Volume 12, Number 4, 2012 ISSN 1562-8353

NONLINEAR DYNAMICS AND SYSTEMS THEORY

An International Journal of Research and Surveys

Volume 12 Number 4 2012

CONTENTS



 ISSN 1562-8353 Printed in Ukraine
To receive contents and abstracts by e-mail, visit our Website at: **http://www.e-ndst.kiev.ua**

NONLINEAR DYNAMICS & SYSTEMS THEORY

**Volume 12, No. 4, 2012**

# Nonlinear Dynamics and Systems Theory

## An International Journal of Research and Surveys



**InforMath Publishing Group**
**http://www.e-ndst.kiev.ua**

# Nonlinear Dynamics and Systems Theory

An International Journal of Research and Surveys






# INSTRUCTIONS FOR CONTRIBUTORS

**(1) General.** Nonlinear Dynamics and Systems Theory (ND&ST) is an international journal devoted to publishing peer-refereed, high quality, original papers, brief notes and review articles focusing on nonlinear dynamics and systems theory and their practical applications in engineering, physical and life sciences. Submission of a manuscript is a representation that the submission has been approved by all of the authors and by the institution where the work was carried out. It also represents that the manuscript has not been previously published, has not been copyrighted, is not being submitted for publication elsewhere, and that the authors have agreed that the copyright in the article shall be assigned exclusively to InforMath Publishing Group by signing a transfer of copyright form. Before submission, the authors should visit the website:

**http://www.e-ndst.kiev.ua**

for information on the preparation of accepted manuscripts. Please download the archive Sample_NDST.zip containing example of article file (you can edit only the file Samplefilename.tex).

**(2) Manuscript and Correspondence.** Manuscripts should be in English and must meet common standards of usage and grammar. To submit a paper, send by e-mail a file in PDF format directly to

*Professor A.A. Martynyuk*, Institute of Mechanics,
Nesterov str.3, 03057, MSP 680, Kiev-57, Ukraine
e-mail: anmart@stability.kiev.ua; center@inmech.kiev.ua

or to one of the Regional Editors or to a member of the Editorial Board. Final version of the manuscript must typeset using LaTex program which is prepared in accordance with the style file of the Journal. Manuscript texts should contain the title of the article, name(s) of the author(s) and complete affiliations. Each article requires an abstract not exceeding 150 words. Formulas and citations should not be included in the abstract. AMS subject classifications and key words must be included in all accepted papers. Each article requires a running head (abbreviated form of the title) of no more than 30 characters. The sizes for regular papers, survey articles, brief notes, letters to editors and book reviews are: (i) 10-14 pages for regular papers, (ii) up to 24 pages for survey articles, and (iii) 2-3 pages for brief notes, letters to the editor and book reviews.

**(3) Tables, Graphs and Illustrations.** Each figure must be of a quality suitable for direct reproduction and must include a caption. Drawings should include all relevant details and should be drawn professionally in black ink on plain white drawing paper. In addition to a hard copy of the artwork, it is necessary to attach the electronic file of the artwork (preferably in PCX format).

**(4) References.** References should be listed alphabetically and numbered, typed and punctuated according to the following examples. Each entry must be cited in the text in form of author(s) together with the number of the referred article or in the form of the number of the referred article alone.

Journal: [1] Poincare, H. Title of the article. *Title of the Journal* **Vol. l** (No.l), Year, Pages. [Language]

Book: [2] Liapunov, A.M. *Title of the book.* Name of the Publishers, Town, Year.

Proceeding: [3] Bellman, R. Title of the article. In: *Title of the book.* (Eds.). Name of the Publishers, Town, Year, Pages. [Language]

**(5) Proofs and Sample Copy.** Proofs sent to authors should be returned to the Editorial Office with corrections within three days after receipt. The corresponding author will receive a sample copy of the issue of the Journal for which his/her paper is published.

**(6) Editorial Policy.** Every submission will undergo a stringent peer review process. An editor will be assigned to handle the review process of the paper. He/she will secure at least two reviewers' reports. The decision on acceptance, rejection or acceptance subject to revision will be made based on these reviewers' reports and the editor's own reading of the paper.

**NONLINEAR DYNAMICS AND SYSTEMS THEORY**
An International Journal of Research and Surveys
Published by InforMath Publishing Group since 2001

Volume 12 Number 4 2012

CONTENTS



*Founded by A.A. Martynyuk in 2001.*
*Registered in Ukraine Number: KB 5267 / 04.07.2001.*

**NONLINEAR DYNAMICS AND SYSTEMS THEORY**

An International Journal of Research and Surveys

*Impact Factor from SCOPUS for 2011: SNIP – 0.84, RIP – 0.77*

**Nonlinear Dynamics and Systems Theory** (ISSN 1562–8353 (Print), ISSN 1813–7385 (Online)) is an international journal published under the auspices of the S.P. Timoshenko Institute of Mechanics of National Academy of Sciences of Ukraine and Curtin University of Technology (Perth, Australia). It aims to publish high quality original scientific papers and surveys in areas of nonlinear dynamics and systems theory and their real world applications.

## AIMS AND SCOPE

**Nonlinear Dynamics and Systems Theory** is a multidisciplinary journal. It publishes papers focusing on proofs of important theorems as well as papers presenting new ideas and new theory, conjectures, numerical algorithms and physical experiments in areas related to nonlinear dynamics and systems theory. Papers that deal with theoretical aspects of nonlinear dynamics and/or systems theory should contain significant mathematical results with an indication of their possible applications. Papers that emphasize applications should contain new mathematical models of real world phenomena and/or description of engineering problems. They should include rigorous analysis of data used and results obtained. Papers that integrate and interrelate ideas and methods of nonlinear dynamics and systems theory will be particularly welcomed. 

## PUBLICATION AND SUBSCRIPTION INFORMATION

**Nonlinear Dynamics and Systems Theory** will have 4 issues in 2013, printed in hard copy (ISSN 1562–8353) and available online (ISSN 1813–7385), by InforMath Publishing Group, Nesterov str., 3, Institute of Mechanics, Kiev, MSP 680, Ukraine, 03057. Subscription prices are available upon request from the Publisher (`mailto:anmart@stability.kiev.ua`), SWETS Information Services B.V. (`mailto:Operation-Academic@nl.swets.com`), EBSCO Information Services (`mailto:journals@ebsco.com`), or website of the Journal: `http://e-ndst.kiev.ua`. Subscriptions are accepted on a calendar year basis. Issues are sent by airmail to all countries of the world. Claims for missing issues should be made within six months of the date of dispatch.

## ABSTRACTING AND INDEXING SERVICES

Papers published in this journal are indexed or abstracted in: Mathematical Reviews / MathSciNet, Zentralblatt MATH / Mathematics Abstracts, PASCAL database (INIST–CNRS) and SCOPUS.

Nonlinear Dynamics and Systems Theory, **12** (4) (2012) 325–332

**PERSONAGE IN SCIENCE**

# Professor Theodore A. Burton

J.H. Dshalalow [1*] and A.A. Martynyuk [2]

[1] *Department of Applied Mathematics Florida Institute of Technology, Melbourne, Fl, 32901, USA*
[2] *S.P. Timoshenko Institute of Mechanics, National Academy of Science of Ukraine, Nesterov Str. 3, Kiev, 03057, Ukraine*

## 1 Brief outline of T.A. Burton's life

T. A. Burton (denoted by T. A. throughout this paper) was born on September 7, 1935 on a farm in Kansas, the fifth child of seven in the family. It was a peak of the Great Depression and when the dust storms wrecked havoc on the Mid-Western United States. Entire buildings were buried in the dust. The economy was so poor that farmers turned their livestock loose and left the area. At the age of five, T. A. and his family moved to Idaho, then to California, and finally to the Cascade Mountains of the state of Washington where he completed an elementary and high school.

On the day he graduated from high school he was drafted into the army for two years, emerging with veteran's rights to a college education. In 1959 he graduated from the Washington State College with a Bachelor of Science with Honors. His record earned him a full fellowship for three years of study toward a Ph.D. in mathematics. On August 5, 1961 he married the love of his life, Fredda Jean Anderson.

His graduate work began in 1959 under the direction of the late Donald W. Bushaw. Bushaw was a student of Solomon Lefschetz and his dissertation concerned the first paper on optimal control. But Lefschetz was also deeply interested in differential equations of various Liénard types and Bushaw inherited that interest, assigning to T. A. a problem on global stability of a nonlinear oscillator. There was much literature on the problem and its generalizations. Lefschetz gathered a number of outstanding foreign and American researchers to study the problem, whose most important aspects were well-defined. The problem was old, going back to Lagrange, and it is taught to every student in a basic course on differential equations.

We consider a number of physical problems, such as a spring-mass-dashpot system, and use Newton's second law of motion under numerous assumptions to obtain the equation of motion

$$x'' + ax' + bx = 0$$

* Corresponding author: mailto:edshalalow@cfl.rr.com

with $a$ and $b$ being positive constants. It is obvious that all solutions and their derivatives tend to zero as $t$ tends to infinity. Taking into account an ample amount of significant real-world problems it stands to reason that $a$ and $b$ must be replaced with general functions to obtain a solution which incorporates a more realistic behavior with many uncertainties. The problem proposed to T. A. in his MA thesis in mathematics was to replace the above linear problem with

$$x'' + f(x)x' + g(x) = 0,$$

where $f(x)$ is a positive function and $g(x)$ is a continuous odd function. His thesis ultimately led to the first necessary and sufficient condition for global asymptotic stability. The result also held when $f(x)$ was replaced with $f(x)h(x')$ where $h$ was also positive. These results have been generalized ever since, but the original ones are still widely quoted.

**[1]** Burton, T. A. The generalized Liénard equation. *J. SIAM on Control* **5** (1965) 223–230.

**[2]** Burton, T. A. On the equation $x'' + f(x)h(x')x' + g(x) = e(t)$. *Annali di Math. Pura Appl.* **LXXXV** (1970) 277–286.

The problem had also brought to its attention a large group of Chinese mathematicians, including Qichang Huang who later became a university president where he used his position to promote research and collaboration with foreign mathematicians around the world. In 1965, just before [1] appeared, Mao Zedong started the Cultural Revolution which sent scholars to farms, steel mills, and other places of hard labor. Huang was sent to a rural village, given a cow, and sent to the mountains using the cow to drag firewood down to the village. Nevertheless, he continued to work on this same problem during the night times and when the Cultural Revolution ended in the early 1980's he returned to his university and got across Burton's paper [1] which he presented in a conference to his fellows mathematicians who were working on the same problem. As a result, Huang was paid a two-years visit to work with T. A. It was the beginning of a cultural and scientific exchange which is still active.

The three year fellowship for graduate study given to T. A. came to an end one year before he was supposed to graduate. To support his fourth year of the graduate study, T.A. took part in a national competition to earn a full scholarship. This was a successful endeavor and T.A. was awarded for his final year followed by his PhD thesis defense in 1964. In the same year he accepted an academic position at the University of Alberta, Edmonton, Canada.

Due to the Russian satellite, Sputnik, American universities were awakening and gearing up for graduate study in all areas of science. Under the leadership of Delyte Morris, a little known university (Southern Illinois University at Carbondale) in Illinois received massive funding for graduate programs. T. A. joined the influx of young professors taking positions there. The opportunities were great and he attracted 13 doctoral students, all of whom succeeded as university professors. To this day he asserts that his main achievement was to guide his doctoral students. All of them were established in areas of mathematics with a future.

Much of his work was international. He was twice a Fulbright senior scholar to Eastern Europe at the University of Szeged, Hungary and at the Technical University of Budapest, once as senior lecturer and once as senior researcher. He had brief research appointments at the University of Florence and the University of Madrid. He was a plenary lecturer at conferences in Europe and Asia almost every year since 1984.

T. A. retired from teaching in 1998, moved to the state of Washington, and spent the last 14 years with the Northwest Research Institute (732 Caroline St., Port Angeles, WA, taburton at olypen.com) conducting research, writing, and lecturing at conferences. He returned to teaching for one semester at the University of Memphis in 2009, offering a graduate course on his book on Liapunov functionals for integral equations. In the summer of 2012 he delivered a plenary lecture at the Conference on Differential and Difference Equations and Applications 2012 in Terchova, Slovakia, a keynote talk at the $10^{th}$ International Conference on Fixed Point Theory and its Applications in Cluj-Napoca, Romania, and a plenary talk at the $8^{th}$ International Conference on Differential Equations and Dynamical Systems at the University of Waterloo, Ontario, Canada.

## 2 Basic Trends of His Scientific Work

### Periodicity and Oscillation

In 1944, N. Levinson studied the equation $x'' + f(x, x')x' + g(x) = e(t)$ under conditions similar to those in [1] and with $e(t)$ periodic. Patterned after the behavior of the constant coefficient analog, he focused on the behavior of solutions of the system form when all solutions entered and remained in a bounded region. It was behavior later named uniform ultimate boundedness. He used a translation argument and Brouwer's fixed point theorem to get a periodic solution. Conditions showing this boundedness were widely sought. Exactly 20 years later, the year T. A. received the Ph.D., G. Sansone and R. Conti published an English version of a 533 page monograph studying such problems, their applications, generalizations, and history. In collaboration with C. G. Townsend, T. A. advanced the necessary and sufficient conditions for global stability of the unforced equation [1] to boundedness and periodicity of solutions of the forced equation under similar conditions. That work appeared as

**[3]** Burton, T. A. and Townsend, C. G. On the generalized Liénard equation with forcing function. *J. Differential Equations* **4** (1968) 620–633.

**[4]** Burton, T. A. and Townsend, C. G. Stability regions of the forced Liénard equation. *J. London Math. Soc.* (2) **3** (1971) 393–402.

It is to be remembered that all of this was in an effort to show that the behavior of solutions of the nonlinear equation was very similar to the behavior of the solutions of the linear constant coefficient equation. The results established clear boundaries for which nonlinear problems would have solutions like the linear problems. The problems are still vigorously studied under increasingly more general assumptions.

This is not to be confused with the problem encountered when the damping, $f(x, y)$, changes sign, a problem which one of T. A.'s doctoral students, John Graef, solved in a similar way in his doctoral dissertation obtaining necessary and sufficient conditions.

The study of periodicity led to the study of oscillation theory, as well as an introduction to functional differential equations. There was then a line of joint papers with R. Grimmer a typical of which was Burton, T. and Grimmer [5]:

**[5]** Burton, T. and Grimmer, R. Oscillation, continuation, and uniqueness of solutions of retarded differential equations. *Trans. Amer. Math. Soc.* **179** (1973) 193–209. (Correction **187** (1974) 429).

### Uniform Asymptotic Stability

At the time T. A. began his work, one of the challenging questions on stability theory by Liapunov's direct method from 1950 to 1992 was to prove or give a counterexample to the following conjecture. Briefly, we have a functional differential equation with bounded delay denoted by $x' = f(t, x_t)$, $x_t(s) = x(t+s)$ for $-r \leq s \leq 0$. We denote by $C_H$ the $H$-ball in the function space of all continuous functions on $[-r, 0]$ into $\Re^n$. The supremum norm is denoted by $\|\cdot\|$ and continuous increasing functions are denoted by $W_i$ where $W_i(0) = 0$.

**Conjecture 2.1** *If there are a continuous and locally Lipschitz functional $V : [0,\infty) \times C_H \to [0,\infty)$ and functions $W_i$ with (i) $W_1(|\phi(0)|) \leq V(t,\phi) \leq W_2(\|\phi\|)$ and (ii) $V'(t,\phi) \leq -W_3(|\phi(0)|)$, then the zero solution is uniformly asymptotically stable.*

A counterexample was given by Geza Makay in 1991 and a more complete one by Junji Kato in 1992, exactly 100 years after the publication of Liapunov's famous work. Details and a history on these are found in [7], pp. 264–293. The conjecture is on p. 269. But something close to it is true. In the 1950's Krasovskii had noted that in most applications the function $W_2$ was actually replaced by something a bit more severe: $V(t,\phi) \leq W_4(\phi(0)| + W_5(|||\phi|||)$, where $|||\cdot|||$ is the $L^2$-norm on $\phi : [-r, 0] \to \Re^n$. He had obtained an asymptotic stability conclusion under the additional assumption that $f(t, x_t)$ is bounded for $x_t$ bounded, the old condition of Marachkoff from 1942.

In 1978, T. A. proved that Krasovskii's result was true without the Marachkoff condition and that the conclusion is actually uniform asymptotic stability, just as in the original conjecture.

Paper [6] introduced the idea of playing $W_3$ against $W_2$ which proved to be very successful in many problems.

**[6]** Burton, T. A. Uniform asymptotic stability in functional differential equations. *Proc. Amer. Math. Soc.* **68** (1978) 195–199.

It opened a way to further results, particularly by Laszlo Hatvani, Tingxiu Wang, and Bo Zhang. A summary is found on pp. 264-293 of:

**[7]** Burton, T. A. *Volterra Integral and Differential Equations, Second Edition.* Elsevier, Amsterdam, 2005.

It is an interesting and important problem. However, the counterexamples and the subsequent advances of Hatvani, Wang, and Zhang show that this old conjecture on which so many investigators had worked for so long was very nearly true.

### Stability in Functional Differential Equations

His next main project involved Liapunov functional methods for functional differential equations with emphasis on integrodifferential equations. The foundation was laid in five main papers:

**[8]** Burton, T. A. Stability theory for Volterra equations. *J. Differential Equations* **32** (1979) 101–118.

**[9]** Burton, T. A. Stability theory for functional differential equations. *Trans. Amer. Math. Soc.* **255** (1979) 263–275.

**[10]** Burton, T. A. Stability theory for delay equations. *Funkcialaj Ekvacioj* **22** (1979) 67–76.

**[11]** Burton, T. A. and Mahfoud, W. E. Stability criteria for Volterra equations. *Trans. Amer. Math. Soc.* **279** (1983) 143–174.

**[12]** Burton, T. A. and Hatvani, L. Stability theorems for nonautonomous functional differential equations by Liapunov functionals. *Tohoku Math. J.* **41** (1989) 65–104.

A unified treatment of existing theory through 1983 is found in

**[13]** Burton, T. A. *Volterra Integral and Differential Equations.* Academic Press, Orlando, 1983,

which was updated in a second edition [7].

## Fixed Point Theory I

The work on stability of integrodifferential equations led naturally to questions of periodic solutions of Volterra integrodifferential equations with infinite delay. This presented special problems in fixed point theory concerning the "sandwich" theorems, asymptotic fixed point theorems, and compactness. Everything depended on two things. There was the need to establish conditions under which solutions are uniformly ultimately bounded and this was done with Liapunov theory. But the translation arguments given by N. Levinson so long ago had no chance of holding for these problems. Everything depended on the study of spaces having unbounded compact sets. It was an interesting study and investigators were constantly on new ground. In such an unexpected way, exactly the same problems occur when we study fractional differential equations. These are developed in [33].

One can trace the evolution of those questions and solutions through the papers:

**[14]** Burton, T. A. Periodic solutions of nonlinear Volterra equations. *Funkcialaj Ekjvacioj* **27** (1984) 301–317.

**[15]** Burton, T. A. Periodic solutions of integrodifferential equations. *Proc. London Math. Soc.* **31** (1985) 537–548.

**[16]** Arino, O. A., Burton, T. A., and Haddock, J. R. Periodic solutions of functional differential equations. *Roy. Soc. Edinburgh Proc. A.* **101A** (1985) 253–271.

All of this was integrated into the existing theory and appeared in:

**[17]** Burton, T. A. *Stability and Periodic Solutions of Ordinary and Functional Differential Equations*. Academic Press, Orlando, 1985; reprinted by Dover, Mineola, New York, 2005.

But a much more final disposition appeared later in:

**[18]** Burton, T. A. and Zhang, Bo. Uniform ultimate boundedness and periodicity in functional differential equations. *Tohoku Math. J.* **42** (1990) 93–100.

## Liapunov Functionals for Integral Equations I

The work on stability and periodic solutions of integrodifferential equations provided a background and insights to attack the old problem of constructing Liapunov functionals for integral equations. The direct method of Liapunov had been applied very successfully for ordinary, functional, and partial differential equations, as well as related areas such as control theory. In all of these problems, the elementary technique of uniting the Liapunov functional with the differential equation was achieved by means of the chain rule, extended in a reasonable way to non-elementary cases. If an integral equation could be differentiated to obtain an integrodifferential equation, then the direct method could be readily applied. In 1992, exactly 100 years after Liapunov's famous paper, T. A. constructed the first successful Liapunov functionals for integral equations and united them in a simple way to the integral equation. The work was presented at the centennial celebration of Liapunov's paper held in Tampa, Florida and sponsored by one of the great investigators of the direct method, V. Laksmikantham, and the International Federation of Nonlinear Analysts. It appeared in the conference proceedings:

**[19]** Burton, T. A. Examples of Lyapunov functionals for non-differentiated equations. *Proc. First World Congress Nonlinear Analysts*, 1992. V. Lakshmikantham, ed. Walter de Gruyter publisher, 1996, New York. pp. 1203–1214.

He was joined the next year by a former doctoral student of Taro Yoshizawa, Tetsuo Furumochi, from Shimane University in Matsue, Japan who came with his family to Southern Illinois University for ten months to develop the theory. A substantial number of papers resulted from the study including:

**[20]** Burton, T. A. and Furumochi, Tetsuo. Periodic solutions of a Volterra equation and robustness. *Nonlinear Analysis* **25** (1995) 1199–1219.

**[21]** Burton, T. A. and Furumochi, Tetsuo. Stability theory for integral equations. *J. Integral Equations and Applications* **6** (1994) 445–477.

The work progressed and a preliminary book was printed for use in a graduate course which he taught at the University of Memphis, Tennessee in the spring of 2009. A pdf file of the preliminary book can be downloaded free of charge at T. A.'s web page, Item 91: **http://www.math.siu.edu/burton/papers.htm**.

**[22]** Burton, T. A. *Liapunov Functionals for Integral Equations*.

The work was preliminary because the method only worked for continuous kernels which was certainly a step up from the earlier requirement that the integral equation be differentiable. It failed to cover so many important real-world problems such as those represented by fractional differential equations with kernel $(t-s)^{q-1}$ for $0 < q < 1$, including many forms of heat equations with $q = 1/2$. Much of the work involved a careful strategy and that is developed in:

**[23]** Burton, T. A. Liapunov functionals, convex kernels, and strategy. *Nonlinear Dynamics and Systems Theory* **10** (2010) 325–337.

We will return to a conclusion later.

## Fixed Point Theory II

Sixty years ago Krasnoselskii studied an old paper by Schauder on elliptic partial differential equations and formulated a principle which we formalize as Krasnoselskii's Hypothesis. The inversion of a perturbed differential operator yields the sum of a contraction and a compact map. Accordingly, he formulated a fixed point theorem which was a combination of the contraction mapping principle and Schauder's fixed point theorem. In recent years the idea emerged that Krasnoselskii was advancing an idea which could unify the broad and disconnected area of differential equations. In the mid 1990s T. A. began a study of Krasnoselskii's theorem with a view to discovering the unification. The first result was

**[24]** Burton, T. A. Integral equations, implicit functions, and fixed points. *Proc. Amer. Math. Soc.* **124** (1996) 2383–2390.

That paper introduced the idea of a large contraction which has proved useful in transforming totally nonlinear differential equations into integral equations. It has played a major role in fractional differential equations, as may be seen in [35], below. Krasnoselskii's theorem had a condition which was very difficult to meet. The next three papers circumvented that problem.

**[25]** Burton, T. A. and Kirk, Colleen. A fixed point theorem of Krasnosel'skii-Schaefer type. *Mathematische Nachrichten* **189** (1998) 23–31.

**[26]** Burton, T. A. A fixed-point theorem of Krasnoselskii. *Appl. Math. Lett.* **11** (1998) 85–88.

**[27]** Burton, T. A. Krasnoselskii's inversion principle and fixed points. *Nonlinear Analysis* **30** (1997) 3975–3986.

With this background and in collaboration with Tetsuo Furumochi and Bo Zhang a comprehensive theory of stability by fixed point methods was developed. There were two main advantages over the Liapunov theory. First, with the fixed point theory the conditions were averages, while Liapunov theory was usually point-wise. Next, the construction of a Liapunov function was replaced by the usually simpler fixed point mapping. The first comprehensive paper on the subject with many examples was

[**28**] Burton, T. A. and Furumochi, Tetsuo. Fixed points and problems in stability theory. *Dynamical Systems and Applications* **10** (2001) 89–116.

Five years later the papers were collected, the techniques compared with Liapunov theory, and published in:

[**29**] Burton, T. A. *Stability by Fixed Point Theory for Functional Differential Equations.* Dover, Mineola, New York, 2006.

It had been clearly established that much stability theory of functional differential equations could be established from Krasnoselskii's theory. There was, however, a major problem. The unification which was promised by his theory was entirely missing. In an interesting way, that unification was achieved when the efforts returned to Liapunov theory for integral equations. Thus, the next topic offers the foundation for both the fixed point problem and the quest for Liapunov functionals for integral equations with singular kernels.

## Liapunov Theory for Integral Equations II

In 2010 Liapunov theory was advanced to integral equations with singular kernels and, in particular, to fractional differential equations in the papers:

[**30**] Burton, T. A. A Liapunov functional for a singular integral equation. *Nonlinear Analysis* **73** (2010) 3873–3882.

[**31**] Burton, T. A. Fractional differential equations and Lyapunov functionals. *Nonlinear Analysis* **74** (2011) 5648–5662.

[**32**] Becker, L. C., Burton, T. A., and Purnaras, I. K., Singular integral equations, Liapunov functionals, and resolvents. *Nonlinear Analysis* **75** (2012) 3277–3291.

In the second paper the fractional differential equation was inverted to an integral equation which was then transformed into an integral equation with completely monotone kernel, $R(t-s)$, with the property that $0 < R(t) \le t^{q-1}$ and

$$\int_0^\infty R(s)ds = 1.$$

That last property yielded an integral equation defining a natural mapping that was very fixed point friendly and yielded a number of papers showing qualitative properties of solutions, culminating in:

[**33**] Burton, T. A. and Zhang, Bo. Fractional equations and generalizations of Schauder's and Krasnoselskii's fixed point theorems. *Nonlinear Analysis* **75** (2012) 6485–6495.

With that, the basic Liapunov theory and its relation to fixed point theory seemed to have been laid and a preliminary book was completed and is available on amazon.com in the United States, Europe, and the United Kingdom as:

[**34**] Burton, T. A. *Liapunov Theory for Integral Equations with Singular Kernels and Fractional Differential Equations* (2012), Amazon.co.uk, 379 pages.

In 2009, T.A. participated in a conference at the N. N. Krasovskii Institute of Mathematics and Mechanics in Ekaterinburg, Russia where he presented a basic work on Liapunov theory for integral equations. As a result of that association a manuscript is being translated into the Russian language by Prof. Sergey I. Kumkov. An editing of the translation will be performed by Prof. Nikolay Yurievich Lukoyanov. The translation is to be published by the Autonomous Nonprofit Organization, Izhevsk Institute of Computer Science, Universitetskaya, I, Izhevsk, 426034 Russia.

**Fixed Point Theory III**

The mapping equation derived in the inversion of the fractional differential equation concerning the new kernel $R(t)$ has proved to be a unifying concept. At the present time scalar fractional differential equations, functional differential equations, and neutral equations are all treated in a unified way using that mapping. It is an intriguing evidence that Krasnoselskii had a very fruitful and general idea. Pursuing that has now become the main project. Paper [35] gives all the details of the transformations, shows the fixed points methods, and illustrates the use of large contractions and the paper [36] employs very different fixed point techniques.

**[35]** Burton, T. A. and Zhang, Bo. Fixed points and fractional differential equations: Examples. *Fixed Point Theory*, in press.

**[36]** Burton, T. A. and Zhang, Bo. $L^p$-solutions of fractional differential equations. *Nonlinear Studies* **19** (2) (2012) 161–177.

## 3 T.A.'s Doctoral Students and Dissertation Titles

John Graef, *Relaxation and Forced Oscillations in a Second Order Nonlinear Differential Equation*, 1970;
John Haddock, *Some Refinements of Liapunov's Direct Method*, 1970;
John Erhart, *Lyapunov Theory and Perturbations of Differential Equations*, 1970;
Alfredo Somolinos, On the Problem of Lurie and its Generalizations, 1974;
Wadi Mahfoud, *Oscillation, Asymptotic Behavior, and Noncontinuation of Solutions of $n^{th}$ Order Nonlinear Delay Differential Equations*, 1975;
Leigh Becker, *Stability Considerations for Volterra Integrodifferential Equations*, 1979;
Muhammed Islam, *Periodic Solutions of Volterra Integral Equations*, 1985;
Shou Wang, *Stability and Boundedness in Ordinary and Functional Differential Equations*, 1987;
Roger Hering, *Boundedness and Stability in Functional Differential Equations*, 1988;
Tingxiu Wang, *On Uniform Asymptotic Stability of the zero Solution of Functional Differential Equations*, 1991;
Bo Zhang, *Periodic Solutions of Nonlinear Abstract Differential Equations with Infinite Delay*, 1991;
David Dwiggins, *Fixed Point Theory and Periodic Solutions for Differential Equations*, 1993;
Geza Makay, *Boundedness and Periodic Solutions of Functional Differential Equations*, 1993.

## 4 Exceptional Master's Student

Colleen Kirk, *Neural Networks: Convergence and Stability*, 1995.

## 5 Journal Editing

T. A. has periodically been an editor of the following journals:
1. *Cubo: A Mathematical Journal*; Chile.
2. *Electronic J. Qualitative Theory of Differential Equations* (jointly founded with Laszlo Hatvani, now honorary editor); Hungary.
3. *Fixed Point Theory*; Romania.
4. *Journal of Fractional Calculus and Applications*; Egypt.
5. *Nonlinear Analysis: TMA*; United Kingdom.
6. *Nonlinear Dynamics and Systems Theory* (editor and honorary editor); Ukraine.
7. *Nonlinear Studies*; United States.
8. *Opuscula Mathematica*; Poland.

Nonlinear Dynamics and Systems Theory, **12** (4) (2012) 333–344

# Flatness-based Control of Throttle Valve Using Neural Observer

I. Aidi [1,2*], M. Ayadi [1], M. Benrejeb [1] and P. Borne [2]

[1] *LARA. Ecole Nationale d'Ingénieurs de Tunis (ENIT)*
*BP 37, Le Belvédère, 1002 Tunis, Tunisia*
[2] *LAGIS. Ecole Centrale de Lille*
*Cité Scientifique BP 48, F 59651, Villeneuve d'Ascq Cedex, Lille, France*

Received: February 10, 2012; Revised: October 8, 2012

**Abstract:** In this paper, a proposed flatness-based controller is designed for an electronic throttle valve in an internal combustion engine. It is based on the use of the state space variables of the flat nonlinear model, estimated by a neural observer, to track a desired trajectory. The case of the control of an electronic throttle valve study shows the efficiency of the developed control method in terms of tracking in the presence of non linearities.

**Keywords:** *flat output; flatness-based controller; neural observer; electronic throttle valve.*

**Mathematics Subject Classification (2010):** 93C10, 93C35.

## 1 Introduction

Quality improvement of the combustion in automobile engine requires the control of the system of injection as well as the quality of air aspired via the admission collector [3]. This desired air flow is obtained by an electronic throttle valve considered as an electro-valve which presents nonlinear phenomena, depending on the position and the applied control voltage, such as: saturation, hysteresis, dead zone, disturbances and parametric uncertainties of the model.

This paper deals with the use of the differential flatness concept to control this nonlinear system. However, this approach has no systematic methods to detect the flat output for a given system, and presents the difficulty concerning the robustness study of the

* Corresponding author: mailto:aidi.imen@gmail.com

proposed process control; but, it constitutes a powerful tool for trajectory tracking for linear and nonlinear systems such as the electronic throttle valve [6, 9].

The aim of this work is to design a flatness-based controller in order to track a desired angular position trajectory of a throttle plate, by using the tracking error, the angular velocity and acceleration of this system. The problem concerning the estimation of the angular velocity and acceleration is solved, in this paper, by the use of a neural observer. This paper is organized as follows. After the description of the studied non linear electronic throttle valve in Section 2, the proposed flatness-based controller with a neural observer is introduced in Section 3. The proposed approach is presented for a numerical example studied in Section 4 to illustrate the efficiency of the proposed method.

## 2 Electronic Throttle Valve Modelization

After a description of the studied electronic throttle valve, a non linear global modal of this system is proposed in this section.

### 2.1 System Description

The considered system is constituted of a DC motor with independent excitation coupled to the throttle valve (Figure 1) [1–3].

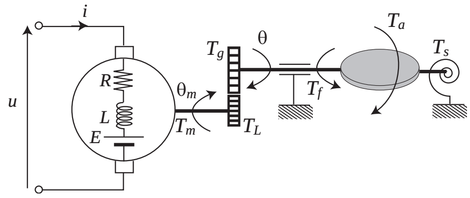


**Figure 1**: Electronic throttle valve model.

The electrical part can be described by:

$$u = L\frac{di}{dt} + Ri + E, \quad E = k\frac{d\theta_m}{dt} = k\omega, \tag{1}$$

where $L$ is the inductance, $R$ is the resistance, $E$ is the electromotive force of its armature, $u$ and $i$ are the voltage and the armature current respectively, $k$ is an electromotive force constant, $\theta$ is the plate position of the throttle and $\omega$ is the rotor angular velocity. The mechanical part of the throttle is modeled by a gear reducer characterized by its reduction ratio $n$ such as:

$$n = \frac{\theta_m}{\theta} = \frac{T_g}{T_L}, \tag{2}$$

where $T_L$ is the load torque, $T_g$ is the gear torque, $J$ is the total inertia of the load submitted to an electromagnetical torque $T_e$, $T_e = k_e i$, and $T_f$, $T_s$ and $T_a$ are other resistive torques; $T_f$ is the stickslip friction torque, $T_s$ is the nonlinear spring torque and $T_a$ is the torque generated by the air flow. By considering $\Omega = \frac{\omega}{n}$, as the reduced rotor angular velocity, the mechanical equation is then given by (3):

$$J\frac{d\Omega}{dt} = T_e - T_f - T_s - T_a. \tag{3}$$

It can be noted that the torque $T_a$, generated by the air flow, can be considered as an external perturbation. The electronic throttle valve involves two complex nonlinearities due to the nonlinear spring torque $T_s$ and the friction torque $T_f$. They are given by their static characteristics [3, 4], as shown in Figure 2:

- a dead zone in which the control voltage signal has no effect on the nominal position of the valve plate;
- two hysteresis combined with a saturation, due to the valve plate movement, limited by the maximum and minimum angle.

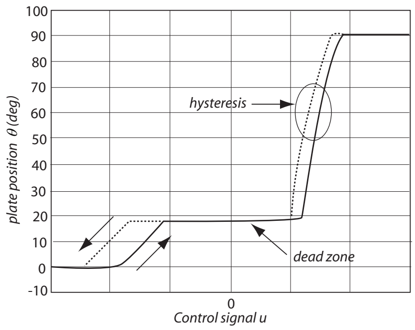


**Figure 2**: Static characteristic of the studied throttle.

The static characteristic of the nonlinear spring torque $T_s$ is defined by

$$T_s = k_r(\theta - \theta_0) + D\,\mathrm{sgn}(\theta - \theta_0) \tag{4}$$

for $\theta_{\min} \leqslant \theta \leqslant \theta_{\max}$ (Figure 3); $k_r$ is the spring constant, $\theta_0$ is the default position and

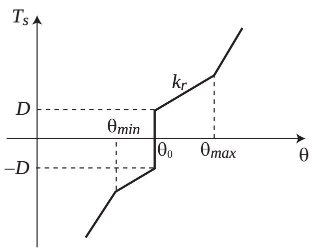


**Figure 3**: Spring torque characteristic.

sgn(·) is the following signum function:

$$\mathrm{sgn}(\theta - \theta_0) = \begin{cases} 1, & \text{if } \theta \geq \theta_0, \\ -1, & \text{else.} \end{cases} \tag{5}$$

The friction torque function $T_f$ of the angular velocity of the throttle plate, given in Figure 4, can be expressed as

$$T_f = f_v\omega + f_c\mathrm{sgn}(\omega), \tag{6}$$

where $f_v$ and $f_c$ are two constants.

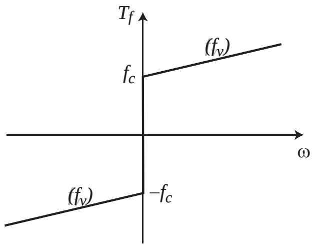


**Figure 4**: Friction torque characteristic.

## 2.2 Global Nonlinear Model

By substituting in equations (1) and (3), $T_e$, $T_f$ and $T_s$ torques by their expressions, the nonlinear differential system can be obtained, for the unload case ($T_a = 0$), as following:

$$\begin{cases} \frac{J}{n}\frac{d\omega}{dt} = k_e i - f_v\omega - f_c\mathrm{sgn}(\omega) - k_r(\theta - \theta_0) - D\,\mathrm{sgn}(\theta - \theta_0), \\ L\frac{di}{dt} = u - Ri - k\omega, \\ \frac{d\theta}{dt} = \frac{1}{n}\omega. \end{cases} \tag{7}$$

By adopting the following notations:

$$\begin{gathered} a_{12} = \tfrac{1}{n},\ a_{21} = -\tfrac{k_r n}{J},\ a_{22} = -\tfrac{f_v n}{J},\ a_{23} = \tfrac{k_e n}{J}, \\ a_{32} = -\tfrac{k}{L},\ a_{33} = -\tfrac{R}{L},\ \mu = \tfrac{f_c n}{J},\ K = \tfrac{Dn}{J},\ b_1 = \tfrac{1}{L}, \end{gathered} \tag{8}$$

and by the choice of the following state variables:

$$x_1 = \theta - \theta_0, \quad x_2 = \dot{x}_1 = a_{12}\omega, \quad x_3 = \dot{x}_2 = a_{12}\dot{\omega}, \tag{9}$$

the differential system (7) can be rewritten as:

$$\begin{cases} \dot{x}_1 = x_2, \\ \dot{x}_2 = x_3, \\ \dot{x}_3 = \ \beta_1(x_1) + \beta_2 x_2 + \beta_3 x_3 + v(x) + bu, \end{cases} \tag{10}$$

with

$$\begin{gathered} \beta_1 = -a_{12}a_{21}a_{33},\ \beta_2 = -a_{22}a_{33} + a_{12}a_{21} + a_{23}a_{32},\ \beta_3 = a_{22} + a_{33}, \\ K'' = a_{12}a_{33}K,\ \mu'' = a_{12}a_{33}\mu,\ b = a_{12}a_{23}b_1,\ K' = Ka_{12},\ \mu' = \mu a_{12}, \end{gathered} \tag{11}$$

and

$$v(x) = K''\mathrm{sgn}(x_1) + \mu''\mathrm{sgn}(x_2) - K'\mathrm{sgn_d}(x_1) - \mu'\mathrm{sgn_d}(x_2), \tag{12}$$

$\mathrm{sgn_d}(\cdot)$ denoting the derivative of the signum function. This system description involves the signum function and its derivatives which present a singularity at the origin. In order to overcome this problem, this signum function can be approximated by the following derivable function in any point:

$$\mathrm{sgn}(\xi) \approx \frac{2}{\pi}\arctan(\alpha\xi), \tag{13}$$

where $\alpha$ is a positive constant, chosen equal to 10 000 for instance. Then the derivative function of $\mathrm{sgn}(\xi)$, noted $\mathrm{sgn_d}(\cdot)$, is given by:

$$\mathrm{sgn_d}(\xi) = \frac{2}{\pi}\frac{\alpha}{1+(\alpha\xi)^2}\dot{\xi}. \tag{14}$$

It comes:

$$v\left(x\right) = \frac{2}{\pi}K'' \arctan\left(\alpha x_1\right) + \frac{2}{\pi}\mu'' \arctan\left(\alpha x_2\right) - \frac{2}{\pi}K' x_2 \frac{\alpha}{1+\left(\alpha x_1\right)^2} - \frac{2}{\pi}\mu' x_3 \frac{\alpha}{1+\left(\alpha x_2\right)^2}. \tag{15}$$

The control of the throttle's angle constitutes a complicated problem because of the strong nonlinearities of the system and the difficulty to measure the disturbances and the uncertainty of the parameters of the model. In order to overcome the problem and to control this throttle, we propose, in the next section, the use of a flatness-based control.

## 3 Flatness-based Control Design of the Throttle's Valve

A nonlinear flatness-based control approach is applied, in this section, to the nonlinear model of the motorized throttle valve. This controller is proposed to follow a given trajectory planned from the flat output [8], see Appendix and Subsection 3.2, and the estimation of its derivatives.

### 3.1 Basic idea

The proposed based-flatness controller uses a state observer as shown in Figure (7).

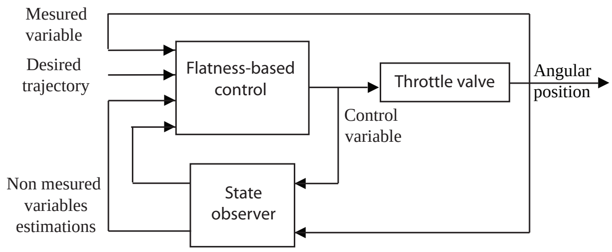


**Figure 5**: Flatness-based control structure with observer.

The idea is to show, firstly, that the studied throttle valve is a flat system and, secondly to generate the angular velocity and acceleration, which cannot be measured, by the use of a proposed neural observer. Then, with the measured angular position values, a flatness-based control has to be, at last, elaborated to make the studied system tracking desired trajectory.

### 3.2 Proposed flatness-based controller

Let's show, first, that the electronic throttle valve is flat. Let's, then consider the equations (10) and (15), and the output $y$ equal to $x_1$:

$$y = x_1. \tag{16}$$

We note that the state variables $x_1$, $x_2$, and $x_3$ and the input $u$ can be expressed as functions of this output $y$ and a finite number of its time derivatives [8], as shown in the following. By replacing $x_1$, $x_2$, and $x_3$ with their expressions given by

$$x_1 = y, \quad x_2 = \dot{y}, \quad x_3 = \ddot{y}, \tag{17}$$

in the expression of $\dot{x}_3$ given by (10), we obtain:

$$\dot{x}_3 = f(y, \dot{y}, \ddot{y}) + bu \tag{18}$$

with $f(.) = \beta_1 y + \beta_2 \dot{y} + \beta_3 \ddot{y} + \frac{2}{\pi} K'' \arctan(\alpha y) + \frac{2}{\pi}\mu'' \arctan(\alpha \dot{y}) - \frac{2}{\pi} K' \dot{y} \frac{\alpha}{1+(\alpha y)^2} - \frac{2}{\pi}\mu' \ddot{y} \frac{\alpha}{1+(\alpha \dot{y})^2}$. The input $u$ of the throttle valve can be expressed by

$$u = \frac{\dot{x}_3 - f(.)}{b} \tag{19}$$

or depending on $y$ and $y^{(3)}$ by

$$u = \frac{y^{(3)} - f(.)}{b}. \tag{20}$$

The electronic throttle valve is therefore a flat system and the output $y$ is the flat output. In order to verify that the proposed approach allows to achieve very smooth transitions, a sinusoidal trajectory shall be planned around $y_0$, the default position of the throttle plate. To the corresponding reference trajectory $y^d$ for the output, is associated the open-loop control $u^d$ given by

$$u^d = \frac{y^{d(3)} - f_d(.)}{b} \tag{21}$$

with $f_d(.) = f\left(y^d, \dot{y}^d, \ddot{y}^d\right)$. An open-loop control is then determined by the knowledge of a derived trajectory $y^d$. For the closed-loop control design, the new variable $v$, chosen such as

$$v = bu + f(.) \tag{22}$$

and introduced in (19), leads to the following linear model of the throttle valve:

$$v = y^{(3)}. \tag{23}$$

Let $v$ be expressed by

$$v = v^d + \sum_{i=0}^{2} a_i e^{(i)}. \tag{24}$$

It comes that:

$$e^{(3)} + \sum_{i=0}^{2} a_i e^{(i)} = 0 \tag{25}$$

such as the error $e$ is defined as $e = y^d - y$, where the coefficient $a_i$ has to be chosen such that the error $e$ converges asymptotically to zero. From the expression of $v$ of equation (22), the closed loop control law becomes:

$$u = \frac{y^{d(3)} + \sum\limits_{i=0}^{2} a_i e^(i) - f(.)}{b}. \tag{26}$$

Replacing $v^d$ by its expression, we find the expression of $u$ in terms of $u^d$:

$$\begin{aligned} u &= u^d + (f_d(.) - f(.) + \sum_{i=0}^{2} a_i e^(i))b^{-1} \\ &= u^d + (f_d(.) - f(.) + a_0 \left(y - y^d\right) + a_1 \left(\dot{y} - \dot{y}^d\right) + a_2 \left(\ddot{y} - \ddot{y}^d\right))b^{-1}. \end{aligned} \tag{27}$$

Finally, by replacing the expression (22) of the open-loop control in the equation (24), we obtain:

$$u = (y^{(3)d} - f(y) + a_0 \left(y - y^d\right) + a_1 \left(\dot{y} - \dot{y}^d\right) + a_2 \left(\ddot{y} - \ddot{y}^d\right))b^{-1}. \tag{28}$$

The controller is then designed to track a reference trajectory $y^d$. The determination of the control signal $u$ needs the estimation of $\dot{y}$ and $\ddot{y}$ variables. A neural network observer will be used and implemented to the electronic throttle's valve, as shown in the next section.

### 3.3 Proposed neural network observer

Many structures of network and learning algorithms, developed in the littrature by using artificial neural networks [10–12], are efficient in various domains such as the pattern recognition, the signal processing, the speech recognition or the automatic control domains [13, 14].

In this section, the neural observer generates state variables $\dot{y}$ and $\ddot{y}$ of the throttle valve system which can not be measured [16]. The multilayer network of the proposed observer has two neurons in input layer, three neurons in hidden layer and two neurons in output layer. For training of this observer, the Levenberg-Marquardt algorithm is used and data $\hat{\dot{y}}$ and $\hat{\ddot{y}}$ are obtained directly from the values of $u$, $y$, $\dot{y}$ and $\ddot{y}$ at each instant. The generation of the derivative of $y$ is generally difficult to realize. Many approximations of the solutions of this problem can be considered:

- by estimation of $\dot{y}$ as following: $\dot{y}(t) = \frac{y(t+\Delta t) - y(t)}{\Delta t}$ which increases the disturbances effect;
- by application of the inverse principle, as shown in Figure (6), with $A$ as a high gain, which makes possible the realization of the derivative operator and decreases the perturbation effect by the use of integration operator [15].

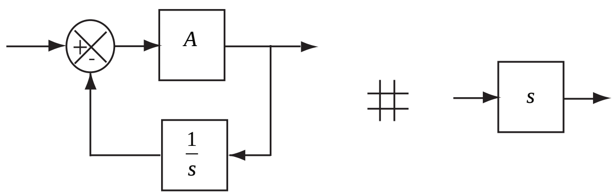


**Figure 6**: Derivative operator realization using the inverse principle.

Validation of the neural observer is based on the error between the target state variables and the real state variables.

| | |
|---|---|
| $\beta_1$ | $-4.8617 \times 10^4$ |
| $\beta_2$ | $-6.7101 \times 10^4$ |
| $\beta_3$ | $-553.852$ |
| $K''$ | $-1.3351 \times 10^5$ |
| $\mu''$ | $-6.0979 \times 10^4$ |
| $b'$ | $1.131 \times 10^5$ |
| $K'$ | $256.3278$ |
| $\mu'$ | $117.0722$ |

**Table 1**: Parameter numerical values.

## 4 Control Electronic Throttle Valve Study by Simulation

Simulations are carried out with the following model parameters (see Table 1) [17].

In order to show the efficiency of the tracking behavior of the throttle's plate with flatness-based control, an open loop and then a closed loop controllers are considered to the throttle valve (10). For the first case, applied trajectory takes into account the flat outputs and its derivatives as shown in relation (21). For sinusoidal desired trajectory output $y^d$, the results, given in Figure 7, show that the obtained angular position is too close to the desired trajectory with an acceptable tracking error. Moreover, a closed loop control is necessary to ameliorate this tracking error and to accelerate the convergence more speedily. A sinusoidal trajectory is also applied to the closed loop system for which

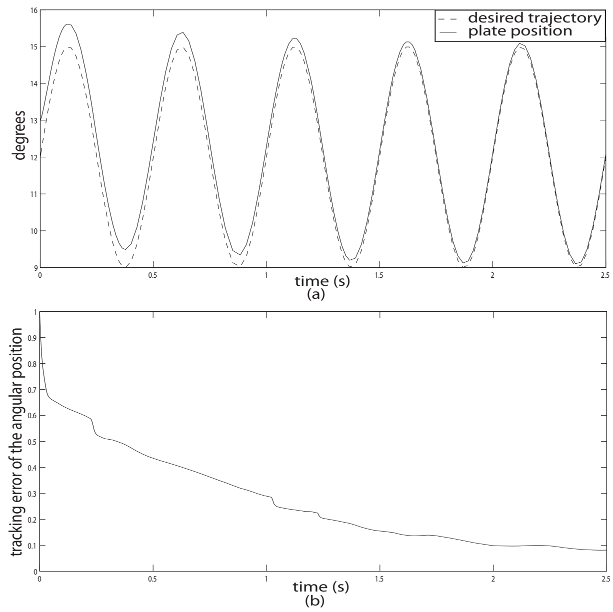


**Figure 7**: (a) Evolution of the angular position in open loop case. (b) Evolution of tracking error of the angular position in open loop case.

the evolutions of the angular velocity and angular acceleration, estimated by a neural observer and their corresponding tracking errors, are given in Figures 8 and 9 .

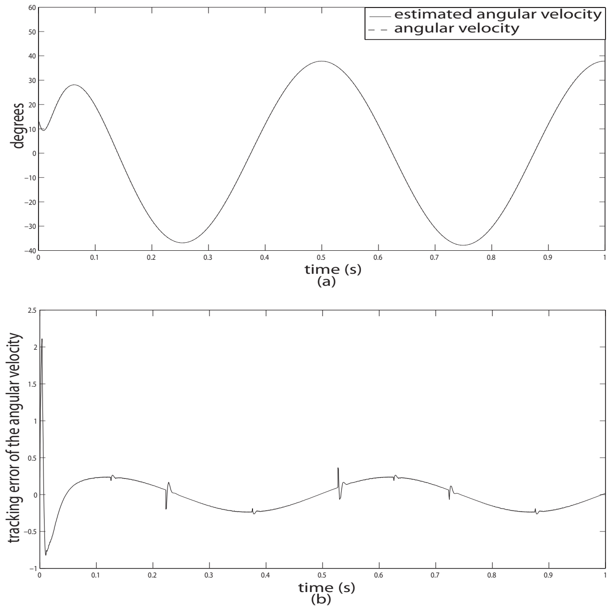


**Figure 8**: (a) Evolution of estimated angular velocity in neural observer case. (b) Evolution tracking error of the angular velocity in neural observer case.

The obtained state variables are very close to the real state variables, which satisfy the assigned objectives. Then, the results show the efficiency of the proposed neural network observer. It must be noted that the evolution of the angular position and the tracking error, in the closed loop case is better than in the open loop case. In fact, the convergence becomes speedily with a small tracking error by the use of the closed loop (Figure 10). The control signal presents minimal and maximum values within the limits imposed on the system, see Figure 11. The obtained control signal ensures a good tracking of trajectories in spite of the strong nonlinearities and commutations present in the throttle.

## 5 Conclusion

In this paper, a flatness-based tracking controller is proposed for a nonlinear electronic throttle valve. The system model has been shown to be differentially flat with the angular position as a flat output. The proposed controller uses angular velocity and angular acceleration which are needed to be estimated. Thus, a neural observer is implemented to estimate these state variables. The application of the neural network observer showed good performances in terms of convergence speed and precision. The proposed method of flatness-based controller with a neural networks observer ensures the track of a desired position of the plate, with a small tracking error, in spite of the strong nonlinearities presented by this system, showing the effectiveness of the proposed approach.

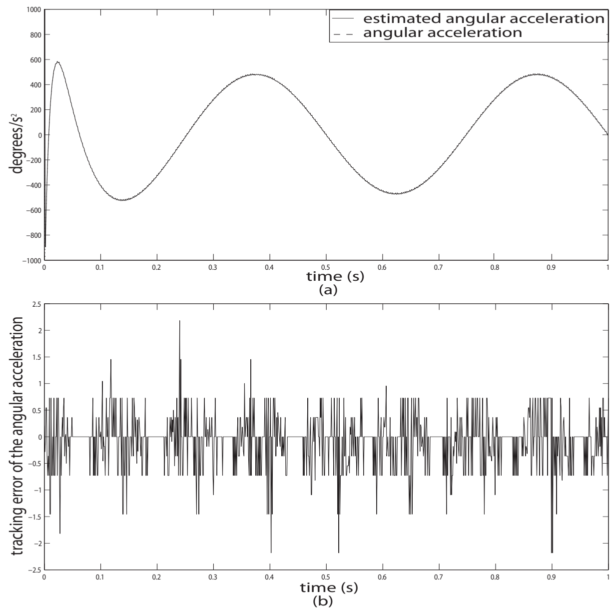


**Figure 9**: (a) Evolution of estimated angular acceleration in neural observer case. (b) Evolution of tracking error of the angular acceleration in neural observer case.

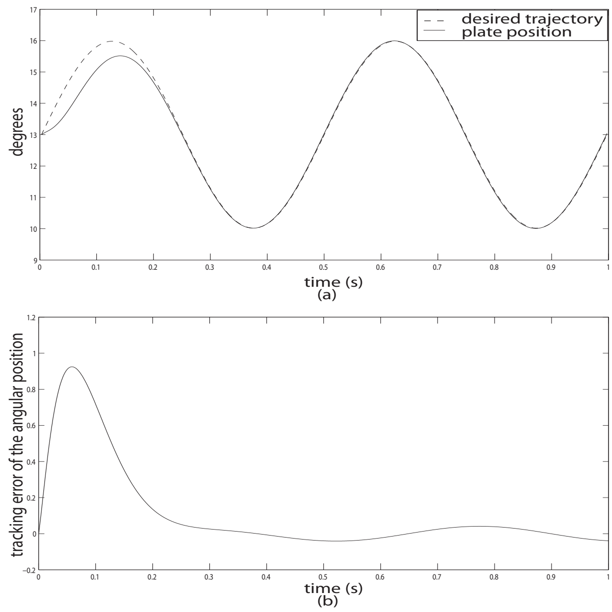


**Figure 10**: (a) Evolution of the angular position in closed loop case. (b) Evolution of tracking error of the angular position in closed loop case.

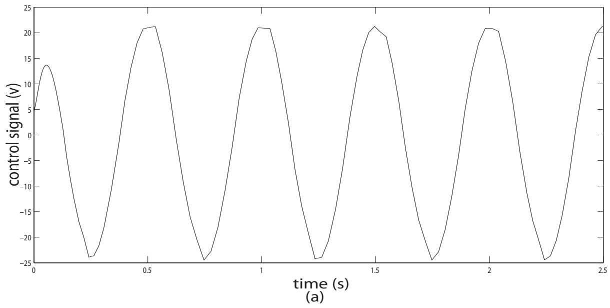


**Figure 11**: Control signal applied to the throttle in closed loop case.

## Appendix

**Flat Systems.** The notion of flatness, introduced in 1992 by M. Fliess and al. [5] constitutes a new perspective in control systems theory. This property, originally developed in the context of nonlinear systems of finite dimension, defines a class of systems characterized by the existence of a variable called flat output, which allows to set all other variables in the system. The following nonlinear system

$$\dot{x} = f\left(x, u\right), \tag{29}$$

$$y = g\left(x, u\right), \tag{30}$$

where $x$ is the state vector, $x \in \mathbb{R}^n$ and $u \in \mathbb{R}^m$ is the input vector which is called flat, if there is a variable $z$, $z \in \mathbb{R}^m$, of the form [7]:

$$z = \psi\big(x, u, \dot{u}, \dots, u^{(r)}\big). \tag{31}$$

The flat output $z$ allows to differentially parameterize the state $x$ and the input $u$ as:

$$x = \phi\big(z, \dot{z}, \dots, z^{(r)}\big), \tag{32}$$

$$u = \chi\big(z, \dot{z}, \dots, z^{(r+1)}\big). \tag{33}$$

The relation (30) defines the $z$ variable as the flat output of the system or as endogenous variable. Thus, the actual output of the process $y$ is given by:

$$y = \xi\big(z, \dot{z}, \dots, z^{(r)}\big). \tag{34}$$

The objective of the trajectories planning is to determine an open-loop control $u^d$, carrying out the objective bringing a given system, of a certain initial state in a known final state: An important consequence of the parametrization given in (33) is that once having chosen a nominal desired reference trajectory $z^d$ for the flat output, this output determines the necessary nominal control $u^d$ that is [8]:

$$u^d = \chi\big(z^d,\ ...,\ z^{d(r+1)}\big), \tag{35}$$

where $z^d$ is the desired path for the flat output, $(r+1)$ once continuously differentiable.

Generating a trajectory leads to the open loop control that can require the system to get the expected behavior. However, as the model is not perfect, a closed loop control is needed to stabilize the system around this trajectory. To accelerate the convergence, stable or unstable systems need a correction term to track a reference trajectory which is added to the open-loop control. Closed loop system is characterized by [9]

$$u = \chi\big(z, \dot{z}, \dots, z^{(r)}, v\big), \quad v = z^{d(r+1)} + \sum_{i=0}^{r} a_i e^{(i)}. \tag{36}$$

The coefficients $a_i$ are chosen so that the error tracking $e = z^d - z$ converges asymptotically to zero.

## References


[1] Grondin, O. Modélisation du moteur à allumage par compression dans la perspective du contrôle et du diagnostic. *PhD thesis*, Université de Rouen, 2004.

[2] Lebbal, H., Chafouk, H., Hoblos, G. and Lefebvre, D. Modeling and identification of non linear throttle system using piecewise ARX models. In: *Congrés Mondial IMACS'2005*, Paris, 2005.

[3] Conaster, R., Wagner, J., Ganta, S. and Walker, I. Diagnosis of automotive electronic throttle control systems. *Engeneering Pratice* **12** (2004) 23–30.

[4] Benrejeb, M. Gasmi, M. and Borne, P. New Stability Conditions for TS Fuzzy Continuous Nonlinear Models. *Nonlinear Dynamics and Systems Theory* **5** (4) (2004) 369–380.

[5] Fliess, M., Levine, J., Martin, P. and Rouchon, P. A Lie Bäcklund approach to equivalence and flatness of nonlinear systems. *IEEE Trans. on Automatic Control* **44** (5) (1999) 922–937.

[6] Levine, J., Lottin, J. and Ponsart, J.Ch. A nonlinear approach to the control of magnetic bearings. *IEEE Trans. on Control Systems Technology* **4** (5) (1996) 524–544.

[7] Martin, P. and Rouchon, P. Systèmes plats: Planification et suivi de trajectoires. *www.math.polytechnique.fr/xups*, Vol. 99.

[8] Fliess, M., Levine, J., Martin, P. and Rouchon, P. Sur les systèmes non linéaires diffrenciellement plats. *Compte Rendu de l'Académie des Sciences de Paris*, Série I, 315 (1992 b) 619–624.

[9] Rotella, F. and Zambettakis, I. Commande des systèmes par platitude. *Techniques de l'Ingénieur* S7 450 (2007) 1–18.

[10] Monirul, M.I. and Murase, K. A new algorithm to design compact two-hidden-Layer artificial neural networks. *Pergamon* **14** (2001) 1265–1278.

[11] Naghavi, S.V. and Safavi, A.A. A Neural Network Observer-Based Approach for Synchronization of Discrete-Time Chaotic Systems. In: *The Intern. Federation of Automatic Control*, pp. 355–3520, 2008.

[12] Zhu, R., Chai, T. and Shao, C. Robust Nonlinear Adaptive Observer Design Using Dynamic Recurrent Neural Networks. In: *Proc. Amer. Cont. Conf.*, pp. 1096–1100, New Mexico, 1997.

[13] Borne,P., Benrejeb, M. et Haggège, J. *Les réseaux de neurones. Présentation et applications.* Editions Technip, Paris, 2007.

[14] Elfelly, N., Dieulot, J. Y. and Borne, P. A Neural Approach of Multimodel Representation of Complex Processes. *Intern. J. of Computers Communications and Control* **3** (2) (2008) 149–160.

[15] Benrejeb, M., Naceur, M. and Soudani, D. On an internal model controller based on the use of specific inverse model. *ACIDCA*, pp. 623–626, Tozeur, 2005.

[16] Aloui, R. and Braiek, N. B. Optimal State Observer Design for Nonlinear Dynamical Systems. *Nonlinear Dynamics and Systems Theory* **12** (1) (2012) 37–48.

[17] Yang, C. Model-based analysis and tuning of electronic throttle controllers. *Visteon corporation*, SAE paper, 2004.

Nonlinear Dynamics and Systems Theory, **12** (4) (2012) 345–364

# Stabilisation of a Class of Underactuated System with Tree Structure Using Backstepping Approach

A. Choukchou-Braham [1], B. Cherki [1] and M. Djemaï [2*]

[1] *Département d'Automatique, Université de Tlemcen, Algérie*
[2] *Univ. Lille Nord de France, F-59000 Lille, France,*
*UVHC, LAMIH, F-59313 Valenciennes, France,*
*CNRS, UMR 8201, F-59313 Valenciennes, France.*

Received: November 17, 2011; Revised: October 7, 2012

**Abstract:** In this paper, a method for transforming the structure of a class of underactuated mechanical system from tree to chain structure through a change of coordinates and control law is proposed. The main goal of this transformation is to allow apply control design methodologies suited to the chain structure, namely, the feedback linearization and backstepping. The effectiveness of the proposed transformation is shown via an example of underactuated system that initially possesses a tree structure and to which backstepping control was applied. However, the designed control law presents a singularity that decreases the stability domain. In order to make the latter global, a hybrid control strategy is adopted allowing to switch the control near the singularities. The stability proof and simulation results for using the hybrid switching are given.

**Keywords:** *underactuated mechanical system; CFD; tree structure; chain structure; systematic backstepping; Tora system; singularity; switching control.*

**Mathematics Subject Classification (2010):** 93C10, 93D15.

* Corresponding author: mailto:mohamed.djemai@univ-valenciennes.fr

## 1 Introduction

Recently, there has been renewed and extensive research interest in the control of underactuated mechanical systems due to their broad applications and due to the large number of open theoretical problems they present. Many real-life control mechanical systems including aircrafts, helicopters, spacecrafts, underwater vehicles, mobile robots, walking robots and flexible systems are examples of underactuated systems. Underactuated systems are systems that have fewer actuators than configuration variables. This limitation in actuators makes the control design for these systems rather complicated.

As a result, an underactuated system presents challenges which are not found in a system with full control. For instance, controllability, at least locally, is not easy to determine. Most underactuated systems are not fully feedback linearizable, and smooth feedback stabilization to a single equilibrium point is not possible [10]. Furthermore, there is no general theory that allows the systematic analysis and control design for all underactuated systems so that, most of time these systems have to be dealt with on a case by case basis [15]. Consequently, different control strategies have been proposed in the literature, among them there is the backstepping and forwarding control in [31], [14], energy and passivity based control in [12], [17], sliding mode control [5], [9] and observation [23], hybrid and switched control in [28], [41], intelligent and fuzzy control in [38], [22] just to mention a few.

In [31], underactuated systems are classified into three types according to their control flow diagram (CFD) which reflects the way generalized forces are transmitted through components, namely, the chain, tree and isolated point structures. Additionally, the author proposes a control design strategy for systems with chain structure. However, the control design issue for other structures is still an open problem.

In this paper, based on the observation that the CFD of a given system is not invariant under change of coordinate, we will show that a subclass of tree structure can be transformed in a chain structure so that the strategy of control for chain structure can be applied. However, as a result of this transformation, one assumption that was laid in the control scheme is satisfied only on a certain domain rather than on the whole space. As a consequence, a singularity in the control law appears which limits the bassin of attraction. To make this stability global, we propose a hybrid control allowing to switch through these singularities.

Others strategies and viewpoints for dealing with singularities involve the use of nilpotent approximations like in [36] and [26].

The outline of the paper is as follows. In Section 2, a standard model for underactuated systems is presented. Next, in Section 3, definitions of the CFD, the chain and the tree structure are given. In Section 4, the main result on the transformation of the structure of an underactuated system from tree to chain is presented. In Section 5, the proposed design procedure is applied to stabilize the so-called Tora system. Finally, the hybrid control that permits to switch near the singularities is presented.

## 2 Dynamics of Underactuated Systems

It is well-known that classical Lagrangian mechanics provides dynamical model of underactuated systems. In this paper, we consider mechanical systems with configuration vector $q \in Q$, which is an n-dimensional manifold, and with a Lagrangian:

$$\mathcal{L} = K - V = \frac{1}{2}\dot{q}^T M(q)\dot{q} - V(q), \tag{1}$$

where K is the kinetic energy, V(q) is the potential energy and $M(q)$ is the inertia matrix of the system which is symmetric and positive definite.

The Euler-Lagrange equation of motion is given by:

$$M(q)\ddot{q} + H(q, \dot{q}) = F(q)u, \tag{2}$$

where $H(q, \dot{q})$ contains Coriolis, centrifugal and gravity terms and $F(q)$ is identity matrix. Suppose that $q = col(q_1, q_2) \in Q_1 \times Q_2$ where the dimension of the manifold $Q_i$ is denoted by $n_i = dim(Q_i)$ for $i = 1, 2$ and $n_1 + n_2 = n$; then, the system (2) can be written as:

$$\begin{aligned} m_{11}(q)\ddot{q}_1 + m_{12}(q)\ddot{q}_2 + h_1(q, \dot{q}) = \tau_1, \\ m_{21}(q)\ddot{q}_1 + m_{22}(q)\ddot{q}_2 + h_2(q, \dot{q}) = \tau_2. \end{aligned} \tag{3}$$

The $\tau_i$'s are the control inputs satisfying the conditions of either one of the following actuation modes:

A1) $\tau = \tau_2 \in \Re^{n_2}$ is the control input and $\tau_1 \equiv 0$;

A2) $\tau = \tau_1 \in \Re^{n_1}$ is the control input and $\tau_2 \equiv 0$.

In both of the above cases, system (3) is an underactuated system. The actuation modes A1 and A2 are important due to their applications in robotics. The Acrobot [33], the Tora system [39] are actuated according to mode A1, while the Pendubot [34] and, the cart-pole system [25] are actuated according to mode A2.

## 3 Control Flow Diagram

In [31] a Control Flow Diagram (CFD) is constructed for each mechanism to represent the interaction forces among the degrees of freedom. Each CFD will be comprised of three possible sructutres: chain (Figure 1(a)), tree (Figure 1(b)) or isolated point (Figure 1(c)).

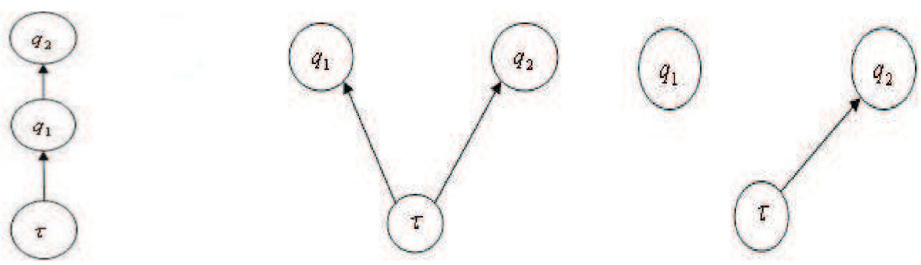


$(a)$ $(b)$ $(c)$

**Figure 1**: CFD structures for an underactuated system with 2 degrees of freedom.

In terms of these structures a precise definition of the degree of complexity is given. It was shown that the chain structure is the least complex, where both, feedback linearization technique [20] and backstepping strategy [29] can be applied. A system with tree structure is more difficult to control since we need to control certain configuration variables in parallel; that is, one control input must control more than one degree of freedom simultaneously. For systems with isolated points, certain control goal are difficult to

achieve because the control input have no influence on some variables at certain states. Control design for the last two classes is currently under investigation.
From the above discussions, it is clear that if we can transform the tree structure (or at least a subclass of tree structure) to a chain structure, then we will considerably simplify the control design for this class of systems.

## 4 Systems with Chain Structure

The configuration variables in a chain structure affect each other in a serial way. The most general representation of this serial connection is a triangular form given by Seto and Baillieul in [31]:

$$\begin{array}{rcl} \ddot{q}_i & = & N_i(q_1, \cdots, q_{i+1}, \dot{q}_1, \cdots, \dot{q}_{i+1}), \quad i = 1, \cdots, n-1, \\ \ddot{q}_n & = & N_n(q, \dot{q}) + G(q, \dot{q})u, \end{array} \tag{4}$$

where $G(q, \dot{q}) \neq 0$, $N_i(.)i = 1, \cdots, n-1$ are smooths functions and either $\frac{\partial N_i}{\partial \dot{q}_{i+1}} \neq 0$ or $\frac{\partial N_i}{\partial \dot{q}_{i+1}} = 0$ but $\frac{\partial N_i}{\partial q_{i+1}} \neq 0 \quad \forall (q, \dot{q}) \in \Re^{2n}$.

The former condition ensures the conrollability of the system while the latter one ensures the connection between the degrees of freedom.

Note that the chain structure proposed here is different from the chained form systems studied in [1], generally represented by the following configuration:

$$\begin{array}{rcl} \ddot{\xi}_1 & = & u_1, \\ \ddot{\xi}_2 & = & u_2, \\ \ddot{\xi}_3 & = & \xi_2 u_1. \end{array} \tag{5}$$

In [31], Seto and Baillieul propose a systematic backstepping control strategy which globally asymptotically stabilize systems in chain structure (4). However, few underatuated systems are naturally in this form, the only examples we found are the mass sliding on a cart system [31] and the robot with joint elasticity [7]. Most of the underatuated systems are either in tree structure as the Acrobot, the Tora system, the Inverted pendulum, or in isolated point as the Ball and Beam system [16], as far as simple systems with two degrees of freedom are considered. As there is no systematic procedure for dealing with tree structure and isolated point, such structures are generally studied on a case by case basis.

In the next section, we propose to transform a subclass with tree structure into a chain structure so that the well established backstepping design procedure associated with chain structure can be applied.

## 5 Transformation from Tree Structure to Chain Structure

The construction of CFD for a given system depends on its coordinates, specially on the choice of generalized coordinates and the external forces. Thus, the CFD is not invariant under coordinate transformation. This simple observation leads us to search for a change of coordinates in order to transform the CFD. Thus, we consider underactuated systems satisfying the following assumptions:

**Assumptions 1**

*B1)* $q_2$ *is the actuated variable (case A1).*

*B2) the considered system possesses a kinetic symmetry property, that is the inertia matrix depends only on the variable* $q_2$ *so that* $M(q) = M(q_2)$.

*B3) the quantity* $m_{11}^{-1}(q_2)m_{12}(q_2)$ *is integrable.*

It is important to note that these assumptions are satisfied by a broad class of underactuated systems. Our main result is presented in the next theorem.

**Theorem 5.1** *Assumming that Assumptions B1)-B3) hold, then an underactuated system with tree structure can be transformed in a system with chain structure.*

***Proof.*** The proof can be broken down in two parts: first, we will show how an underactuated system can be partially linearized. Next, we will show how the linearized system can be expressed under a chain form.

In [32], Spong shows that all underatuated systems can be partially linearized using the following change of control law:

$$\tau = \alpha(q)u + \beta(q, \dot{q}) \tag{6}$$

which transforms the dynamics of (3) into

$$\begin{aligned} \dot{q}_1 &= p_1, \\ \dot{p}_1 &= f(q,p) + g_0(q)u, \\ \dot{q}_2 &= p_2, \\ \dot{p}_2 &= u, \end{aligned} \tag{7}$$

where $\alpha(q)$ is an $m \times m$ positive definite symmetric matrix and

$$g_0(q) = -m_{11}^{-1}(q)m_{12}(q).$$

In fact, from the first line of (3), for $\tau_1 = 0$ we have

$$\ddot{q}_1 = -m_{11}^{-1}(q)h_1(q,\dot{q}) - m_{11}^{-1}(q)m_{12}\ddot{q}_2$$

which yields the expression for $g_0(q)$. Substituting this in the second line of (3), we get

$$(m_{22}(q) - m_{21}(q)m_{11}^{-1}(q)m_{12}(q))\ddot{q}_2 + h_2(q,\dot{q}) - m_{21}(q)m_{11}^{-1}(q)h_1(q,\dot{q}) = \tau$$

thus, defining

$$\begin{aligned} \alpha(q) &= m_{22}(q) - m_{21}(q)m_{11}^{-1}(q)m_{12}(q), \\ \beta(q,\dot{q}) &= h_2(q,\dot{q}) - m_{21}(q)m_{11}^{-1}(q)h_1(q,\dot{q}), \end{aligned}$$

and observing that $\alpha(q)$ is positive definite and symmetric complete the first part of the proof.

However, after applying this change of control law, the new control input $u$ appears both in linear and nonlinear subsystems. This means that (7) has a tree structure. The idea is to decouple the linear and nonlinear subsystems so that the system (7) will be in a triangular form.

According to [25], an underactuated system which satisfies the preceding assumptions can be transformed in a strict feedback normal form. In fact, the following change of coordinates:

$$\begin{aligned} q_r &= q_1 + \gamma(q_2), \\ p_r &= m_{11}(q_2)p_1 + m_{12}(q_2)p_2 := \frac{\partial \mathcal{L}}{\partial \dot{q}_1}, \end{aligned} \tag{8}$$

transforms the dynamics of the system (7) into a cascade nonlinear system in strict feedback form:

$$\begin{aligned} \dot{q}_r &= m_{11}^{-1}(q_2)p_r, \\ \dot{p}_r &= g(q_r, q_2), \\ \dot{q}_2 &= p_2, \\ \dot{p}_2 &= u, \end{aligned} \tag{9}$$

where

$$\gamma(q_2) = \int_0^{q_2} m_{11}^{-1}(\theta)m_{12}(\theta)\,d\theta, \quad g(q_r, q_2) = -\frac{\partial V(q)}{\partial q_1}.$$

The so obtained system is also in a triangular form. More precisely, in a chain structure, since the control appears in the last equation and each variable affects the other in a serial way. Hence, the tree structure is transformed in a chain structure.

**Remark 5.1** For case A2 (i.e. $q_2$ is not actuated) there is an other change of coordinates to transform the initial system but the obtained normal form is not in strict feedback form. It means that some tree structure could not be transformed in chain structure as the cart pole system, the pendubot, the rotating pendulum and others.

In the next section, we will illustrate this procedure design by an example.

## 6 Application

The problem of controlling the Tora (Translational oscillator with rotational actuator) system was introduced first by Wan, Brenstein and Coppola at the University of Michigan [39] and has attracted much attention of control theorists recently; since it exhibits nonlinear interaction between the translational and rotational motions. As a result, it has been extensively used as a benchmark for nonlinear controllers for cascade systems; namely for passivity based approaches [19], integrator backstepping procedure [39], sliding mode and robust controllers [24], dynamic surface control [27], Tensor product distributed compensation and linear matrix inequality based controller [3], speed gradient [13] and even fuzzy controller with [18]. In the best of our knowledge, this work is the first one where a switched control is applied to the Tora system. As a matter of fact, this constitutes the second contribution of the present paper.

The Tora system, depicted in Figure 2, consists of a platform that can oscillate without damping in the horizontal plane. On the platform a rotating eccentric mass is actuated by a DC motor whose motion applies a force to the platform which can be used to damp the translational oscillations. Assuming that the motor torque is the control variable, our task is to find a control law that stabilizes both rotation and translation to the rest. This implies the Tora is an underactuated mechanical system.

Note that this system possesses 2 degrees of freedom $(q_1, q_2)$ where $q_1$ is the unactuated variable and $q_2$ is the actuated one. The Euler-Lagrange equation of motion for the

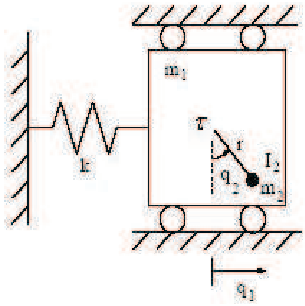


**Figure 2**: The Tora system.

Tora system is given by:

$$\begin{aligned} (m_1+m_2)\ddot{q}_1 + m_2 r\cos(q_2)\ddot{q}_2 - m_2 r\sin(q_2)\dot{q}_2^2 + kq_1 &= 0, \\ m_2 r\cos(q_2)\ddot{q}_1 + (m_2 r^2 + I_2)\ddot{q}_2 + m_2 g r\sin(q_2) &= \tau, \end{aligned} \tag{10}$$

where $m_1$ is the mass of the cart, $m_2$ is the mass of the eccentric mass, $r$ is the radius of the rotation, $k$ is the spring constant, $g$ is the gravity acceleration and $\tau$ is the torque input.

The system (10) can be rewritten as:

$$\begin{aligned} \ddot{q}_1 &= \frac{1}{detM(q_2)}(-m_2 r\cos(q_2)\tau + g m_2^2 r_2^2 \cos(q_2)\sin(q_2) \\ &\quad -(m_2 r^2 + I_2)(kq_1 - m_2 r\sin(q_2)\dot{q}_2^2)), \\ \ddot{q}_2 &= \frac{1}{detM(q_2)}((m_1+m_2)\tau - (m_1+m_2)m_2 g r\sin(q_2) \\ &\quad + m_2 r\cos(q_2)(kq_1 - m_2 r\sin(q_2)\dot{q}_2^2)), \end{aligned} \tag{11}$$

with $detM(q_2) = (m_1+m_2)(m_2 r^2 + I_2) - (m_2 r\cos(q_2))^2$.

The associated CFD to (11) is given by Figure 3 which is in tree structure. After a partial linearization using change of control input:

$$\tau = \alpha(q)u + \beta(q,\dot{q}) \tag{12}$$

with

$$\begin{aligned} \alpha(q_2) &= (m_2 r^2 + I_2) - \frac{(m_2 r\cos(q_2))^2}{m_1+m_2} \quad \forall q_2 \in [-\pi,\pi], \\ \beta(q,\dot{q}) &= m_2 g r\sin(q_2) - \frac{m_2 r\cos(q_2)}{m_1+m_2}(kq_1 - m_2 r\sin(q_2)\dot{q}_2^2). \end{aligned}$$

The dynamics of the Tora becomes

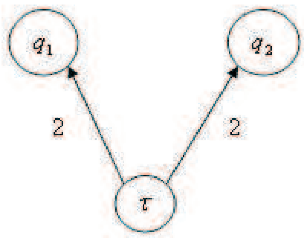


**Figure 3**: Tora system CFD.

$$\begin{aligned} \dot{q}_1 &= p_1, \\ \dot{p}_1 &= f_0(q,p) + g_0(q)u, \\ \dot{q}_2 &= p_2, \\ \dot{p}_2 &= u, \end{aligned} \tag{13}$$

with

$$f_0(q,p) = \frac{(m_2 r \sin(q_2))p_2 - kq_1}{m_1 + m_2}, \quad g_0 = \frac{m_2 r \cos(q_2)}{m_1 + m_2}.$$

Note that $M(q) = M(q_2)$, that the Tora system is actuated according to mode A1 and the function $\gamma(q_2)$ can be calculated explicitly as

$$\gamma(q_2) = \int_0^{q_2} \frac{m_2 r \cos(\theta)}{m_1 + m_2} d\theta = \frac{m_2 r \sin(q_2)}{m_1 + m_2}$$

so all the assumptions B1-B3 are verified. Thus, the global change of coordinates:

$$\begin{aligned} q_r &= q_1 + \frac{m_2 r \sin(q_2)}{m_1 + m_2}, \\ p_r &= (m_1 + m_2)p_1 + m_2 r \cos(q_2) p_2, \end{aligned} \tag{14}$$

transforms the dynamics of the Tora system into cascade nonlinear system in strict feedback form:

$$\begin{aligned} \dot{q}_r &= \frac{1}{(m_1 + m_2)} p_r, \\ \dot{p}_r &= -kq_r + k\gamma(q_2), \\ \dot{q}_2 &= p_2, \\ \dot{p}_2 &= u. \end{aligned} \tag{15}$$

The system (15) can be written as:

$$\begin{aligned} \ddot{q}_r &= -\frac{k}{m_1 + m_2} q_r + \frac{k m_2 r}{(m_1 + m_2)^2} \sin(q_2), \\ \ddot{q}_2 &= u, \end{aligned} \tag{16}$$

which is in the form of a chain structure. The associated CFD to (16) is given by Figure 4 Hence, the change of control (12) and the coordinates transformation (14) transform

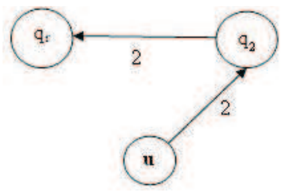


**Figure 4**: CFD of the transformed Tora system.

the tree structure of the Tora system into a chain structure.

Next, as the Tora is now expressed as a chain structure, we can then apply the procedure proposed by Seto and Baillieul in [31], to design the control law that globally asymptotically stabilizes the system. In order to apply this procedure, one must first verify the following assumptions:

**Assumptions 2**

*C1)* $N_i(0) = 0, i = 1, \cdots, n.$

*C2)* *For each* $i = 1, \cdots, n-1, N_i(.)$ *are smooth functions with bounded states* $q_1, \cdots, q_i, \dot{q}_1, \cdots, \dot{q}_i$, *the boundedness of the function* $N_i$ *implies the boundedness of the states* $q_{i+1}$ *and* $\dot{q}_{i+1}$.

*C3)* *Either* $\frac{\partial N_i}{\partial \dot{q}_{i+1}} \neq 0$ *or* $\frac{\partial N_i}{\partial \dot{q}_{i+1}} = 0$ *but* $\frac{\partial N_i}{\partial q_{i+1}} \neq 0 \quad \forall (q, \dot{q}) \in \Re^{2n}$.

*C4)* *For any* $\frac{\partial N_i}{\partial \dot{q}_{i+1}} \neq 0$ *, the nonlinear system* $N_i(0, \cdots, 0, q_{i+1}, 0, \cdots, 0, \dot{q}_{i+1}) = 0$ *is globally asmptotically stable at the origin, or when* $\frac{\partial N_i}{\partial \dot{q}_{i+1}} = 0$ *but* $\frac{\partial N_i}{\partial q_{i+1}} \neq 0$, *the nonlinear system* $N_i(0, \cdots, 0, q_{i+1}, 0, \cdots, 0) = 0$ *is globally asmptotically stable at the origin.*

Assumption C1 is a necessary condition for the origin to be an equilibrium point of the closed loop system. C2 is necessary to avoid the peaking phenomenon, C3 ensures the connection between degrees of freedom of the system and C4 is equivalent to the condition on the global asymptotic stability of the zero dynamics.

Then, the procedure is defined as follows. Let $\bar{q}_1 = [q_1, \dot{q}_1]^T$, $b = [0, 1]^T$, $P$ is a positive definite matrix with all elements being positive and $N_i$, $N_n$ and $G$ are variables defined in (4). The sequences $e_i$, $G_i$ and $W_i$ are defined as:

$$e_1 = \bar{q}_1^T P b, \qquad G_1 = 1, \qquad W_1 = 0,$$

for $i = 1, \cdots, n-1$,

$$\left.\begin{array}{l} e_{i+1} = G_i N_i + W_i + k_i e_i, \\ G_{i+1} = \frac{\partial N_i}{\partial \dot{q}_{i+1}} G_i, \\ W_{i+1} = \sum_{j=1}^{i+1} \frac{\partial e_{i+1}}{\partial q_j} \dot{q}_j + \sum_{j=1}^{i} \frac{\partial e_{i+1}}{\partial \dot{q}_j} N_j + e_i, \end{array}\right\} if \frac{\partial N_i}{\partial \dot{q}_{i+1}} \neq 0; \tag{17}$$

$$\left.\begin{array}{l} e_{i+1} = G_{i+1}\dot{q}_{i+1} + W_{(i+1)1} + k_{(i+1)1}e_{(i+1)1}, \\ e_{(i+1)1} = G_i N_i + W_i + k_i e_i, \\ G_{i+1} = \frac{\partial N_i}{\partial q_{i+1}} G_i, \\ W_{i+1} = \sum_{j=1}^{i+1} \frac{\partial e_{i+1}}{\partial q_j}\dot{q}_j + \sum_{j=1}^{i} \frac{\partial e_{i+1}}{\partial \dot{q}_j} N_j + e_{(i+1)1}, \\ W_{(i+1)1} = \sum_{j=1}^{i} (\frac{\partial e_{(i+1)1}}{\partial q_j}\dot{q}_j + \frac{\partial e_{(i+1)1}}{\partial \dot{q}_j} N_j) + e_i, \end{array}\right\} if \frac{\partial N_i}{\partial \dot{q}_{i+1}} = 0;$$

and $k_{(i+1)1}$, $k_i$, $i = 1, \cdots n-1$, $k_n$ are positive constants.

The control law is chosen according to the following theorem.

**Theorem 6.1** *[31] Under assumptions C1-C4, the system (4) is globally asymptotically stable at the origin if the control law is chosen as*

$$u = -(G_n N_n + w_n + k_n e_n)(G_n G)^{-1}. \tag{18}$$

The application of the above control scheme to the Tora system leads to the following control law:

$$u_{nL} = -\frac{(m_1+m_2)^2}{k\cos(q_2)}(c_1\dot{q}_r + \frac{k}{(m_1+m_2)^2}\dot{q}_2(c_2\cos(q_2) - \dot{q}_2) + c_3 q_r + c_4\sin(q_2)), \tag{19}$$

where $c_1, c_2, c_3, c_4$ are positive constants. Clearly the obtained control law is simple and easy to implement. In addition, the rate of convergence can be controlled by adjusting the gain constants $c_i$.

Nevertheless, this control is valid for any $q_2 \neq (2k+1)\pi/2$. This is a consequence of the fact that assumption C3, is not always verified $\forall (q, \dot{q}) \in \Re^{2n}$, since for the Tora system $\frac{\partial N_i}{\partial q_{i+1}} \neq 0$ only for $q_2 \neq (2k+1)\pi/2$.

This means that the control has singularities that make the bassin of attraction not the entire space and hence the stability is not global.

One solution to avoid divergence of the states is to adjust the gains such that the trajectories are kept near the equilibrium. However, keeping trajectories near the equilibrium will imply little effort but will induce large settling time. Moreover, if the initial conditions of $q_2$ are chosen greater or equal to $\pi/2$, the states and the control will diverge due to the singularity; therefore, this solution must be discarded.

In the next section, we present a solution to make the asymptotic stability global; i.e. a control system that is valid for any initial conditions.

## 7 Switching Through Singularities

The idea is to use a hybrid control law which switches between the designed control law (19) away from singularities and another control law that will be designed close the singularities. Control techniques based on switching between different controllers have been applied extensively in recent years [35, 40, 41]. The importance of such control stems from the existence of systems that cannot be asymptotically stabilized by a single continuous feedback control law.

Now, we must design the second control law and the procedure we used is very simple. The idea is to use the Jacobian linearized system around the singularity point to calculate a linear control law that will be applied near singularities. Once the trajectories go through the neighborhood of singularities, we come back to the nonlinear control law to achieve global asymptotic stabilization of all the states.

### 7.1 Expression of the linear control law

The linearized model of the Tora system around $(q_r, p_r, q_2, p_2) = (0, 0, \pi/2, 0)$ is given by:

$$\begin{aligned} \dot{\delta q_r} &= \frac{1}{(m_1 + m_2)}\delta p_r, \\ \dot{\delta p_r} &= -k\delta q_r, \\ \dot{\delta q_2} &= \delta p_2, \\ \dot{\delta p_2} &= \delta u. \end{aligned} \tag{20}$$

The new problem that appears now is that the subsystem $(\delta q_r, \delta p_r)$ is not controllable; fortunately, it is stable. Due to Borckett in [4], if the uncontrollable modes are stable, the whole system can still be stabilized.

The linear control law is given by:

$$u_L = -Kx, \tag{21}$$

where $x = [\delta q_2, \delta p_2]^T$ and $K = [K_1 \quad K_2]$ is a matrix gain fixed either by LQR or by pole placement approaches.

**Remark 7.1** Note that, even the uncontrolled modes of the linearized system around the singularity point are stable, it does not mean that the whole system is stable. Indeed, if any control is applied to the Tora system, all trajectories will go to infinity since $\frac{1}{cosq_2}$ becomes very large.

The application in simulation of this switched control to the Tora system with the parameters $m_1 = 10kg, m_2 = 1kg, k = 5N/m, r = 1m, I = 1kg/m$, shows the effectiveness of the proposed procedure, see Figure 5. In fact, even for hard initial conditions like the singularity point $q_2 = \pi/2$ (Figure 6) or a far initial point $q_2 = \pi$ (Figure 7), the proposed control law still stabilizes the system. The switch from one control to the other is orchestrated by the state $q_2$, so that, while $|q_2|$ is out of the interval $\frac{\pi}{2} \pm e$, the nonlinear control $u_{nL}$ is applied and when $|q_2|$ goes through this interval, we switch to the linear control $u_L$ )Figure 8). The size of this interval is directly related to the control effort. In fact, we have noted that small value of $e$ (around 0.2 or 0.3) (Figure 9) leads to more important effort than larger value of $e$ (like 0.5 or 0.6) (Figure 5). This is due to the fact that with a large interval, we do not allow $cos(q_2)$ to become too small in order to avoid great value for $u_{nl}$.

### 7.2 Stability proof of the hybrid control

Mathematically, a switched system can be described by a differential equation of the form:

$$\dot{x} = f_p(x), \qquad p \in \mathcal{P}, \tag{22}$$

where $\mathcal{P}$ is an index set and let $\sigma(t) = p = \{1, 2\}$ be a switching signal. We are assuming here that the individual subsystems have the origin as a common equilibrium point $f_p(0) = 0$.

**Remark 7.2** A necessary condition for asymptotic stability under arbitrary switching is that all of the individual subsystems are asymptotically stable. However, this condition is not sufficient [21]. Nevertheless, if switching among asymptotically stable subsystems is slow enough, one would intuitively expect a stable response.

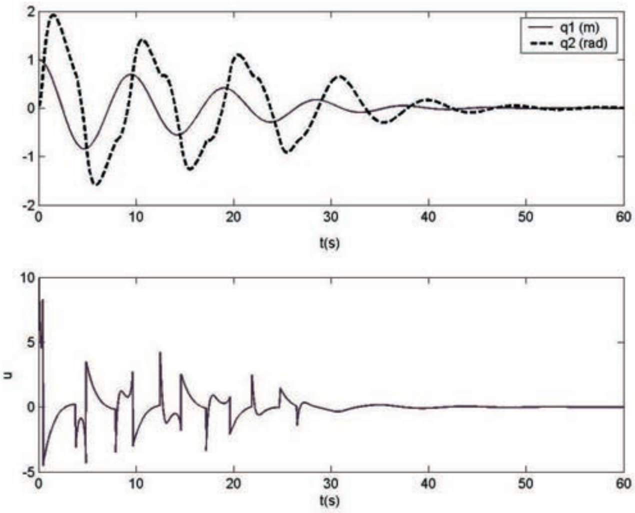


**Figure 5**: States trajectories and control input of the Tora system for the initial condition $(q_1, q_2, p_1, p_2) = (1, 0, 0, 0)$.

It is easy to see that if the family of systems (22) has a common Lyapunov function $V$ such that $\nabla V(x) f_p(x) < 0$ for all $x \neq 0$ and all $p \in \mathcal{P}$, then the switched system is asymptotically stable for any switched signal $\sigma$ [21]. Hence, one possible approach to prove the stability of the hybrid system is to find a common Lyapunov function for the family (22). If we can not find such function, one tool for proving stability in such cases employs multiple Lyapunov functions (see [2], [8] and the references therein). Since the individual subsystems in the family (22) are assumed to be asymptotically stable, there is a family of Lyapunov functions $[V_p : p \in \mathcal{P}]$ such that the value of $V_p$ decreases on each interval where the $p-th$ subsystem is active. Then, the switched system is globally asymptotically stable if for every $p$ the value of $V_p$ at the end of each such interval exceeds the value at the end of the next interval on which the $p-th$ subsystem term is active [21]

For the Tora system, these functions are given by:

$V_{nL} = \frac{1}{2}\bar{q}_1^T P \bar{q}_1 + \frac{1}{2}e_{21}^2 + \frac{1}{2}e_2^2$ for the nonlinear subsystem,

$V_L = \frac{1}{2}\tilde{x}^T R \tilde{x}$ for the linearized subsystem,

where $\bar{q}_1$, $P$, $e_{21}$ and $e_2$ are variables defined in the sequences of the control scheme (17), $\tilde{x} = (\delta q_r, \delta p_r, \delta q_2, \delta p_2)$ is the vector of coordinates of the linearized system and $R$ is a symmetric positive definite matrix.

In a previous work [6], we give the proof that $V_{nL}$ is a Lyapunov function for the nonlinear subsystem under $u_{nL}$ control. We first recall briefly this proof and then give the one related to the linearized subsystem under $u_L$ control.

In [31], the authors did not give the proof of Theorem 6.1 and refer the reader to the proof given for the adaptive case for system with parametric uncertainties in [30]. Moreover, the proof there is given only for the control derived from the first sequences in (17). We propose to give the proof of Theorem 6.1 for system with no parametric uncertainties and for the case when the control is derived from the second sequences in

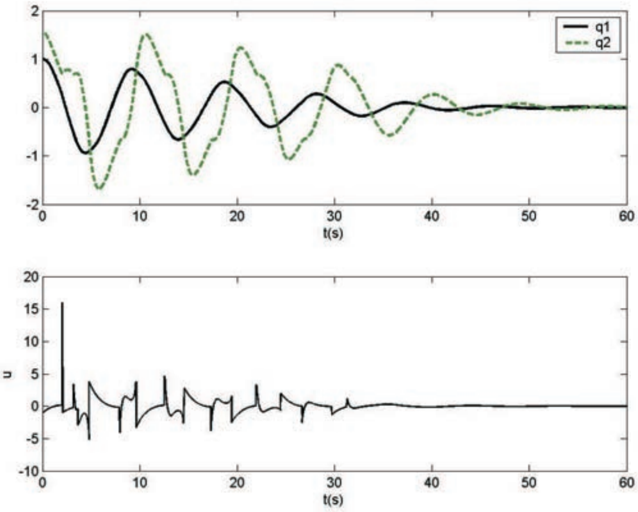


**Figure 6**: States trajectories and control input of the Tora system for the initial condition $(q_1, q_2, p_1, p_2) = (1, \frac{\pi}{2}, 0, 0)$.

(17) since for the Tora system $\frac{\partial N_i}{\partial \dot{q}_{i+1}} = 0$ but $\frac{\partial N_i}{\partial q_{i+1}} \neq 0$.

***Proof.*** As the Tora system possesses two degrees of freedom, we limit the proof to the case $n = 2$. For each degree of freedom $q_i$, $q_{i+1}$ can be considered as a "control variable" which governs the behavior of $q_i$. Hence, we determine a reference position $q_{r2}$ for $q_2$ such that when $q_2 \to q_{r2}$, $q_1$ will behave as desired.

Step 1 $i = 1$.

When $\frac{\partial N_1}{\partial \dot{q}_2} = 0$ and $\frac{\partial N_1}{\partial q_2} \neq 0$, we obtain the differential equation

$$\ddot{q}_1 = N_1(q_1, q_2, \dot{q}_1) \tag{23}$$

and define a reference position $q_{r2}$ as $q_{r2} = q_2 - N_1 - k_1 q_1 - k_2 \dot{q}_1$. The error between the reference and the actual position is given by

$e_{21} = q_2 - q_{r2} = N_1 + k_1 q_1 + k_2 \dot{q}_1 \Rightarrow N_1 = e_{21} - k_1 q_1 - k_2 \dot{q}_1$. Define

$$\bar{q}_1 = \begin{pmatrix} q_1 \\ q_2 \end{pmatrix}, A = \begin{pmatrix} 0 & 1 \\ -k_1 & -k_2 \end{pmatrix}, b = \begin{pmatrix} 0 \\ 1 \end{pmatrix},$$

where $k_1$ and $k_2$ are chosen such that $\ddot{q}_1 + k_2 \dot{q}_1 + k_1 q_1 = 0$ is asymptotically stable at $(q_1, \dot{q}_1) = (0, 0)$. This implies the existence of a positive definite matrix $P$ such that $A^T P + PA = -Q < 0$. Applying the above definitions to (23), we get

$$\dot{\bar{q}}_1 = A\bar{q}_1 + be_{21}.$$

Consider the following Lyapunov function

$$V_{11} = \frac{1}{2}(\bar{q}_1^T P \bar{q}_1 + e_{21}^2) \tag{24}$$

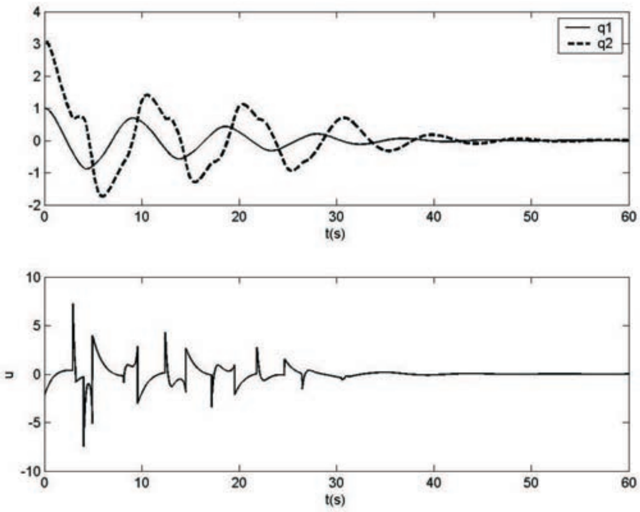


**Figure 7**: States trajectories and control input of the Tora system for the initial condition $(q_1, q_2, p_1, p_2) = (1, \pi, 0, 0)$.

The time derivative $\dot{V}$ is given by

$$\dot{V}_{11} = -\frac{1}{2}\bar{q}_1^T Q \bar{q}_1 + \bar{q}_1^T P b e_{21} + e_{21}\dot{e_{21}},$$

if $e_1 = \bar{q}_1^T P b$ and $\nu_{11} = \frac{1}{2}\bar{q}_1^T Q \bar{q}_1$, then

$$\begin{aligned}
\dot{V}_{11} &= -\nu_{11} + e_{21}(\dot{e}_{21} + e_1) \\
&= -\nu_{11} + e_{21}(\dot{N}_1 + k_1\dot{q}_1 + k_2\ddot{q}_1 + e_1) \\
&= -\nu_{11} + e_{21}(\frac{\partial N_1}{\partial q_1}\dot{q}_1 + \frac{\partial N_1}{\partial q_2}\dot{q}_2 + \frac{\partial N_1}{\partial \dot{q}_1}\ddot{q}_1 + \frac{\partial N_1}{\partial \dot{q}_2}\ddot{q}_2 \\
&\quad + k_1\dot{q}_1 + k_2\ddot{q}_1 + e_1) \\
&= -\nu_{11} + e_{21}((\frac{\partial N_1}{\partial q_1} - k_1)\dot{q}_1 + \frac{\partial e_{21}}{\partial q_2}\dot{q}_2 + (\frac{\partial e_{21}}{\partial \dot{q}_1} - k_2)\ddot{q}_1 \\
&\quad + k_1\dot{q}_1 + k_2\ddot{q}_1 + e_1) \\
&= -\nu_{11} + e_{21}(\underbrace{\frac{\partial N_1}{\partial q_2}}_{\stackrel{def}{=} G_2}\dot{q}_2 + \underbrace{\frac{\partial e_{21}}{\partial q_1}\dot{q}_1 + \frac{\partial e_{12}}{\partial \dot{q}_1}N_1 + e_1)}_{\stackrel{def}{=} W_{21}} \\
&= -\nu_{11} + e_{21}(G_2\dot{q}_2 + W_{21}).
\end{aligned}$$

Note that, we cannot reach $u$ through $\dot{q}_2$ but rather through $\ddot{q}_2$. Hence, we add a step where we determine a reference velocity $\dot{q}_{r2}$ for $\dot{q}_2$ such that $e_{21}(G_2\dot{q}_2 + W_{21})$ is made nonpositive $\dot{q}_{r2} = \dot{q}_2 - G_2\dot{q}_2 - W_{21} - k_{21}e_{21}$.

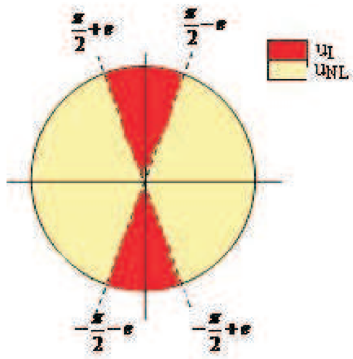


**Figure 8**: Switching regions for the control.

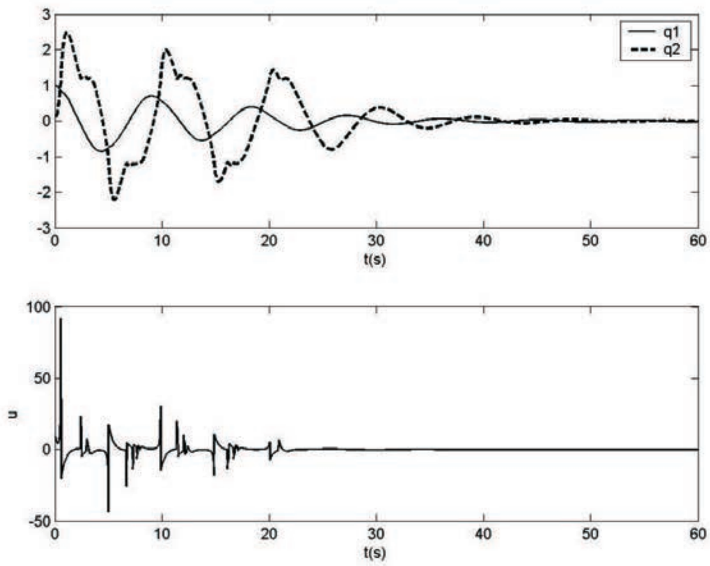


**Figure 9**: States trajectories and control input of the Tora system for the initial condition $(q_1, q_2, p_1, p_2) = (1, 0, 0, 0)$ and $e = 0.2$.

The error between the reference and the actual velocity is given by $e_2 = \dot{q}_2 - \dot{q}_{r2} = G_2\dot{x}_2 + W_{21} + k_{21}e_{21} \Rightarrow G_2\dot{q}_2 + W_{21} = e_2 - k_{21}e_{21}$, then

$$\begin{aligned}\dot{V}_{11} &= -\nu_{11} + e_{21}(e_2 - k_{21}e_{21}) \\ &= -\nu_{11} - k_{21}e_{21}^2 + e_{21}e_2 \\ &= -\nu_1 + e_{21}e_2\end{aligned}$$

with $\nu_1 = \nu_{11} + k_{21}e_{21}^2$.

To compensate for $e_2$, we modify the scalar function $V_{11}$ as $V_1 = V_{11} + \frac{1}{2}e_2^2$. Differentiating $V_1$, we obtain

$$\begin{aligned}\dot{V}_1 &= \dot{V}_{11} + e_2\dot{e}_2 \\ &= -\nu_1 + e_{21}e_2 + e_2\dot{e}_2 \\ &= -\nu_1 + e_2(\dot{e_2} + e_{21}) \\ &= -\nu_1 + e_2(\underbrace{\frac{\partial e_2}{\partial q_1}\dot{q}_1 + \frac{\partial e_2}{\partial q_2}\dot{q}_2 + \frac{\partial e_2}{\partial \dot{q}_1}\ddot{q}_1 + e_{21}}_{\stackrel{def}{=} W_2} + \underbrace{\frac{\partial e_2}{\partial \dot{q}_2}}_{G_2}\ddot{q}_2) \\ &= -\nu_1 + e_2(G_2\ddot{q}_2 + W_2) \\ &= -\nu_1 + e_2(G_2(N_2 + Gu) + W_2).\end{aligned}$$

Finally, the expression of the Lyapunov derivative is

$$\dot{V}_1 = -\nu_1 + e_2(G_2N_2 + G_2Gu + W_2). \tag{25}$$

In order to make $\dot{V}_1$ nonpositive, it is enough to choose $u$ such that

$$e_2(G_2N_2 + G_2Gu + W_2) = -k_2e_2^2. \tag{26}$$

Thus the expression of the control law that globally asymptotically stabilizes the system is given by

$$u = -(G_nN_n + w_n + k_ne_n)(G_nG)^{-1}.$$

Note that, $G_nG$ is invertible since both $G_n$ and $G$ are different from 0 by assumptions ($G \neq 0$ to ensure controllability and $G_n \neq 0$ because of $G_n$ definition in sequences (17) and of assumption C3).

Step 2 $i = 2$.

The final Lyapunov function is given by $V_2 = V_1$ such that $\dot{V}_2 = -\nu_2 - k_2e_2^2$.
In this work, we take $V_{nL} = V_2$ as the Lyapunov function of the nonlinear subsystem.
Next, as the subsystem (20) is linear, we can choose a Lyapunov function of the form

$$V_L = \frac{1}{2}\tilde{x}^T R\tilde{x}.$$

If the matrix $R$ is chosen diagonal then, $V_L$ can be expressed as:

$$V_L = \frac{1}{2}(R_1\tilde{x}_1^2 + R_2\tilde{x}_2^2 + R_3\tilde{x}_3^2 + R_4\tilde{x}_4^2).$$

Differentiating $V_L$, we obtain:

$$\begin{aligned}\dot{V_L} &= R_1\tilde{x}_1\dot{\tilde{x}}_1 + R_2\tilde{x}_2\dot{\tilde{x}}_2 + R_3\tilde{x}_3\dot{\tilde{x}}_3 + R_4\tilde{x}_4\dot{\tilde{x}}_4 \\ &= (\frac{R_1}{m_1+m_2} - R_2k)\tilde{x}_1\tilde{x}_2 + (R_3 - K_1R_4)\tilde{x}_3\tilde{x}_4 - K_2R_4\tilde{x}_4^2.\end{aligned} \tag{27}$$

If the elements of the matrix R are chosen so that the conditions

$$\begin{cases} \frac{R_1}{m_1+m_2} &= R_2k, \\ R_3 &= K_1R_4, \end{cases}$$

are verified. Then

$$\dot{V_L} = -K_2R_4\tilde{x}_4^2.$$

The use of the LaSalle invariance principle finishes the proof.

The analysis of the stability of switched control is very difficult by means of analytical tools, so, often we are bounded to use numerical calculations [11]. The energy profile of the switched control is illustrated in Figure 10.

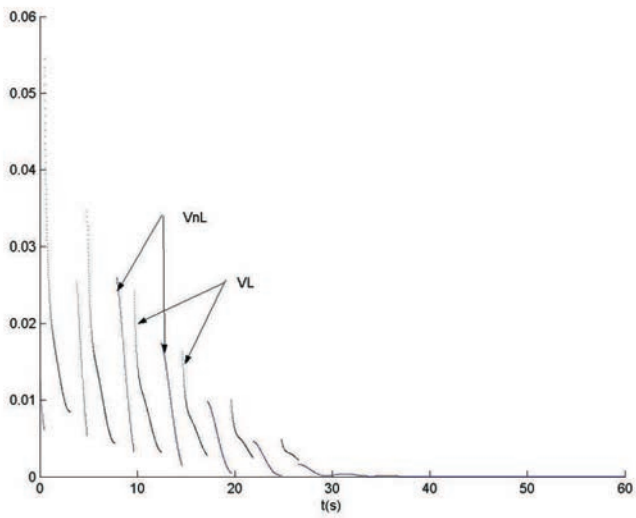


**Figure 10**: Energy profile of the switched system.

According to this figure, the Lyapunov functions $V_{nL}$ and $V_L$ satisfy the above condition and hence we can conclude that the Tora system is globally asmptotically stable.

## 8 Conclusion

In this paper, a transformation methodology for a class of underactuated system with tree structure to another underactuated system with chain structure is proposed by using a change of control and coordinates; so that control design strategies pertaining to the last structure can be applied. This transformation is possible under some conditions on integrability, symmetry property and actuation of certain variables that hold for broad applications of underactuated systems such as the Acrobot, Tora, Inertia-wheel pendulum, VTOL aircraft and others. As an illustrating example, the design procedure has been applied to an underactuated system with initially tree structure. However, as the obtained control law contains singularities, a hybrid control scheme that switches between a linear control law, in a neighborhood of the singularities, and a nonlinear one outside of this neighborhood is presented. Simulation results have shown the good performance and effectiveness of the proposed control strategy.

## Acknowledgment

This work has been supported, for M. Djemai, by International Campus on Safety and Intermodality in Transportation, the European Community, the Delegation Regionale a la Recherche et a la Technologie, the Ministere de lEnseignement superieur et de la Recherche, the Region Nord Pas de Calais and the Centre National de la Recherche Scientifique.

## References

[1] Aneke, N., Nijmeijer, H. and De Jager, A. Tracking control of second-order chained form systems by cascaded backstepping. *International Journal of Robust and Nonlinear Control* **13** (2003) 95–115.

[2] Branicky, M. S. Multiple Lyapunov Functions and others analysis tools for switched and hybrid systems. *IEEE Transaction on Automatic and control* **43** (4) (1998) 475–482.

[3] Baranyi, P. and Varkonyi, P.L. Exact tensor product distributed compensation based stabilization of the Tora system. In: *Proc. on Dynamical systems and Control WSEAS Int.*. Nov. 2005, pp. 38–43.

[4] Brockett, R. W. Asymptotic stability and feedback stabilization. In: *Differential Geometric Control Theory*, R. S. Millman, R.W. Brockett and H. J. Sussmann, eds. Birkhausser, 1983.

[5] Choukchou-Braham, A., Bensalah, C. and Cherki, B. Stabilization of an under-actuated mechanical system by sliding control. In: *Proceeding of the* $1^{st}$ *conference on intelligent systems and automation CISA'08*, vol. 1019, pp. 80–84, June 2008.

[6] Choukchou-Braham, A. and Cherki, B. An extention to backstepping control for a class of underactuated mechanical system in tree structure. In: *Proceeding of the* $2^{nd}$ *Conference on intelligent systems and automation CISA'09*, vol. 1107, pp. 120–125, March 2009.

[7] De Luca, A., Iannitti, S., Mattone, R. and Oriolo, G. Underactuated manipulators: control properties and techniques. *Machine intelligence and robotic* **4** (2003) 113–125.

[8] Decarlo, R. A., Branicky, M. S., Petterson, S. and Lennartson, B. Perspectives and results on the stability and stabilization of hybrid systems. In: *Proceeding of The IEEE*, Vol. 88, No. 7, pp. 1069–1082, July 2000.

[9] Fahimi, F. Slinding mode formation control for underactuated surface vessels. *IEEE Transaction on Robotics* **23** (3) (2007) 617–622.

[10] Fazal-ur-Rehman. Feedback Stabilization of the extended Nonholonomic double integrator *Nonlinear Dynamics and Systems Theory* **5** (4) (2005) 381–394.

[11] Flaus, J.M. Stabilité des systèmes dynamiques hybrides. In: *Systèmes dynamiques hybrides, J. Zytoon, Hermes*, 2001.

[12] Fontoni, I. and Lozano, R. *Nonlinear Control of Underactuated Mechanical System.* Springer-Verlag, London, 2002.

[13] Frafkov, A. L., Makarov, I. A., Shiriaev, A. and Tomchina, O. P. Control of oscillations in Hamiltonian systems. In: *Proceeding of the* $4^{th}$ *European control conference*, 1997.

[14] Gronard, F., Sepulchre, R. and Bastin, G. Slow control for global stabilization of feed-forward systems with exponentially unstable jacobian linearisation. *Systems and Control Letters* **37** (1999) 107–115.

[15] Guisheng Zhai, Isatada Matsune, Tomoaki Kobayashi and Joe Imae. A Study on Stabilization of Nonholonomic Systems via a Hybrid Control Method. *Nonlinear Dynamics and Systems Theory* **7** (3) (2007) 327–338.

[16] Hauser, J., Sastry, S. and Kokotović, P. Nonlinear control via approximate input-output linearization: the ball and beam example. *IEEE Transaction on Automatic and control* **37** (1992) 392–398.

[17] Hu, G., Makkar, C., and Dixon, W.E. Energy based nonlinear control of underactuated Euler Lagrange systems subject to impacts. *IEEE Transaction on Automatic control* **52** (9) (2007) 1742–1748.

[18] Hung, L., Lin, H., and Chung, H. Design of self tuning fuzzy sliding mode control for Tora system. *Journal of Expert systems with applications* **32** (1) (2007) 201–212.

[19] Jankovic, M., Fontaine, D. and Kokotović, P. Tora example: cascade and passivity based control designs. *Transaction on Control System Technique* **4** (3) (1996) 292–297.

[20] Khalil, H. K. *Nonlinear systems.* Prentice Hall, New Jersey, 2002.

[21] Liberzon, D. and Morse, A.S. Basic problems in stability and design of switched systems. *IEEE Control Systems Magazine* **19** (5) (1999) 59–70.

[22] Lin, C. Robust adaptive critic control of nonlinear systems using fuzzy basis function network: an LMI approach. *Journal of Information Sciences* **177** (22) (2007) 4934–4946.

[23] Manamanni, N., Djemaï, M., Boukhobza, T. and M'Sirdi, N. Nonlinear Sliding observer Based control for a Pneumatic Robot Leg. *Intern. Journal of Robotics and Automation* **16** (2) (2001) 100–112.

[24] Nazrulla, S., Khalil, H.K. A Novel nonlinear output feedback control applied to the TORA benchmark system. In: *Proceeding of the* $47^{th}$ *IEEE Conference on Decision and Control*, pp. 3565–3570, Dec. 2008.

[25] Olfati-saber, R. Normal forms for underactuated mechanical systems with symmetry. *IEEE Transaction on Automatic Control* **47** (2) (2002) 305–308.

[26] Oriolo, G. and Venditelli, M. A framework for the stabilization of general nonholonomic systems with an application to the plat-ball mechanism. *IEEE Transaction on Robotics* **21** (2) (2005) 162–175.

[27] Qaiser, N., Hussain, A., Iqbal, N. and Qaiser, N. Dynamic surface control for stabilization of the oscillationg eccentric rotor. In: *Proc. IMechE, Systems and Control Engineering*, 2007, vol. 221, 311–319.

[28] Reyhanoglu, M. and Bommer, A. Tracking control of an underactuated autonomous surface vessel using switching feedback. In: *Proceeding of the* $32^{nd}$ *Conference on Industrial Electronics*, pp. 3833–3838, Nov. 2006.

[29] Sepulchre, R., Janković, M. and Kokotović, P. *Contructive Nonlinear Control.* Springer-Verlag, 1997.

[30] Seto, D., Annaswamy, A. M. and Baillieul, J. Adaptative control of a class of nonlinear systems with a triangular structure. *IEEE Transaction on Automatic Control* **39** (7) (1994) 1411–1428.

[31] Seto, D. and Baillieul, J. Control problems in super-articulted mechanical systems. *IEEE Transaction on Automatic Control* **39** (12) (1994) 2442–2453.

[32] Spong, M. W. Underactuated mechanical systems. In: *Contol Problems in Robotics and Automation*. B. Siciliano and K. P. Valavanis, eds. Springer-Velag, London, vol. 230, pp. 135–150, 1998.

[33] Spong, M.W., Energy based control of a class of underactuated mechanical systems. In: *IFAC World Congress*, pp. 431–435, July 1996.

[34] Spong, M.W. and Bolck, D.J. The Pendubot: A mechatronic system for control research and education. In: *Proceeding of the* $34^{th}$ *Conference on Decision and Control*, pp. 555–556, Dec. 1995.

[35] Tomlin, C. J. and Sastry, S. S. Switching through singularities. In: *Proceeding of the* $36^{th}$ *Conference on Decision and Control*, vol. 1, pp. 1–6, 1997.

[36] Venditelli, M., Oriolo, G., Jean, F. and Laumond, J. P. Nonhomogeneous nilpotent approximations for nonholonomic systems with singularities. *IEEE Transaction on Automatic Control* **49** (2) (2004) 261–266.

[37] Voytsekhovsky, D. A. and Hirschorn, R. M. Stabilization of Single-Input Nonlinear Systems Using Higher Order Compensating Sliding Mode Control. In: *Proceeding of the* $44^{th}$ *Conference on Decision and Control, and the European Control conference*, pp. 566–570, Dec. 2005.

[38] Wai, R. and Lee, M. Cascade direct adaptive fuzzy control design for a nonlinear two axis inverted pendulum servomechanism. *IEEE Transaction on Systems, Man and Cybernetics* **38** (2) (2008) 439–454.

[39] Wan, C.J., Bernstein, D.S. and Coppola, V.T. Global stabilization of the oscillating eccentric rotor. *Nonlinear Dynamics* **10** (1996) 49–62.

[40] Zhang, M. and Tarn,T. J. Hybrid control of the Pendubot. *IEEE ASME Transaction on Mechatronics* **7** (1) (2002) 79–86.

[41] Zhang, M. and Tarn, T. J. A hybrid switching control strategy for nonlinear and underactuated mechanical systems. *IEEE Transaction on Automatic Control* **48** (10) (2003) 1777–1782.

Nonlinear Dynamics and Systems Theory, **12** (4) (2012) 365–374

# Travelling Wave Solutions of Nonlocal Models for Media with Oscillating Inclusions

V.A. Danylenko and S.I. Skurativskyi *

*Division of Geodynamics of Explosion, Subbotin Institute of geophysics, National Academy of Sciences of Ukraine, 63 G Bohdan Khmelnytsky str., 01054, Kyiv-54, Ukraine*

Received: November 2, 2011; Revised: October 7, 2012

**Abstract:** Continual model of a complex medium with oscillating inclusions is considered. Travelling wave (TW) solutions to the source system are shown to satisfy a four-dimensional dynamical system. Qualitative study of the factorized system enables to show the existence of homoclinic and heteroclinic contours in vicinities of fixed points. Existence of the homoclinic loops results in the complex global behavior of phase trajectories, including the bifurcations of tori, that are investigated numerically.

**Keywords:** *travelling wave solutions; homoclinic curve; invariant tori; nonlinear normal modes.*

**Mathematics Subject Classification (2010):** 74D10, 74D30, 37G20, 34A45.

## 1 Introduction

Experimental investigations of deformations of geomedia in the wide range of loading velocities, carried out in the last decades, testify that geomedia possess two basic features, namely, a discrete structure and oscillating motion of the discrete elements [1, 2].

Oscillating modes can be incorporated into the continual model by means of adding extra volumetric forces, causing the movements of the elements of the structure. In the papers [3, 4] a linear mathematical model for structured media taking into account the oscillations of structural elements has been suggested. In the simplest form the equations of motion can be written as follows:

$$\rho\frac{\partial^2 u}{\partial t^2} = \frac{\partial \sigma}{\partial x} - m\rho\frac{\partial^2 w}{\partial t^2}, \qquad \frac{\partial^2 w}{\partial t^2} + \omega^2 (w-u) = 0, \tag{1}$$

* Corresponding author: mailto:skurserg@rambler.ru

where $\rho$ is the density, $\sigma$ is the stress, $u\left(x,t\right)$, $w\left(x,t\right)$ are the displacements of the bulk medium and typical oscillator with natural frequency $\omega$, $m\rho$ is the density of oscillating inclusions.

But it is well known that the real geomaterials manifest a strong nonlinear effects when being subjected to high-intense impulse loading. In the situation when the medium is far from equilibrium, various relaxing processes within the elements of structure take place and the linear model becomes completely incorrect.

Thus, generally speaking, one should take into account both physical nonlinearity and nonlocal effects. This can be done by incorporating into the modelling system the following equation of state [5, 6]:

$$\sigma = E_1\varepsilon + E_3\varepsilon^3 + \theta\left(\sigma_{xx} - \sigma_x\frac{\varepsilon_x}{\varepsilon+1} - \eta\left[\varepsilon_{xx} - \frac{\left(\varepsilon_x\right)^2}{\varepsilon+1}\right]\right). \tag{2}$$

Equations (1), (2) form a closed system, which will be studied below. In our previous work [7], preliminary investigations of the system with $\theta = 0$ were carried out, revealing, in particular, the existence of periodic and soliton-like (especially important in nonlinear physics and engineering applications [8]) TW solutions.

The aim of the present paper is to study a set of TW solutions to (1)-(2) in the general case and to investigate an influence of spatial nonlocality on the structure of wave regimes.

## 2 Qualitative Analysis of the Dynamical System Describing Autowave Solutions

We restrict our consideration to the set of TW solutions, having the form

$$u = U(s), \quad w = W(s), \quad s = x - Dt. \tag{3}$$

Here the parameter $D$ stands for the constant velocity of the wave front. Substituting (3) into the equations (1), (2), we obtain the dynamical system

$$D^2U'' = F' - mD^2W'', \tag{4}$$

$$W'' + \Omega^2\left(W - U\right) = 0, \tag{5}$$

$$F = e_1U' + e_3\left(U'\right)^3 + \theta\left(F'' - F'\frac{U''}{U'+1} - \eta\left[U''' - \frac{\left(U''\right)^2}{U'+1}\right]\right), \tag{6}$$

where $\Omega = \omega D^{-1}$.

Integrating once equation (4), we get

$$F = D^2\left(U' + mW'\right). \tag{7}$$

Excluding the function $F$ with the help of formula (7), we obtain the following system:

$$\begin{gathered} W'' + \Omega^2\left(W - U\right) = 0, \\ D^2\left(U' + mW'\right) = e_1U' + e_3\left(U'\right)^3 + \theta\left(F'' - F'\frac{U''}{U'+1} - \eta\left[U''' - \frac{\left(U''\right)^2}{U'+1}\right]\right). \end{gathered} \tag{8}$$

It is easily seen, that this system can be rewritten as four-dimensional dynamical system (8):

$$\begin{gathered} Z' = Y, \quad Y' = -\Omega^2 (Z - R), \quad R' = X, \\ X' = \frac{1}{\theta (D^2 - \eta)} \Big( -e_1 R - e_3 R^3 + \frac{X^2 \left\{ D^2 - \eta \right\} \theta + D^2 \theta m X Y}{R + 1} + \\ + \theta m D^2 \Omega^2 \{ Z - R \} + D^2 \{ R + m Z \} \Big) \end{gathered} \tag{9}$$

Analysis shows that system (9) has three fixed (or stationary) points: the point $M_1$ coinciding with the origin, and the pair of the points $M_{2,3}$, given by the formulae

$$X = Y = 0, \qquad Z_2 = R_2 = \pm \sqrt{\frac{D^2 (1 + m) - e_1}{e_3}} \equiv \pm G.$$

It is easy to get convinced, that the Jacobi matrix of the system has the form:

$$J = \begin{pmatrix} 0 & 1 & 0 & 0 \\ -\Omega^2 & 0 & \Omega^2 & 0 \\ 0 & 0 & 0 & 1 \\ K_1 & 0 & K_2 & 0 \end{pmatrix},$$

where $K_1 = \dfrac{m D^2 \left(1 + \Omega^2 \theta\right)}{(D^2 - \eta)\, \theta}$, and $K_2 = \dfrac{D^2 - e_1 - m \omega^2 \theta}{(D^2 - \eta)\, \theta}$ at the point $M_1$, and $K_2 = \dfrac{2 e_1 - D^2 \left(2 + 3m + m \Omega^2 \theta\right)}{(D^2 - \eta)\, \theta}$ at the points $M_{2,3}$. The eigenvalues of the matrix $J$ satisfy the biquadratic equation

$$\lambda^4 + \lambda^2 \left(\Omega^2 - K_2\right) - (K_1 + K_2)\, \Omega^2 = 0.$$

It is then obvious that $\lambda^2 = \frac{1}{2} \left( K_2 - \Omega^2 \pm \sqrt{\left(\Omega^2 + K_2\right)^2 + 4 \Omega^2 K_1} \right)$. Depending on the values of $\lambda$ the fixed points of the dynamical system are centers, saddles, or degenerate ones.

Some analytical results concerning the behavior of solutions in some vicinities of the fixed points can be obtained on the basis of the local asymptotic analysis. Let us consider the dynamical system (9) in the vicinity of the points $M_{2,3}$. For convenience, we replace the origin at the point $M_i$, $i = 1,\ 2$, making the change of variables $Z = x_1 + G$, $Y = y_1$, $R = x_2 + G$, $X = y_2$:

$$\begin{aligned} & x_1' = y_1, \quad y_1' = -\Omega^2 (x_1 - x_2), \quad x_2' = y_2, \\ & y_2' = K_1 x_1 + K_2 x_2 - \frac{3 G e_3}{(D^2 - \eta)\theta} x_2^2 - \frac{e_3}{(D^2 - \eta)\theta} x_2^3 + \frac{y_2 \left(-\eta y_2 + D^2 m y_1 + D^2 y_2\right)}{(D^2 - \eta)(1 + x_2 + G)} \end{aligned} \tag{10}$$

To analyze the dynamics in a vicinity of the critical point of system (10), we introduce a formal parameter $\varepsilon$. Using the scaling transformation $x_i = \varepsilon x_i$, $y_i = \varepsilon y_i$ and the expansion in series $\dfrac{1}{1 + \varepsilon x_2 + G} = \sum\limits_{j=0} \dfrac{(-1)^j \varepsilon^j x_2^j}{(1 + G)^{j+1}}$ we can rewrite our system up to $O(\varepsilon^3)$ in the following form:

$$\begin{aligned} &x_1' = y_1, \quad y_1' = -\Omega^2 \left(x_1 - x_2\right), \quad x_2' = y_2, \\ &y_2' = K_1 x_1 + K_2 x_2 + \varepsilon \left(H_1 x_2^2 + H_2 y_1 y_2 + H_3 y_2^2\right) + \varepsilon^2 \left(L_1 x_2^3 + L_2 x_2 y_1 y_2 + L_3 x_2 y_2^2\right), \end{aligned} \tag{11}$$

where $H_1 = \dfrac{-3e_3 G}{(D^2-\eta)\theta}$, $H_2 = \dfrac{D^2 m}{(1+G)(D^2-\eta)}$, $H_3 = \dfrac{1}{1+G}$, $L_1 = \dfrac{-e_3}{(D^2-\eta)\theta}$, $L_2 = -\dfrac{D^2 m}{(1+G)^2(D^2-\eta)}$, $L_3 = -\dfrac{1}{(1+G)^2}$.

The expansion of the dynamical system (9) in vicinity of the stationary point $M_1$ can be written in the same form but with different coefficients $K_i,\ i = 1, 2$ and $H_i,\ L_i,\ i = 1, 2, 3$.

Now let us remind, that any linear system of coupled oscillators can be presented in an uncoupled form by means of passing to the normal modes (see e.g. [9]). This procedure is connected with the separation of general system dynamics onto the simpler motions described by systems with single degree of freedom, and expresses the principle of superposition for linear systems. For nonlinear systems analogs of the superposition principle can also be stated in many cases. For weakly non-linear systems like (11) the superposition principle can be established on the basis of the method of nonlinear normal modes [10,11]. In accordance with [12], we assume that it is possible to split the degrees of freedoms into the "master" coordinates $x_1 = u,\ y_1 = v$ and the "slave" coordinates $x_2,\ y_2$ functionally, dependent on the "master" ones: $x_2 = X_2(u, v),\ y_2 = Y_2(u, v)$. Such relations just express the nonlinear principle of superposition. On the other hand, the nonlinear normal modes technique could be regarded as the next step of a local asymptotic analysis, following the qualitative analysis of the linearized system.

If we assume that the master system has the form

$$\begin{aligned} x_1' &= y_1, \qquad y_1' = f_1(x_i, y_i), \\ x_2' &= y_2, \qquad y_2' = f_2(x_i, y_i), \end{aligned}$$

then $X_2$ and $Y_2$ satisfy the equations

$$\begin{aligned} Y_2 &= \frac{\partial X_2}{\partial u} v + \frac{\partial X_2}{\partial v} f_1(u, v, X_2, Y_2), \\ f_2(u, v, X_2, Y_2) &= \frac{\partial Y_2}{\partial u} v + \frac{\partial Y_2}{\partial v} f_1(u, v, X_2, Y_2). \end{aligned} \tag{12}$$

Now we are going to find the solution of (12) in the form of the following series expansions:

$$\begin{aligned} X_2 &= a_1 u + a_2 v + a_3 u^2 + a_4 uv + a_5 v^2 + a_6 u^3 + a_7 u^2 v + a_8 uv^2 + a_9 v^3 + ..., \\ Y_2 &= b_1 u + b_2 v + b_3 u^2 + b_4 uv + b_5 v^2 + b_6 u^3 + b_7 u^2 v + b_8 uv^2 + b_9 v^3 + .... \end{aligned} \tag{13}$$

Inserting (13) into (12) and equating to zero the coefficients of the same monomials $u^i v^j$, we get a set of algebraic equations with respect to the parameters $a_i$, $b_i$. The first four coefficients obtained in this way are as follows:

**for mode I**

$$\begin{aligned} a_1 &= \frac{1}{2\Omega^2}(K_2 + \Omega^2 - \sqrt{(K_2+\Omega^2)^2 + 4K_1\Omega^2}), a_2 = 0, \\ b_1 &= 0, b_2 = \frac{1}{2\Omega^2}(K_2 + \Omega^2 - \sqrt{(K_2+\Omega^2)^2 + 4K_1\Omega^2}). \end{aligned} \tag{14}$$

**for mode II**

$$
\begin{aligned}
a_1 &= \frac{1}{2\Omega^2}(K_2 + \Omega^2 + \sqrt{(K_2+\Omega^2)^2 + 4K_1\Omega^2}), a_2 = 0,\\
b_1 &= 0, b_2 = \frac{1}{2\Omega^2}(K_2 + \Omega^2 + \sqrt{(K_2+\Omega^2)^2 + 4K_1\Omega^2}).
\end{aligned} \tag{15}
$$

Note that the sets of the parameters (14) and (15) correspond to the case when the linearly coupled system breaks up into a pair of uncoupled equations describing linear oscillations.

Using (14), we can express the coefficients of the quadratic monomials in the following form:

**for mode I and II**

$$
\begin{gathered}
a_3 = -\frac{a_1\left(2\,H_2\,\Omega^4\,(a_1-1)^2 + \left(H_1\,\left(K_2+\Omega^2\,(2-3\,a_1)\right) + 2\,H_3\,\Omega^4\,(a_1-1)^2\right)\,a_1\right)}{\left(K_2+\Omega^2\,(4-5\,a_1)\right)\,\left(K_2-\Omega^2\,a_1\right)},\\
a_4 = 0,\\
a_5 = -\frac{a_1\,\left(H_2\,\left(K_2+\Omega^2\,(2-3\,a_1)\right) + \left(2\,H_1 + H_3\,\left(K_2+\Omega^2\,(2-3\,a_1)\right)\right)\,a_1\right)}{\left(K_2+\Omega^2\,(4-5\,a_1)\right)\,\left(K_2-\Omega^2\,a_1\right)},\\
b_3 = 0,\\
b_4 = \frac{-2\,a_1\,\left(H_2\,\Omega^2\,(a_1-1) + \left(H_1 + H_3\,\Omega^2\,(a_1-1)\right)\,a_1\right)}{K_2+\Omega^2\,(4-5\,a_1)}, \quad b_5 = 0.
\end{gathered} \tag{16}
$$

**Remark.** One can easily see, that the coefficients defined by (16) become infinite, when the corresponding denominators nullify. This occurs if $K_2 - \Omega^2 a_1 = 0$, $K_2 - \Omega^2\,(5\,a_1 - 4) = 0$, $K_2 - \Omega^2\,(10\,a_1 - 9) = 0$, and so on. In these cases the corresponding resonances take place, namely $1:1$, $1:2$, $1:3$, ..., and the coupled system cannot be presented as a pair of uncoupled ones.

In the third order approximation we get:

**for mode I and II**

$$
a_7 = a_9 = 0, b_6 = b_8 = 0, \tag{17}
$$

while the rest ones are nonzero. We don't present them because they are very cumbersome.

Since $u' = v, \quad v' = f_1(u, v, X_2, Y_2)$, then taking into account the parameters values corresponding to the first mode, we get the following planar system (instead of the fourth order one):

$$
u' = v, v' = \mu_1 u + \mu_2 u^2 + \mu_3 v^2 + \mu_4 u^3 + \mu_5 u v^2, \tag{18}
$$

where $\mu_1 = \Omega^2(a_1 - 1)$, $\mu_2 = \Omega^2 a_3$, $\mu_3 = \Omega^2 a_5$, $\mu_4 = \Omega^2 a_6$, $\mu_5 = \Omega^2 a_8$. Note that the value $\sqrt{\mu_1}$ coincides with the pair of eigenvalues of the matrix $J$.

Nonlinear system (18) proves to be completely integrable. Indeed, dividing the second equation by the first one, we obtain the following equation:

$$
\frac{1}{2}\frac{d\rho}{du} = \mu_1 u + \mu_2 u^2 + \mu_3 \rho + \mu_4 u^3 + \mu_5 u\rho, \tag{19}
$$

where $\rho = v^2$. The general solution of (19) can be presented in the form

$$
\begin{aligned}
v^2 = 2\int_{u_0}^{u} &\left(\mu_1\tau + \mu_2\tau^2 + \mu_4\tau^3\right)\exp\left[(u-\tau)(2\mu_3 + \mu_5(u+\tau))\right]d\tau + \\
&+ v_0^2 \exp\left[(u-u_0)(2\mu_3 + \mu_5(u+u_0))\right],
\end{aligned} \tag{20}
$$

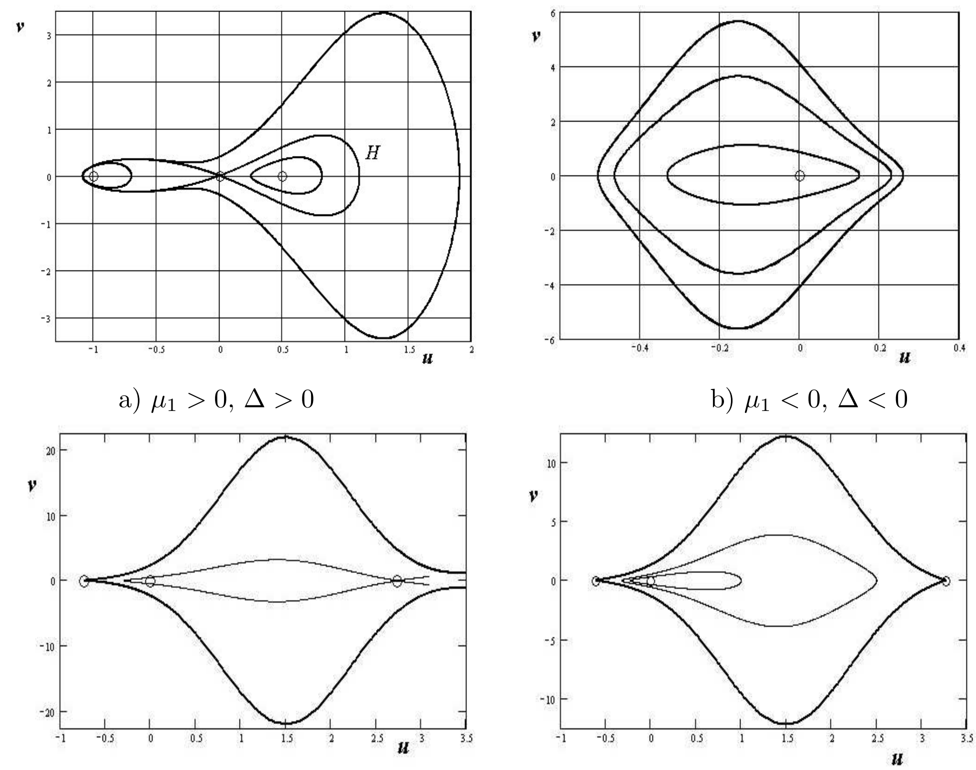


a) $\mu_1 > 0$, $\Delta > 0$ b) $\mu_1 < 0$, $\Delta < 0$

c) $\mu_1 < 0$, $\Delta > 0$ d) $\mu_1 < 0$, $\Delta > 0$, $\mu_2 = -1.3274589$

**Figure 1**: The phase portraits of dynamical system (19) at the different values of the parameters $\mu_i$.

where $(u_0,\, v_0)$ stand for the initial data. Hence, the general solution of system (18) has the form $s = \int v^{-1} du$. To analyze the behavior of the solution obtained, it is desired to perform the qualitative integration [13] of the planar system (18).

The fixed points of system (18) have the coordinates

$$v = 0, u_1 = 0, u_2 = \frac{-\mu_2 - \sqrt{\mu_2^2 - 4\mu_1\mu_4}}{2\mu_4}, u_3 = \frac{-\mu_2 + \sqrt{\mu_2^2 - 4\mu_1\mu_4}}{2\mu_4}.$$

The fixed points $(u_{2,3}; 0)$ exist if $\Delta \equiv \mu_2^2 - 4\mu_1\mu_4 \geq 0$. The type of the fixed points is defined by the eigenvalues $\lambda$ of the linearized matrix

$$M = \begin{pmatrix} 0 & 1 \\ \mu_1 + 2\mu_2 u_i + 3u_i^2 & 0 \end{pmatrix}.$$

For the fixed point $(0; 0)$ $\lambda^2 = \mu_1$ then if $\mu_1 < 0$ the fixed point is a center, if $\mu_1 > 0$ then it is a saddle. For another fixed points, if $\lambda^2 = \mu_1 + 2\mu_2 u_i + 3u_i^2 < 0$ then the fixed points are centers otherwise they are saddles. Let us consider the typical phase portraits of dynamical system (18).

We can distinguish the following cases

- $\mu_1 > 0$. The phase plane has a saddle $(0; 0)$ if $\Delta < 0$; the phase plane has a saddle $(0; 0)$ and a pair $(u_{2,3}; 0)$ of centers, if $\Delta > 0$ (Figure 1a).
- $\mu_1 < 0$. In the case when $\Delta < 0$, there is a center $(0; 0)$ at the origin, Figure 1b. In the case $\Delta > 0$ the center is accompanied by the pair of saddles $(u_{2,3}; 0)$. Separatrices of one of the saddles form a homoclinic loop, whereas the separatrices of another one do not intersect, and surround the homoclinic loop (Figure 1c).

The last case is more complicated and interesting. Indeed, small changes of the parameters (e.g. $\mu_2$) may cause a global qualitative changes of the phase portrait. The saddle separatrices under certain conditions can interconnect, forming a heteroclinic loop.

Using the exact solution (20), one can estimate the conditions of the heteroclinic loop creation. Suppose that a trajectory connecting the fixed points $(u_2,\ 0)$ and $(u_3,\ 0)$ exists. Then the coordinates of the fixed points must satisfy relation (20), where $u_0 = u_2$, $v_0 = 0$, $u = u_3$, $v = 0$. As a result, the following relation is derived

$$\int_{u_3}^{u_2} \left(\mu_1\tau + \mu_2\tau^2 + \mu_4\tau^3\right) \exp\left[(u_2 - \tau)(2\mu_3 + \mu_5(u_2 + \tau))\right] d\tau = 0.$$

It poses certain restrictions on the parameters of the dynamical system, the value of some parameter can be calculated precisely. Following this way, we succeeded in constructing the figure 1d, corresponding to $\mu_1 = -1$, $\mu_3 = 3$, $\mu_4 = 0.5$, and $\mu_5 = -2$.

## 3 Application of Local Analysis to the Dynamical System

Let us apply the results presented above to the investigation of the local dynamics of the system (9) in the vicinity of the fixed points. For the parameters values $D = 0.9$, $\omega = 1$, $m = 0.8$, $e_1 = 1$, $e_3 = 0.7$, $\eta = 0.105$, $\theta = 0.7$ the linearization matrix $J$ taken at the fixed point $(Z_1; 0; R_1; 0)$ has the eigenvalues $(\pm 1.767i; \pm 0.606)$. At the fixed point $(Z_2; 0; R_2; 0)$ the eigenvalues of $J$ are the following: $(\pm 2.256i; \pm 0.671i)$. In the vicinity of each fixed point the system (9) splits into a pair of separated planar dynamical systems,both written in the form (18), but differing by the values of the parameters $\mu_i$.

Thus, for fixed point $(Z_2; 0; R_2; 0)$, the mode I is described by the dynamical system (18) with $\mu_i = \{-5.0882, -17.8235, -4.1475, -128.7057, -26.4049\}$. The corresponding phase plane of the system is depicted in Figure 1b.

The parameters $\mu_i = \{-0.4504, -0.4457, 0.3738, 0.4805, -2.4475\}$ relate to the mode II. Then dynamical system (18) has three fixed points $(0; 0)$, $(-0.6097; 0)$, $(1.5373; 0)$ and the phase plane is presented in Figure 2.

The analysis of the system (18) in the vicinity of the fixed point $(Z_1; 0; R_1; 0)$ is carried out in the same way. The parameter values $\mu_i = \{-3.1214, -4.7475, -1.6104, -16.4902, -5.3289\}$ correspond to the mode I. Corresponding phase portrait is shown in Figure 1b.

For the mode II we have the following values of the parameters $\mu_i = \{0.367067, -0.06678, 0.9554, -0.8903, 0.0763\}$. The phase plane of the system (18) contains the fixed points with the coordinates $(0; 0)$, $(0.6057; 0)$, $(-0.6807; 0)$. Its phase portrait is illustrated by Figure 1a.

It is well known, that the presence of the homoclinic loops in the phase space of the multidimensional dynamical system can lead to the very complex dynamical behaviour [14]. In the case under consideration the homoclinic loops observed in the phase portrait of system (18) can rupture in the next approximations, causing the presence of

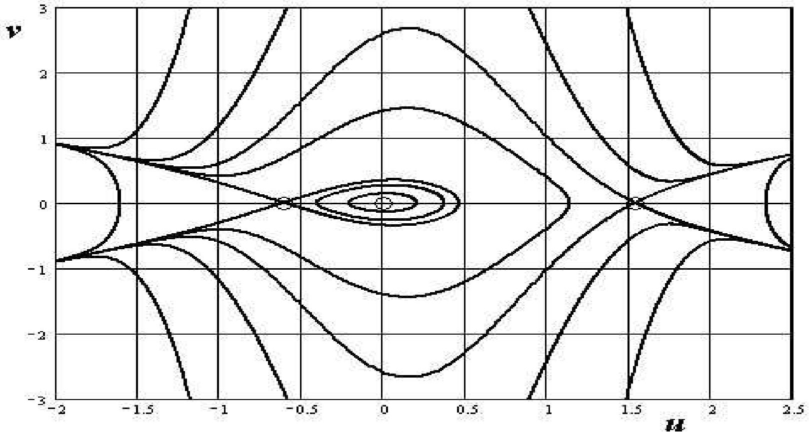


**Figure 2**: Phase plane of dynamical system (18).

complicated dynamics, coexisting with the homoclinic loops. In this case the complex trajectories can be observed in the phase space of a dynamical system.

In order to check the existence of complicated regimes, we integrated the dynamical system (9) numerically. In numerical experiments all the parameters but one were fixed. The $\theta$ played the rule of the bifurcation parameter. We started from the value $\theta$ of the order 0.01. Starting from the initial data $\left(10^{-6};0;0;0\right)$, we obtained the trajectories oscillating closely to the saddle separatices of the stationary point placed at the origin. Note, that for small $\theta$ a qualitative behavior of separatrices can be obtained by means of the asymptotic analysis.

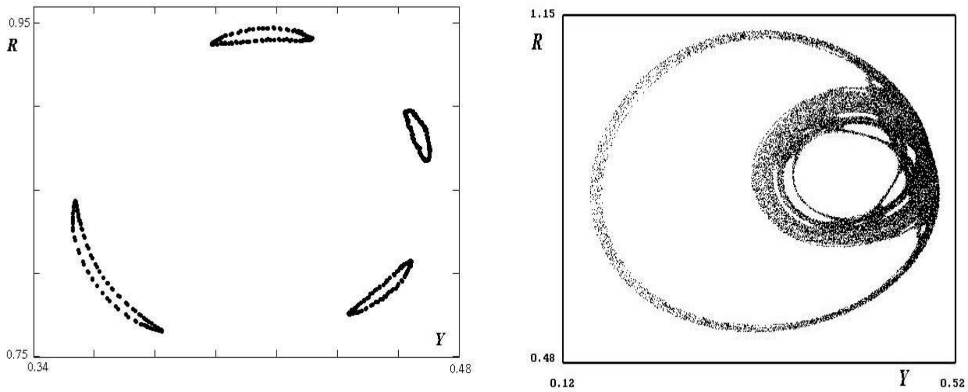


a b

**Figure 3**: The Poincare sections of the tori existing in the phase space of dynamical system (9) at a) $\theta = 0.7$, b) $\theta = 0.72$.

Now let us consider the case when $\theta \sim O(1)$. It is evident that different initial data for dynamical system (9) lead to surfaces with different structure. We considered the

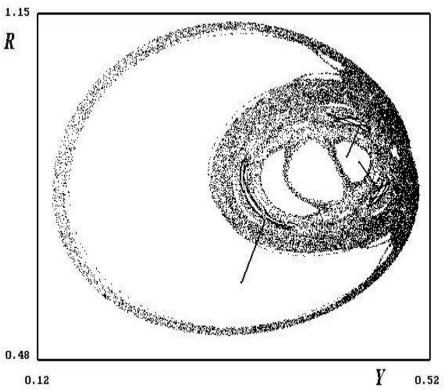


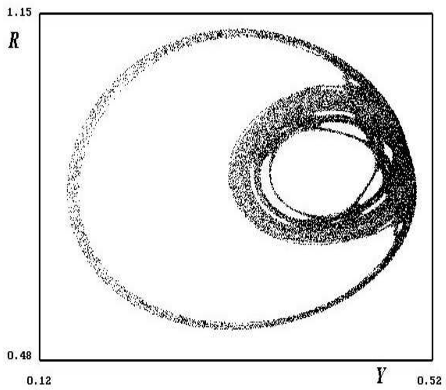


**Figure 4**: The Poincare sections of the tori existing in the phase space of dynamical system (9) at a) $\theta = 0.74$, b) $\theta = 0.7517$.

most interesting of them only. Integrating the dynamical system (9) with the initial data $(0.6; 0.3; 0.8; 0.4)$ and $\theta = 0.7$, one can observe the torus. For its visualization, we used the Poincare section technique. Let the surface $Z = 0.8$ be the target hyperplane. The locus of the intersection of the trajectories with the hyperplane $Z = 0.8$ is a 3D set. The part of this set is projected on the two-dimensional coordinate plane $(Y; R)$ and is depicted in figure 3a. Analyzing the obtained Poincare section, we see that the torus surface consists of four separated pipes.

Let us choose $\theta = 0.72$ and integrate dynamical system (9) from the same initial data. Using the same section plane, we get another Poincare diagram (fig.3b). The main peculiarities of the diagram are the appearance of the pipe of large radius and the presence of tightly enclosed pipes. The set of curves drown in the diagram looks like a fractal structure, though this has not been studied in detail yet. If parameter $\theta$ increases (Figure 4) the structure of the internal region changes most of all. Besides, one can select the regions that the running point visits more frequently (see the pointers in Figure 4).

The analysis of the Poincare sections shows that the trajectories in the four dimensional phase space of dynamical system (9) form a complex object which undergoes bifurcations as the parameter $\theta$ increases.

Applying the results of the local asymptotic analysis of the dynamical system (9) we can state, that the complex behavior of the phase space is connected with the reorganization of the homoclinic trajectories and their neighborhoods.

## 4 Conclusion

In summary, we would like to stress a key role of nonlocal effects, nonlinearity, and oscillating degrees of freedom in the formation of complex wave regimes. When the load applied senses the internal structure of media (and this is the case when the spatio-temporal characteristics of the load and the elements of the internal structure are comparable), then we cannot neglect the dynamics of internal degrees of freedom. Let us stress, that results obtained in this study essentially differ from those predicted by linear models (both local and nonlocal ones) [7].

From the mathematical point of view investigations of the modelling system (1)-(2) are more difficult in comparison with their local analogs, nevertheless, under some additional assumptions they can be treated within the traditional asymptotic techniques. Besides, the variety of observed regimes indicate the existence of another important type of solutions, inherent for essentially nonlocal models.

## Acknowledgment

The authors would like to thank Professor Vladimirov V.A. (University of Science and Technology, Faculty of Applied Mathematics, Poland) for helpful suggestions and discussions. One of the authors (S.S.) is grateful to the Organizers of the 11th Conference "Mathematics in Technical and Natural Sciences", 8 – 12 September 2010, Krynica, Poland, where the essential part of this material has been presented.

## References

[1] Rodionov, V. N. *An essay of geomechanics.* Moscow: Scientific World, 1996.

[2] Sadovskyi, M.A. Self-similarity of geodynamical processes. *Herald of the RAS* **8** (1986) 3–12. [Russian]

[3] Palmov, V.A. On a model of medium of complex structure. *J. Appl. Math. Mech* **4** (1969) 768–773.

[4] Slepyan, L.I. Wave of deformation in a rod with flexible mounted masses. *Mechanics of Solids* **5** (1967) 34–40.

[5] Danevich, T.B. and Danylenko, V.A. Nonlinear nonlocal models of multicomponent relaxing media with interior oscillators. *Reports of NAS of Ukraine* **1** (2005) 106–110.

[6] Danylenko, V.A. and Skurativskyy, S.I. Resonans modes of propagation of nonlinear wave fields in media with oscillating inclusions. *Reports of NAS of Ukraine* **11** (2008) 108–112.

[7] Skurativskyi, S. and Skurativska, I. Localized autowave solutions of the nonlinear model for a complex medium. *Electronic Journal "Technical Acoustics"* **6** (2010) http://www.ejta.org.

[8] Biswas, M. H. A., Rahman, M. A. and Das, T. Optical soliton in nonlinear dynamics and its graphical representation. *Nonlinear Dynamics and Systems Theory* **11** (4) (2011) 383–396.

[9] Landau, L.D. and Lifshitz, E.M. *Mechanics.* Academic Press, New York, 1987.

[10] Shaw, S.W. and Pierre, C. Normal modes for nonlinear vibratory systems. *Journal of sound and vibration* **164**(1) (1993) 85–124.

[11] Vakakis, A.F., Manevich, L.I., Mikhlin, Y. V. and Pilipchuk, V. N. *Normal Modes and Localization in Nonlinear Systems.* Wiley, 1996; (see also the special issue in *Nonlinear Dynamics*, **25(1-3)** (2001) 1–292).

[12] Warmiński, J. Nonlinear normal modes of coupled self-excited oscillators in regular and chaotic vibration regimes. *J. Theor. Applied Mech.* **46** (3) (2008) 693–714.

[13] Shil'nikov, L.P., Shil'nikov, A.L., Turaev, D.V. and Chua, L.O. *Methods of qualitative theory in nonlinear dynamics. Part I.* World Scientific, Singapore, New Jersey, London, Hong Kong, 1998.

[14] Butenin, N., Neymark, Yu. and Fufayev, N. *Introduction to the theory of nonlinear oscillations.* Moscow: Nauka, 1987. [Russian]

Nonlinear Dynamics and Systems Theory, **12** (4) (2012) 375–382

# Nonlinear Plane Waves in Rotating Stratified Boussinesq Equations

B. S. Desale* and Vivek Sharma

*School of Mathematical Sciences, North Maharashtra University, Jalgaon 425001, India.*

Received: September 13, 2011; Revised: October 9, 2012

**Abstract:** In this paper we have built special exact solutions to rotating stratified Boussinesq equations in the form of nonlinear plane waves. We also conclude that these solutions grow exponentially in unstable stratifications. Whereas, in the special case of stable stratification these waves are oscillatory in nature. Consequently, we determined internal gravity waves and some sinusoidal wave forms.

**Keywords:** *plane waves; rotating stratified Boussinesq equation; sinusoidal waves.*

**Mathematics Subject Classification (2010):** 34A05, 35J35.

## 1 Introduction

The stratified Boussinesq equations form a system of PDEs modelling the movements of planetary atmospheres. It may be noted that the Boussinesq approximation in the literature is also referred to as the Oberbeck-Boussinesq approximation for which, the reader is referred to an interesting paper of Rajagopal et al [1] providing a rigorous mathematical justification of use of these equations as perturbations of the Navier-Stokes equations. Majda & Shefter [2] have chosen certain special solutions of this system of PDEs to demonstrate onset of instability when the Richardson number is less than 1/4. In their study of instability in stratified fluids at large Richardson number, Majda & Shefter [2] have obtained the exact solutions to stratified Boussinesq equations neglecting the effects of rotations and viscosity. Further, in the absence of strain field Srinivasan et al [3] have shown that the reduced system of ODEs is completely integrable. Desale and Dasre [4] have obtained the numerical solutions of this reduced system of ODEs. For the similar kind of work the reader may refer to Maas [5,6]. In his monograph Majda [7] has

* Corresponding author: mailto:bsdesale@rediffmail.com

obtained the special solution of stratified Boussinesq equations excluding the effects of viscosity and finite rotation. Whereas, Desale & Sharma [8] included the effect of rotation. In his earlier study Desale [9] has proved the complete integrability of the system of six coupled ODEs, which arises in the reduction of rotating stratified Boussinesq equations in context to the theory of basin scale dynamics. Since the rotating stratified Boussinesq equations admit the periodic solution near the critical point. On the other hand Desale & Patil [10] deployed the Painlevé test to determine the complete integrability of the same system. Further, the stability criteria can be resolved via Floquet theory. In their paper Slane & Tragesser [11] explained the use of Floquet theory to discuss the stability of homogeneous parametrically excited system.

In this paper we deploy the procedure of Majda & Shefter [2] to build the exact solutions of rotating stratified Boussinesq equations in the form of nonlinear plane waves. In the steady state these solutions increase exponentially. We conclude that the steady state is unstable. Whereas, in the special case of stable stratification these waves are oscillatory in nature. In this case, we also find internal gravity waves as some sinusoidal wave forms.

## 2 Nondimensional Rotating Stratified Boussinesq Equations

The motion of an incompressible flow of fluid in the atmosphere and in the ocean is considered where, the flow velocities are too slow to account for compressible effects. The flow of fluid is governed by the following rotating stratified Boussinesq equations (we ignore the effects of viscosity and heat dissipation) that involve the interaction of gravity with density stratification about the reference state.

$$\begin{aligned} \frac{D\vec{\mathbf{v}}}{Dt} + f(\hat{\mathbf{e_3}} \times \vec{\mathbf{v}}) &= -\nabla \frac{\tilde{p}}{\rho_b} - \frac{g\rho}{\rho_b}\hat{\mathbf{e_3}}, \\ \operatorname{div} \vec{\mathbf{v}} &= 0, \\ \frac{D\tilde{\rho}}{Dt} &= 0, \end{aligned} \tag{1}$$

where $D/Dt = \partial/\partial t + \vec{\mathbf{v}} \cdot \nabla$, the unit vector in vertical direction is $\hat{\mathbf{e_3}} = (0, 0, 1)$, the space variable $\vec{\mathbf{x}} = (x_1, x_2, x_3)$ and fluid velocity is given by $\vec{\mathbf{v}} = (v_1, v_2, v_3)$. The full density $\tilde{\rho}$ consists of perturbations $\rho$ about the density $\overline{\rho}$ in hydrostatic balance, which itself creates only small deviations from the baseline constant $\rho_b$, $\tilde{\rho}(\vec{\mathbf{x}}, t) = \rho_b + \overline{\rho}(x_3) + \rho(\vec{\mathbf{x}}, t)$. We make the usual assumption valid for local consideration that $d\overline{\rho}/dx_3$ is constant.

Now we consider the following nondimensional form of (1). For more details one may refer to Desale & Sharma [8].

$$\begin{aligned} \frac{D\vec{\mathbf{v}}}{Dt} + \frac{1}{R_0}\vec{\mathbf{u}} &= -\overline{P}\nabla p - \Gamma\rho\hat{\mathbf{e_3}}, \\ \operatorname{div} \vec{\mathbf{v}} &= 0, \\ \frac{D\tilde{\rho}}{Dt} &= \frac{D\rho}{Dt} + \left(\frac{d\overline{\rho}}{dx_3}\right) v_3 = 0. \end{aligned} \tag{2}$$

Here, we have $\vec{\mathbf{u}} = (u_1, u_2, u_3) = \hat{\mathbf{e_3}} \times \vec{\mathbf{v}}$, $\Gamma$ is the nondimensional number, $R_0$ is the Rossby number and $\overline{P}$ is the Euler number. Nondimensional density function is

$$\tilde{\rho}(\vec{\mathbf{x}}, t) = \rho_b + \overline{\rho}(x_3) + \rho(\vec{\mathbf{x}}, t). \tag{3}$$

The more elaborative discussion about the nondimensional analysis of rotating stratified Boussinesq equations is also given by Majda in his monograph [7]. In the following section we have obtained exact solutions of (2) in the form of nonlinear plane waves.

## 3 Nonlinear Plane Waves

In this section we have determined the exact solutions of rotating stratified Boussinesq equations (2) in the form of nonlinear plane waves. These solutions are suggested by the following Theorem 3.1. The following trivial lemma is useful step towards the proof of Theorem 3.1.

**Lemma 3.1** *For* $\vec{\mathbf{v}}$ *of the form* $\vec{\mathbf{v}} = \vec{\mathbf{A}}(t)F(\vec{\alpha}(t)\cdot\vec{\mathbf{x}})$, div $\vec{\mathbf{v}} = 0$ *implies*

(i) $\vec{\mathbf{A}}(t)\cdot\vec{\alpha}(t) = 0$ *and*
(ii) $\vec{\mathbf{v}}\cdot\nabla W(\vec{\alpha}(t)\cdot\vec{\mathbf{x}}) = 0$,

*for arbitrary* $W$, *where* $\vec{\mathbf{A}}(t) = (A_1(t), A_2(t), A_3(t))$ *and* $\vec{\alpha}(t) = (\alpha_1(t), \alpha_2(t), \alpha_3(t))$.

For the proof of this lemma one may refer to Majda [7], pp. 20.

**Theorem 3.1** *The rotating stratified Boussinesq equations (2) have exact solutions in the form of nonlinear plane waves*

$$\vec{\mathbf{v}} = \vec{\mathbf{A}}(t)F(\vec{\alpha}(t)\cdot\vec{\mathbf{x}}), \quad \rho = B(t)F(\vec{\alpha}(t)\cdot\vec{\mathbf{x}}), \quad p = P(t)G(\vec{\alpha}(t)\cdot\vec{\mathbf{x}}), \tag{4}$$

*where* $F$ *and* $G$ *are arbitrary functions of* $\vec{\alpha}(t)\cdot\vec{\mathbf{v}}$ *with the condition* $G'(s) = F(s)$ *provided that* $\vec{\alpha}(t)$, $\vec{\mathbf{A}}(t)$, $B(t)$ *and* $P(t)$ *satisfy the following ODEs:*

$$\begin{aligned}
&\frac{d\vec{\alpha}}{dt} = 0,\\
&\vec{\mathbf{A}}(t)\cdot\vec{\alpha}(t) = 0,\\
&P(t) = -\frac{1}{R_0\overline{P}}\left(\frac{\vec{\alpha}(t)\cdot(\hat{\mathbf{e_3}}\times\vec{\mathbf{A}}(t))}{|\vec{\alpha}(t)|^2}\right) - \frac{\Gamma\alpha_3(t)}{\overline{P}|\vec{\alpha}(t)|^2}B(t),\\
&\frac{d\vec{\mathbf{A}}(t)}{dt} = \frac{-1}{R_0}(\hat{\mathbf{e_3}}\times\vec{\mathbf{A}}(t)) + \left[\frac{\vec{\alpha}(t)\cdot(\hat{\mathbf{e_3}}\times\vec{\mathbf{A}}(t))}{R_0|\vec{\alpha}(t)|^2} + \frac{\Gamma\alpha_3(t)}{|\vec{\alpha}(t)|^2}B(t)\right]\vec{\alpha}(t) - \Gamma B(t)\hat{\mathbf{e_3}},\\
&\frac{dB(t)}{dt} + \frac{d\overline{\rho}}{dx_3}A_3(t) = 0.
\end{aligned}\tag{5}$$

***Proof.*** Now we begin with the first equation of (2)

$$\frac{\partial\vec{\mathbf{v}}}{\partial t} + \vec{\mathbf{v}}\cdot\nabla\vec{\mathbf{v}} = -\frac{1}{R_0}(\hat{\mathbf{e_3}}\times\vec{\mathbf{v}}) - \overline{P}\nabla p - \Gamma\rho\hat{\mathbf{e_3}}.$$

We have $\vec{\mathbf{v}} = \vec{\mathbf{A}}(t)F(\vec{\alpha}(t)\cdot\vec{\mathbf{x}})$, $\rho = B(t)F(\vec{\alpha}(t)\cdot\vec{\mathbf{x}})$, $p = P(t)G(\vec{\alpha}(t)\cdot\vec{\mathbf{x}})$ and div $\vec{\mathbf{v}} = 0$. Hence by substituting $\vec{\mathbf{v}}$, $\rho$ and $p$ in above equation with $G'(s) = F(s)$ and using Lemma 3.1 we get

$$\left(\frac{d\vec{\mathbf{A}}}{dt} + \frac{1}{R_0}(\hat{\mathbf{e_3}}\times\vec{\mathbf{A}}) + \overline{P}P(t)\vec{\alpha}(t) + \Gamma B(t)\hat{\mathbf{e_3}}\right)F(\vec{\alpha}\cdot\vec{\mathbf{x}}) = -\vec{\mathbf{A}}\left(\frac{d\vec{\alpha}}{dt}\cdot\vec{\mathbf{x}}\right)F'(\vec{\alpha}\cdot\vec{\mathbf{x}}). \tag{6}$$

Since $F$ and $F'$ are arbitrary functions, they must be treated as independent terms implying $\frac{d\vec{\alpha}(t)}{dt} = 0$, which is the first equation of (5). Consequently, (6) gives us

$$\frac{d\vec{\mathbf{A}}(t)}{dt} = -\frac{1}{R_0}(\hat{\mathbf{e_3}} \times \vec{\mathbf{A}}(t)) - \overline{P}P(t)\vec{\alpha}(t) - \Gamma B(t)\hat{\mathbf{e_3}}. \tag{7}$$

Lemma 3.1 proves the second equation of (5). Taking time derivative of $\vec{\mathbf{A}}(t) \cdot \vec{\alpha}(t) = 0$ with the validity of the first equation of (5), we have $\frac{d\vec{\mathbf{A}}(t)}{dt} \cdot \vec{\alpha}(t) = 0$. Then we take the dot product of the equation above for $\frac{d\vec{\mathbf{A}}(t)}{dt}$ with $\vec{\alpha}(t)$ and we determine equation for $P(t)$ as in the required form in (5). Plugging back $P(t)$ into (7) and recasting it we get the fourth equation of (5). Finally plugging plane waves into the third equation of (2) we get the differential equation for $B(t)$ as in the form of the last equation of (5). Hence we complete the proof of the theorem. □

The first equation in (5) shows that vector $\vec{\alpha}(t)$ is a constant vector and we have $\frac{d\overline{\rho}}{dx_3}$ is constant. We can write $\vec{\alpha} = (\alpha_1, \alpha_2, \alpha_3)$ and the last two equations of (5) can be written in component form as:

$$\begin{aligned}
\frac{dA_1(t)}{dt} &= \frac{1}{R_0}A_2(t) + \left[\frac{A_1(t)\alpha_2 - A_2(t)\alpha_1}{R_0|\vec{\alpha}|^2} + \frac{\Gamma\alpha_3 B(t)}{|\vec{\alpha}|^2}\right]\alpha_1, \\
\frac{dA_2(t)}{dt} &= -\frac{1}{R_0}A_1(t) + \left[\frac{A_1(t)\alpha_2 - A_2(t)\alpha_2}{R_0|\vec{\alpha}|^2} + \frac{\Gamma\alpha_3 B(t)}{|\vec{\alpha}|^2}\right]\alpha_2, \\
\frac{dA_3(t)}{dt} &= \left[\frac{A_1(t)\alpha_2 - A_2(t)\alpha_2}{R_0|\vec{\alpha}|^2} + \frac{\Gamma\alpha_3 B(t)}{|\vec{\alpha}|^2}\right]\alpha_3 - \Gamma B(t), \\
\frac{dB(t)}{dt} &+ \left(\frac{d\overline{\rho}}{dx_3}\right)A_3(t) = 0.
\end{aligned} \tag{8}$$

We see that above system (8) is a linear system with constant coefficients, hence there exists a unique solution passing through the given initial values that satisfy the condition $\vec{\mathbf{A}}(t) \cdot \vec{\alpha} = 0$. Plugging these solutions into plane waves given by (4), we determine the physical terms velocity, density and pressure.

In the following section we classified the fluids in the special case of plane waves in which the vectors $\hat{\mathbf{e_3}}, \vec{\mathbf{A}}(t)$ and $\vec{\alpha}$ are coplanar. Consequently we determined the internal gravity waves and sinusoidal waves.

## 4 Classification in the Special Case of Plane Waves

In this section we consider the special case of plane waves in which $\hat{\mathbf{e_3}}, \vec{\mathbf{A}}(t)$ and $\vec{\alpha}$ are coplanar. It means we consider $\hat{\mathbf{e_3}} \cdot (\vec{\mathbf{A}}(t) \times \vec{\alpha}) = 0$. So that equations (8) reduce to

$$\begin{aligned}
\frac{dA_1(t)}{dt} &= \frac{1}{R_0}A_2(t) + \frac{\Gamma\alpha_3\alpha_1}{|\vec{\alpha}|^2}B(t), \\
\frac{dA_2(t)}{dt} &= -\frac{1}{R_0}A_1(t) + \frac{\Gamma\alpha_3\alpha_2}{|\vec{\alpha}|^2}B(t), \\
\frac{dA_3(t)}{dt} &= \left(\frac{\alpha_3^2}{|\vec{\alpha}|^2} - 1\right)\Gamma B(t), \\
\frac{dB(t)}{dt} &= \left(-\frac{d\overline{\rho}}{dx_3}\right)A_3(t).
\end{aligned} \tag{9}$$

The scalar function $P(t)$ in pressure term becomes

$$P(t) = -\frac{\Gamma \alpha_3}{\overline{P}|\vec{\alpha}|^2} B(t). \tag{10}$$

Differentiating the last equation of (9) with respective time variable $t$ we get

$$\frac{d^2 B(t)}{dt^2} = \left(-\frac{d\overline{\rho}}{dx_3}\right) \frac{dA_3(t)}{dt}. \tag{11}$$

We recast the above equation by plugging back the equation for $\frac{dA_3(t)}{dt}$ from the third equation of (9) as follows

$$\frac{d^2 B(t)}{dt^2} = \frac{d\overline{\rho}}{dx_3} \left(1 - \frac{\alpha_3^2}{|\vec{\alpha}|^2}\right) \Gamma B(t) = -\omega^2(\vec{\alpha}) B(t). \tag{12}$$

Thus we observe that the behavior of solutions depends on the sign of $\omega^2$. Because the $\Gamma$ is nondimensional positive number and angular term in parentheses is always positive, the overall sign depends on the sign of the density gradient $\frac{d\overline{\rho}}{dx_3}$.

- **Case(i):** $\frac{d\overline{\rho}}{dx_3} > 0$ **(Heavier fluids on top).** This case will have exponentially growing solutions of the form $e^{|\omega| t}$. We conclude that steady state is unstable.
- **Case(ii):** $\frac{d\overline{\rho}}{dx_3} < 0$ **(Heavier fluids at bottom).** In this case equation (12) suggests that solutions will be oscillatory in nature. Hence we refer to it as stable stratification.

### 4.1 Sinusoidal Waves

In this subsection we determine sinusoidal plane waves in stable stratifications for $\frac{d\overline{\rho}}{dx_3} < 0$. We write the nondimensional form of buoyancy frequency or Brunt-Väisälä frequency

$$N = \left(-\Gamma \frac{d\overline{\rho}}{dx_3}\right)^{1/2}. \tag{13}$$

We use the notation to the general parameter $\vec{\alpha}$ as wave vector $\vec{\mathbf{k}} = (k_1, k_2, k_3) = (\vec{\mathbf{k}}_H, k_3) = \vec{\alpha} = (\alpha_1, \alpha_2, \alpha_3)$, so that $\omega$ as defined in (12) is given by

$$\omega(\vec{\mathbf{k}}) = N \frac{|\vec{\mathbf{k}}_H|}{|\vec{\mathbf{k}}|}. \tag{14}$$

The general solution of (12) is

$$B(t) = c_1 \sin(\omega(\vec{\mathbf{k}})t) + c_2 \cos(\omega(\vec{\mathbf{k}})t), \tag{15}$$

where $c_1$ and $c_2$ are arbitrary constants. The scalar function in pressure terms is given by

$$P(t) = -\frac{\Gamma k_3}{\overline{P}|\vec{\mathbf{k}}|^2} \Big[c_1 \sin(\omega(\vec{\mathbf{k}})t) + c_2 \cos(\omega(\vec{\mathbf{k}})t)\Big]. \tag{16}$$

Substituting (15) into the last equation of (9) we determine $A_3(t)$ as:

$$A_3(t) = \frac{\Gamma |\vec{\mathbf{k}}_H|}{N|\vec{\mathbf{k}}|} \Big[c_1 \cos(\omega(\vec{\mathbf{k}})t) - c_2 \sin(\omega(\vec{\mathbf{k}})t)\Big]. \tag{17}$$

Now to determine $A_1(t)$ and $A_2(t)$ we have the vector $\hat{\mathbf{e_3}}, \vec{\mathbf{A}}(t)$ and $\vec{\mathbf{k}}$ are coplanar. So that they satisfy the equation $A_2(t)k_1 - A_1(t)k_2 = 0$. But $A(t)$ is a function of time variable $t$ and wave vector $\vec{\mathbf{k}}$ is constant. Hence to meet the requirement $A_2(t)k_1 - A_1(t)k_2 = 0$, we consider the following cases that are related with the magnitude $\vec{\mathbf{k}}_H$.

1. $|\vec{\mathbf{k}}_H| \neq 0$**:** In this case we have the following possibilities.

   (a) Suppose that $k_1 \neq 0$, $k_2 = 0$. But this assumption along with $A_2(t)k_1 - A_1(t)k_2 = 0$ implies that $A_2(t) = 0$. If we plug $A_2(t) = 0$ in the first and second equations of (9) and solve these equations we get $A_1(t) = 0$. This is also true in either case $k_1 = 0$ and $k_2 \neq 0$.

   (b) Suppose $k_1 \neq 0$, $k_2 \neq 0$. But we required that $A_2(t)k_1 - A_1(t)k_2 = 0$, so that $A_1(t)$ must be equal to the constant multiple of $A_2(t)$. But in order to satisfy the first and second equations of (9) we conclude that $A_1(t)$ and $A_2(t)$ must be equal to zero.

   In this case we have

$$
\begin{aligned}
&A_1(t) = 0, \quad A_2(t) = 0,\\
&A_3(t) = \frac{\Gamma|\vec{\mathbf{k}}_H|}{N|\vec{\mathbf{k}}_H|}\Big(c_1\cos(\omega(\vec{\mathbf{k}})t) - c_2\sin(\omega(\vec{\mathbf{k}})t)\Big),\\
&B(t) = c_1\sin(\omega(\vec{\mathbf{k}})t) + c_2\cos(\omega(\vec{\mathbf{k}})t),\\
&P(t) = -\frac{\Gamma k_3}{\overline{P}|\vec{\mathbf{k}}|^2}\Big[c_1\sin(\omega(\vec{\mathbf{k}})t) + c_2\cos(\omega(\vec{\mathbf{k}})t)\Big].
\end{aligned}
\tag{18}
$$

   In order to write the physical variables, we must merely remember their definitions in Theorem 3.1. Recalling that $G'(s) = F(s)$, we have

$$
\begin{aligned}
&\vec{\mathbf{v}} = \frac{\Gamma|\vec{\mathbf{k}}_H|}{N|\vec{\mathbf{k}}|}\Big[c_1\cos(\omega(\vec{\mathbf{k}})t) - c_2\sin(\omega(\vec{\mathbf{k}})t)\Big]F(\vec{\mathbf{k}}\cdot\vec{\mathbf{x}})\hat{\mathbf{e_3}},\\
&\rho = \Big[c_1\sin(\omega(\vec{\mathbf{k}})t) + c_2\cos(\omega(\vec{\mathbf{k}})t)\Big]F(\vec{\mathbf{k}}\cdot\vec{\mathbf{x}}),\\
&p = -\frac{\Gamma k_3}{\overline{P}|\vec{\mathbf{k}}|^2}\Big[c_1\sin(\omega(\vec{\mathbf{k}})t) + c_2\cos(\omega(\vec{\mathbf{k}})t)\Big]G(\vec{\mathbf{k}}\cdot\vec{\mathbf{x}}).
\end{aligned}
\tag{19}
$$

   Equations (19) represent the special case of nonlinear plane waves with $k_3 \neq 0$ and are supported by the stable stratification, so we call them the internal gravity waves.

   In order to find sinusoidal wave forms, we put

$$
F(\vec{\mathbf{k}}\cdot\vec{\mathbf{x}}) = \sin(\vec{\mathbf{k}}\cdot\vec{\mathbf{x}}). \tag{20}
$$

   The density function in this case is

$$
\begin{aligned}
\rho &= \frac{c_1}{2}\Big[\cos(\omega(\vec{\mathbf{k}})t - \vec{\mathbf{k}}\cdot\vec{\mathbf{x}}) - \cos(\omega(\vec{\mathbf{k}})t + \vec{\mathbf{k}}\cdot\vec{\mathbf{x}})\Big]\\
&+ \frac{c_2}{2}\Big[\sin(\omega(\vec{\mathbf{k}})t + \vec{\mathbf{k}}\cdot\vec{\mathbf{x}}) - \sin(\omega(\vec{\mathbf{k}})t - \vec{\mathbf{k}}\cdot\vec{\mathbf{x}})\Big].
\end{aligned}
\tag{21}
$$

These calculations illustrate that there are waves moving in different directions corresponding to the two branches of dispersion relation. Let us simplify the case $c_2 = 0$ and we write the solutions

$$\begin{aligned} \rho &= \frac{c_1}{2}\left[\cos(\omega(\vec{\mathbf{k}})t - \vec{\mathbf{k}}\cdot\vec{\mathbf{x}}) - \cos(\omega(\vec{\mathbf{k}})t + \vec{\mathbf{k}}\cdot\vec{\mathbf{x}})\right], \\ p &= \frac{c_1}{2}\frac{\Gamma k_3}{\overline{P}|\vec{\mathbf{k}}|^2}\left[\sin(\omega(\vec{\mathbf{k}})t - \vec{\mathbf{k}}\cdot\vec{\mathbf{x}}) + \sin(\omega(\vec{\mathbf{k}})t + \vec{\mathbf{k}}\cdot\vec{\mathbf{x}})\right], \\ \vec{\mathbf{v}} &= \frac{c_1}{2}\frac{\Gamma|\vec{\mathbf{k}}_H|}{N|\vec{\mathbf{k}}|}\left[\sin(\omega(\vec{\mathbf{k}})t + \vec{\mathbf{k}}\cdot\vec{\mathbf{x}}) - \sin(\omega(\vec{\mathbf{k}})t - \vec{\mathbf{k}}\cdot\vec{\mathbf{x}})\right]\hat{\mathbf{e_3}}. \end{aligned} \tag{22}$$

2. $|\vec{\mathbf{k}}_H| = 0$ **:** In this case the horizontal components of wave vector are $k_1 = k_2 = 0$. The vector $\vec{\mathbf{A}}(t)$ and scalar function $B(t)$ have to satisfy the following differential equations:

$$\begin{aligned} &\frac{dA_1(t)}{dt} = \frac{1}{R_0}A_2(t), \quad \frac{dA_2(t)}{dt} = -\frac{1}{R_0}A_1(t), \\ &\frac{dA_3(t)}{dt} = 0, \quad \frac{dB(t)}{dt} = \left(-\frac{d\overline{\rho}}{dx_3}\right)A_3(t). \end{aligned} \tag{23}$$

Solving these equations, we get

$$\begin{aligned} A_1(t) &= c_1\cos(t/R_0) + c_2\sin(t/R_0), \\ A_2(t) &= -c_1\sin(t/R_0) + c_2\cos(t/R_0), \\ A_3(t) &= c_3, \quad B(t) = c_4(-\tfrac{d\overline{\rho}}{dx_3})t + c_5, \end{aligned} \tag{24}$$

where $c_1$, $c_2$, $c_3$, $c_4$ and $c_5$ are arbitrary constants. The scalar function $P(t)$ in pressure term is

$$P(t) = -\frac{\Gamma}{\overline{P}k_3}\left[c_4\left(-\frac{d\overline{\rho}}{dx_3}\right)t + c_5\right]. \tag{25}$$

In this special case of plane waves, the physical terms, namely the velocity, density and pressure involved in (2) are given by the following equations

$$\begin{aligned} \vec{\mathbf{v}} &= \Big(c_1\cos(\tfrac{t}{R_0}) + c_2\sin(\tfrac{t}{R_0}),\ -c_1\sin(\tfrac{t}{R_0}) + c_2\cos(\tfrac{t}{R_0}),\ c_3\Big)F(k_3x_3), \\ \rho &= \Big(c_4(-\tfrac{d\overline{\rho}}{dx_3})t + c_5\Big)F(k_3x_3), \\ p &= -\tfrac{\Gamma}{\overline{P}k_3}\left[c_4\left(-\tfrac{d\overline{\rho}}{dx_3}\right)t + c_5\right]G(k_3x_3). \end{aligned} \tag{26}$$

Now we put $F(\vec{\mathbf{k}}\cdot\vec{\mathbf{x}}) = F(k_3x_3) = \sin(k_3x_3)$ in equations (26) with $G'(s) = F(s)$ to determine the sinusoidal wave forms. These wave forms are:

$$\begin{aligned} \vec{\mathbf{v}} = \Big( &\tfrac{c_1}{2}\left[\sin(\tfrac{t}{R_0} + k_3x_3) - \sin(\tfrac{t}{R_0} - k_3x_3)\right] + \tfrac{c_2}{2}\left[\cos(\tfrac{t}{R_0} - k_3x_3) - \cos(\tfrac{t}{R_0} + k_3x_3)\right], \\ &-\tfrac{c_1}{2}\left[\cos(\tfrac{t}{R_0} - k_3x_3) - \cos(\tfrac{t}{R_0} + k_3x_3)\right] + \tfrac{c_2}{2}\left[\sin(\tfrac{t}{R_0} + k_3x_3) - \sin(\tfrac{t}{R_0} - k_3x_3)\right], \\ &c_3\sin(k_3x_3)\Big), \\ \rho = &\left[c_3(-\tfrac{d\overline{\rho}}{dx_3})t + c_4\right]\sin(k_3x_3), \\ p = &\tfrac{\Gamma}{\overline{P}k_3^2}\left[c_3\left(-\tfrac{d\overline{\rho}}{dx_3}\right)t + c_4\right]\cos(k_3x_3). \end{aligned} \tag{27}$$

The sinusoidal waves given by (27) with $k_3 \neq 0$ are supported by stable stratification so termed as internal gravity waves.

## 5 Conclusion

The special exact solutions of rotating stratified Boussinesq equations (2) in the form of nonlinear plane waves are obtained from the solutions of linear system (8). In the special case of fluids in which $\hat{\mathbf{e_3}}$, $\vec{\mathbf{A}}(t)$, $\vec{\alpha} = \vec{\mathbf{k}}$ are coplanar and $\frac{d\overline{\rho}}{dx_3} > 0$, the nonlinear plane waves given by (9) with $P(t)$ as in (10) grow exponentially. Whereas, if heavier fluids are at the bottom with $k_3 \neq 0$ then the plane waves given by (19) and (26) are oscillatory in nature. These waves are called the internal gravity waves. The exact solutions of (2) in the form of sinusoidal waves are given by (22) and (27).

## 6 Acknowledgement

The support of this research by the University Grants Commission, New Delhi 110 002, India (Research project F. No. 41-1380/2012(SR)) is greatly acknowledged.

## References

[1] Rajagopal, K. R., Ruzicka, M. and Srinivasa, A. R. On the Oberbeck-Boussinesq Approximation. *Mathematical Models and Methods in Applied Sciences* **6** (1996) 1157–1167.

[2] Majda, A. J. and Shefter, M. G. Elementary stratified flows with instability at large Richardson number. *J. Fluid Mechanics* **376** (1998) 319–350.

[3] Srinivasan, G. K., Sharma, V. D. and Desale, B. S. An integrable system of ODE reductions of the stratified Boussinesq equations. *Computers and Mathematics with Applications* **53** (2007) 296–304.

[4] Desale, B. S. and Dasre, N. R. Numerical Solutions of System of Non-linear ODEs by Euler Modified Method. *Nonlinear Dynamics and Systems Theory* **12(3)** (2012) 215–236.

[5] Maas, Leo R. M. Theory of Basin Scale Dynamics of a Stratified Rotating Fluid. *Surveys in Geophysics* **25** (2004) 249–279.

[6] Maas, Leo R. M. A Simple Model for the Three-dimensional Thermally and Wind-driven Ocean Circulation. *Tellus* **46A** (1994) 671–680.

[7] Majda, A. J. *I*ntroduction to PDEs and Waves for the Atmosphere and Ocean. Courant Lecture Notes in Mathematics 9. American Mathematical Society, Providence, Rhode Island, 2003.

[8] Desale, B. S. and Sharma, V. Special Solutions to Rotating Stratified Boussinesq Equations. *Nonlinear Dynamics and Systems Theory* **10(1)** (2010) 29–38.

[9] Desale, B. S. Complete analysis of an ideal rotating uniformly stratified system of ODEs. *Nonlinear Dynamics and Systems Theory* **9(3)** (2009) 263–275.

[10] Desale, B. S. and Patil K. D. Painlevé Test to a Reduced System of Six Coupled Nonlinear ODEs. *Nonlinear Dynamics and Systems Theory* **10(4)** (2010) 340–361.

[11] Slane, J. and Tragesser, S. Analysis of Periodic Nonautonomous Inhomogeneous Systems. *Nonlinear Dynamics and Systems Theory* **11(2)** (2011) 183–198.

Nonlinear Dynamics and Systems Theory, **12** (4) (2012) 383–388

# A Compactness Condition for Solutions of Nonlocal Boundary Value Problems of Orders $n = 3, 4$ & $5$ [†]

J. Henderson [*]

*Department of Mathematics, Baylor University, Waco, TX 76798-7328, USA*

Received: May 6, 2011; Revised: October 7, 2012

**Abstract:** For the ordinary differential equation, $y^{(n)} = f(x, y, y', \ldots, y^{(n-1)})$, of order $n = 3, 4$, or 5, it is shown that the existence of unique solutions of certain 4-point nonlocal boundary value problems implies a compactness condition on uniformly bounded sequences of solutions.

**Keywords:** *boundary value problem; nonlocal; continuous dependence; compactness condition.*

**Mathematics Subject Classification (2010):** 34B10, 34B15.

## 1 Introduction

In a recent paper, for $n \geq 3$ and $1 \leq k \leq n-1$, Henderson [6] studied solutions of the ordinary differential equation,

$$y^{(n)} = f(x, y, y', \ldots, y^{(n-1)}), \quad a < x < b, \tag{1}$$

satisfying the $(k+2)$-point nonlocal boundary conditions,

$$\begin{aligned} &y^{(i-1)}(x_j) = y_{ij},\ 1 \leq i \leq m_j,\ 1 \leq j \leq k, \\ &y(x_{k+1}) - y(x_{k+2}) = y_n, \end{aligned} \tag{2}$$

for positive integers $m_1, \ldots, m_k$ such that $m_1 + \cdots + m_k = n-1$, points $a < x_1 < x_2 < \cdots < x_k < x_{k+1} < x_{k+2} < b$, real values $y_{ij}, 1 \leq i \leq m_j, 1 \leq j \leq k$, and $y_n \in \mathbb{R}$. In particular, sufficient conditions were given under which the existence of solutions for 4-point nonlocal boundary value problems for (1), (2), (that is, when $k = 2$), led to the existence of unique solutions of $(k+2)$-point nonlocal boundary value problems for (1), (2), for all $1 \leq k \leq n-1$.

Fundamental to that paper's main result was the following list of assumptions on solutions of (1).

[†] In memory of Professor Keith W. Schrader, April 22, 1938 – December 27, 2010.

[*] Corresponding author: mailto:Johnny_Henderson@baylor.edu

(A) $f : (a, b) \times \mathbb{R}^n \to \mathbb{R}$ is continuous.

(B) Solutions of initial value problems for (1) are unique and extend to $(a, b)$.

(C) Boundary value problems (1), (2), for $k = 2$, have solutions on $(a, b)$.

(D) Boundary value problems (1), (2), for $k = n - 2$, have at most one solution.

(E) If $\{y_\nu(x)\}$ is a sequence of solutions of (1) which is uniformly bounded on a nondegenerate compact subinterval $[c, d] \subset (a, b)$, then there is a subsequence $\{y_{\nu_j}(x)\}$ such that $\{y^{(i)}_{\nu_j}(x)\}$ converges uniformly on each compact subinterval of $(a, b)$, for each $i = 0, \ldots, n - 1$.

Under these assumptions, and in conjunction with a uniqueness implies existence result by Eloe and Henderson [3], the following existence result was the main result of paper [6].

**Theorem 1.1** *Assume that with respect to* (1), *conditions* (A)–(E) *are satisfied. Then, for each* $1 \leq k \leq n - 1$, *solutions of* (1), (2) *exist and are unique on* $(a, b)$.

One question that arises, and which is the motivation for this paper, is whether conditions (A) – (D) imply the so-called "Compactness Condition" (E) on sequences of solutions of (1). The study of hypotheses sufficient to imply (E) has a long history, especially in the context of boundary value problems for (1) satisfying $\ell$-point *conjugate* boundary conditions, for $2 \leq \ell \leq n$, of the form,

$$y^{(i-1)}(t_j) = r_{ij},\ 1 \leq i \leq p_j,\ 1 \leq j \leq \ell, \tag{3}$$

where $p_1, \ldots, p_\ell$ are positive integers such that $p_1 + \cdots + p_\ell = n$, $a < t_1 < \cdots < t_\ell < b$, and $r_{ij} \in \mathbb{R}, 1 \leq i \leq p_j, 1 \leq j \leq \ell$.

In the conjugate boundary value problem context, a principal question of the 1960's through the mid-1980's involved whether conditions (A) and (B) and uniqueness of solutions of $n$-point conjugate boundary value problems (1), (3) implied the Compactness Condition (E). This was answered in the affirmative for equation (1), when $n = 2$ and 3, by Jackson [10] and Jackson and Schrader [13]. Other extensive inroads were made in addressing the question for (1) of arbitrary order $n$ in the papers [1, 5, 7–9, 11, 12, 14–17]. In 1985, in an unpublished paper, Schrader [18] announced that the conjecture had been verified. Later, Agarwal [2] gave a detailed presentation of the history and resolution of the conjecture for conjugate boundary value problems.

Much in the spirit of the work done regarding (E) with respect to solutions of conjugate boundary value problems, we show in this paper that when (1) is of any of the orders, $n = 3,\ 4$, or 5, then existence of unique solutions of (1), (2), for $k = 2$, and conditions (A) and (B) imply the Compactness Condition (E).

Each of these cases for $n$ will depend on continuous dependence of solutions of (1), (2) on boundary conditions. We will refer to the following continuous dependence theorem [3], whose proof relies on a standard application of the Brouwer theorem on invariance of domain [19].

**Theorem 1.2** *Assume that with respect to* (1), (2), *conditions* (A) *and* (B) *are satisfied. Assume that, for* $k = 2$ *and any positive integers* $m_1$ *and* $m_2$ *such that* $m_1 + m_2 = n - 1$, *solutions of the corresponding nonlocal boundary value problem* (1), (2) *are unique, when they exist. Given a solution* $y(x)$ *of* (1), *an interval* $[c, d]$, *points* $c < x_1 <$

*$x_2 < x_3 < x_4 < d$ and an $\epsilon > 0$, there exists $\delta(\epsilon, [c,d]) > 0$ such that, if $|x_i - \xi_i| < \delta$, $i = 1,2,3,4$, and $c < \xi_1 < \xi_2 < \xi_3 < \xi_4 < d$, and if $|y^{(i-1)}(x_j) - z_{ij}| < \delta$, $1 \le i \le m_j$, $j = 1,2$ and $|y(x_3) - y(x_4) - z_n| < \delta$, then there exists a solution $z(x)$ of* (1) *satisfying $z^{(i-1)}(\xi_j) = z_{ij}$, $1 \le i \le m_j$, $j = 1,2$, $z(\xi_3) - z(\xi_4) = z_n$, and $|y^{(i)}(x) - z^{(i)}(x)| < \epsilon$ on $[c,d]$, $0 \le i \le n-1$.*

## 2 The Compactness Condition: n =3, 4, 5

In this section, we show that, for $n = 3,4$, or 5, conditions (A) and (B) and the existence of unique solutions of (1), (2), for $k = 2$, imply the Compactness Condition (E).

**Theorem 2.1** *For $n = 3$, 4, or 5, assume that with respect to* (1), *conditions* (A) *and* (B) *hold, and in addition, that there exist unique solutions of* (1), (2), *for $k = 2$. Then condition* (E) *also holds.*

***Proof.*** We will address the case of each $n$ independently.
(a) $n = 3$. In this case, we are assuming that, for each pair of positive integers $m_1$ and $m_2$ such that $m_1 + m_2 = n - 1 = 2$ (that is, $m_1 = m_2 = 1$), there exist unique solutions of (1), (2); that is, there exists a unique solution of (1) satisfying

$$y(x_1) = y_1,\ y(x_2) = y_2,\ y(x_3) - y(x_4) = y_3,$$

where $a < x_1 < x_2 < x_3 < x_4 < b$ and $y_1, y_2, y_3 \in \mathbb{R}$. From Rolle's theorem, solutions of 3-point conjugate boundary value problems (1), (3) are unique, when they exist. As a consequence of the Jackson and Schrader [13] result for third order conjugate boundary value problems, or as a result of the more general result by Schrader [18] which was detailed in the Introduction, it follows that the Compactness Condition (E) is satisfied.

(b) $n = 4$. In this case, we are assuming that, for each pair of positive integers $m_1$ and $m_2$ such that $m_1 + m_2 = n - 1 = 3$, there are unique solutions of (1), (2); that is, for any $a < x_1 < x_2 < x_3 < x_4 < b$ and $y_1, y_2, y_3, y_4 \in \mathbb{R}$, there exists a unique solution of (1) satisfying

$$y(x_1) = y_1,\ y'(x_1) = y_2,\ y(x_2) = y_3,\ y(x_3) - y(x_4) = y_4,$$

and there exists a unique solution of (1) satisfying

$$y(x_1) = y_1,\ y(x_2) = y_2,\ y'(x_2) = y_3,\ y(x_3) - y(x_4) = y_4.$$

We now assume there are $a < c < d < b$, a number $M > 0$, and a sequence $\{y_\nu\}$ of solutions of (1) such that, for each $\nu \ge 1$,

$$|y_\nu(x)| \le M, \quad c \le x \le d.$$

Next, let the points $c < \eta_1 < x_2 < x_3 < x_4 < d$ be given. Then, for each $\nu \ge 1$, there exists $\xi_\nu \in (c, \eta_1)$ such that

$$|y'_\nu(\xi_\nu)| \le \frac{2M}{\eta_1 - c}.$$

This leads to the five bounded sequences of real numbers,

$$\{\xi_\nu\} \subset (c, \eta_1), \quad \{y_\nu(\xi_\nu)\} \subset [-M, M], \quad \{y'_\nu(\xi_\nu)\} \subset \left[\frac{-2M}{\eta_1 - c}, \frac{2M}{\eta_1 - c}\right],$$
$$\{y_\nu(x_2)\} \subset [-M, M], \text{ and } \{y_\nu(x_3) - y_\nu(x_4)\} \subset [-2M, 2M].$$

Hence, there exist a subsequence $\{\nu_j\} \subset \{\nu\}$, a point $x_1 \in [c, \eta_1]$ and $\gamma_1, \gamma_2, \gamma_3, \gamma_4 \in \mathbb{R}$ such that

$$\xi_{\nu_j} \to x_1, \quad y_{\nu_j}(\xi_{\nu_j}) \to \gamma_1, \quad y'_{\nu_j}(\xi_{\nu_j}) \to \gamma_2,$$
$$y_{\nu_j}(x_2) \to \gamma_3, \text{ and } \quad \{y_{\nu_j}(x_3) - y_{\nu_j}(x_4)\} \to \gamma_4.$$

Now, let $y(x)$ be the solution of (1), (2), for $k = 2$, satisfying

$$y(x_1) = \gamma_1, \; y'(x_1) = \gamma_2, \; y(x_2) = \gamma_3, \text{ and } y(x_3) - y(x_4) = \gamma_4.$$

It follows from Theorem 1.2 that

$$\lim y^{(i)}_{\nu_j}(x) = y^{(i)}(x) \text{ uniformly on } [c, d],$$

for each $i = 0, 1, 2, 3$. It follows in turn, from (A) and (B) and the Kamke Convergence Theorem [4, page 14, Theorem 3.2], that these convergences are uniform on each compact subinterval of $(a, b)$.

(c) $n = 5$. This time, we assume that, for each pair of positive integers $m_1$ and $m_2$ such that $m_1 + m_2 = n - 1 = 4$, there are unique solutions of (1), (2); that is, for any $a < x_1 < x_2 < x_3 < x_4 < b$ and $y_1, y_2, y_3, y_4, y_5 \in \mathbb{R}$, there exists a unique solution of (1) satisfying

$$y(x_1) = y_1, \; y'(x_1) = y_2, \; y''(x_1) = y_3, \; y(x_2) = y_4, \; y(x_3) - y(x_4) = y_5,$$

there exists a unique solution of (1) satisfying

$$y(x_1) = y_1, \; y'(x_1) = y_2, \; y(x_2) = y_3, \; y'(x_2) = y_4, \; y(x_3) - y(x_4) = y_5,$$

and there exists a unique solution of (1) satisfying

$$y(x_1) = y_1, \; y(x_2) = y_2, \; y'(x_2) = y_3, \; y''(x_2) = y_4, \; y(x_3) - y(x_4) = y_5.$$

Again, we assume there are $a < c < d < b$, a number $M > 0$, and a sequence $\{y_\nu\}$ of solutions of (1) such that, for each $\nu \geq 1$,

$$|y_\nu(x)| \leq M, \quad c \leq x \leq d.$$

Let the points $c < \eta_1 < \eta_2 < \eta_3 < x_3 < x_4 < d$ be given. Then, for each $\nu \geq 1$, there exist $\xi_\nu \in (c, \eta_1)$ and $\sigma_\nu \in (\eta_2, \eta_3)$ such that

$$|y'_\nu(\xi_\nu)| \leq \frac{2M}{\eta_1 - c} \text{ and } |y'_\nu(\sigma_\nu)| \leq \frac{2M}{\eta_3 - \eta_2}.$$

Then we have the seven bounded sequences of real numbers,

$$\{\xi_\nu\} \subset (c, \eta_1), \; \{\sigma_\nu\} \subset (\eta_2, \eta_3), \; \{y_\nu(\xi_\nu)\} \subset [-M, M], \; \{y'_\nu(\xi_\nu)\} \subset \left[\frac{-2M}{\eta_1 - c}, \frac{2M}{\eta_1 - c}\right],$$
$$\{y_\nu(\sigma_\nu)\} \subset [-M, M], \; \{y'_\nu(\sigma_\nu)\} \subset \left[\frac{-2M}{\eta_3 - \eta_2}, \frac{2M}{\eta_3 - \eta_2}\right], \; \& \; \{y_\nu(x_3) - y_\nu(x_4)\} \subset [-2M, 2M].$$

As in the previous case, there exist a subsequence $\{\nu_j\} \subset \{\nu\}$, points $x_1 \in [c, \eta_1]$ and $x_2 \in [\eta_2, \eta_3]$, and $\gamma_1, \gamma_2, \gamma_3, \gamma_4, \gamma_5 \in \mathbb{R}$ such that,

$$\xi_{\nu_j} \to x_1,\ \sigma_{\nu_j} \to x_2,\ y_{\nu_j}(\xi_{\nu_j}) \to \gamma_1,\ y'_{\nu_j}(\xi_{\nu_j}) \to \gamma_2,$$
$$y_{\nu_j}(\sigma_{\nu_j}) \to \gamma_3,\ y'_{\nu_j}(\sigma_{\nu_j}) \to \gamma_4,\ \text{and} \quad \{y_{\nu_j}(x_3) - y_{\nu_j}(x_4)\} \to \gamma_5.$$

Let $y(x)$ be the solution of (1), (2), for $k = 2$, satisfying

$$y(x_1) = \gamma_1,\ y'(x_1) = \gamma_2,\ y(x_2) = \gamma_3,\ y'(x_2) = \gamma_4,\ \text{and}\ y(x_3) - y(x_4) = \gamma_5.$$

As above, it follows from Theorem 1.2 that

$$\lim y^{(i)}_{\nu_j}(x) = y^{(i)}(x) \text{ uniformly on } [c, d],$$

for each $i = 0, 1, 2, 3, 4$, and from (A) and (B) and the Kamke Convergence Theorem [4, page 14, Theorem 3.2], these convergences are uniform on each compact subinterval of $(a, b)$. □

We remark that in [6], it was proved that condition (D) implies uniqueness of solutions of (1), (2), when solutions exist, for $1 \le k \le n - 2$. As a consequence of that and by Theorem 2.1, we can give a stronger result than Theorem 1.2, for $n = 3, 4, 5$.

**Theorem 2.2** *For $n = 3,\ 4,$ or $5$, assume that with respect to* (1)*, conditions* (A)–(D) *are satisfied. Then, for each $1 \le k \le n-1$, solutions of* (1)*,* (2) *exist and are unique on* $(a, b)$.

## References


[1] Agarwal, R. P. *Boundary value problems for higher order differential equations.* World Scientific, Singapore, 1986.

[2] Agarwal, R. P. Compactness condition for boundary value problems. In: *Proceedings Conference on Differential Equations and Applications, EQUDIFF 9, Brno, August 25–29, 1997* (R. P. Agarwal, F. Neuman and J. Vosmanský, eds.). Electronic Publishing House, Stony Brook, 1998, 1–23.

[3] Eloe, P. W. and Henderson, J. Uniqueness implies existence and uniqueness conditions for nonlocal boundary value problems for $n$th order differential equations. *J. Math. Anal. Appl.* **331** (2007) 240–247.

[4] Hartman, P. *Ordinary differential equations.* Wiley, New York, 1964.

[5] Hartman, P. On $N$-parameter families and interpolation problems for nonlinear ordinary differential equations. *Trans. Amer. Math. Soc.* **154** (1971) 201–226.

[6] Henderson, J. Existence and uniqueness of solutions of $(k + 2)$-point nonlocal boundary value problems for ordinary differential equations. *Nonlinear Anal.* **74** (2011) 2576–2584.

[7] Henderson, J. and Jackson, L. K. Existence and uniqueness of solutions of $k$-point boundary value problems for ordinary differential equations. *J. Differential Equations* **48** (1983) 373–385.

[8] Jackson, L. K. Uniqueness and existence of solutions of boundary value problems for ordinary differential equations. In: *Proceedings NRL-MRC Conference on Ordinary Differential Equations, Washington, DC.* Academic Press, New York, 1972, 137–149.

[9] Jackson, L. K. Uniqueness of solutions of boundary value problems for ordinary differential equations. *SIAM J. Appl. Math.* **24** (1973), 535–538.

[10] Jackson, L. K. Existence and uniqueness of solutions for third order differential equations. *J. Differential Equations* **13** (1973) 432–437.

[11] Jackson, L. K. A compactness condition for solutions of ordinary differential equations. *Proc. Amer. Math. Soc.* **57** (1) (1976) 89–92.

[12] Jackson, L. K. and Klaasen, G. Uniqueness of solutions of boundary value problems for ordinary differential equations. *SIAM J. Appl. Math.* **19** (1970) 542–546.

[13] Jackson, L. K. and Schrader, K. Existence and uniqueness of solutions of boundary value problems for third order differential equations. *J. Differential Equations* **9** (1971) 46–54.

[14] Klaasen, G. A. Existence theorems for boundary value problems for $n$th order ordinary differential equations. *Rocky Mountain. J. Math.* **3** (1973) 457–472.

[15] Klaasen, G. A. Continuous dependence for $N$-point boundary value problems. *SIAM J. Appl. Math.* **29** (1975) 99–102.

[16] Schrader, K. A pointwise convergence theorem for sequences of continuous functions. *Trans. Amer. Math. Soc.* **159** (1971) 155–163.

[17] Schrader, K. A generalization of the Helly selection theorem. *Bull. Amer. Math. Soc.* **78** (1972) 415–419.

[18] Schrader, K. Uniqueness implies existence for solutions of nonlinear boundary value problems. *Abstracts Amer. Math. Soc.* **6** (1985) 235.

[19] Spanier, E. H. *Algebraic topology.* McGraw-Hill, New York, 1966.

Nonlinear Dynamics and Systems Theory, **12** (4) (2012) 389–396

# A computational Method for Solving a System of Volterra Integro-differential Equations

H. Jafari [1*] and A. Azad [2]

[1] *Department of Mathematics, University of Mazandaran, Babolsar, Iran.*
[2] *Young Research Club, Islamic Azad University-Ayatollah Amoli Branch, Amol, Iran*

Received: December 6, 2011; Revised: October 8, 2012

**Abstract:** In this paper we present a reliable algorithm for solving a system of Volterra integro-differential equations using Taylor series expansion method and computer algebra. This method converts a system of Volterra integro-differential equations to a system of linear algebraic equations. Some illustrative examples have been presented to illustrate the implementation of the algorithm and efficiency of the method.

**Keywords:** *system of Volterra integro-differential equations; Taylor-series expansion method; ordinary differential equations; system of linear algebraic equations.*

**Mathematics Subject Classification (2010):** 45J05, 34K28.

## 1 Introduction

A number of problems in chemistry, physics and engineering are modeled in terms of system of Volterra integro-differential equations. Various methods have been developed to prove existence and uniqueness of solutions to integro-differential equations [3].

In this paper, we use a modified Taylor-series expansion method for solving system of Volterra integro-differential equations. This method was first presented by Kanwal and Liu et. al. [1] for solving integral equations and in [2, 6] for solving Fredholm integral equations of second kind. Daftardar-Gejji et. al. have used this method for solving system of ordinary differential equations [4]. Maleknejad et. al. have applied this method for solving Volterra integral equations and system of Volterra integral equations

* Corresponding author: mailto:jafari@umz.ac.ir

of second kind [5,7]. Yalcinbas and Sezer [8] have studied the following type of nonlinear Fredholm-Volterra integral equations

$$y(x) = f(x) + \lambda_1 \int_a^x k_1(x,t)[y(t)]^p \, dt + \lambda_2 \int_a^b k_2(x,t) y(t) \, dt, \tag{1}$$

and the high-order linear and nonlinear Volterra-Fredholm integro-differential equations have been considered in [9,10]

$$\sum_{j=0}^{m} P_j(x) \, y^{(j)}(x) = f(x) + \lambda_1 \int_a^x k_1(x,t) y(t) \, dt + \lambda_2 \int_a^b k_2(x,t) y(t) \, dt, \tag{2}$$

$$\sum_{j=0}^{m} P_j(x) \, y^{(j)}(x) = f(x) + \lambda_1 \int_a^x k_1(x,t)[y(t)]^p \, dt + \lambda_2 \int_a^b k_2(x,t)[y(t)]^q \, dt. \tag{3}$$

In this paper, the basic ideas of the previous work [6] are developed and applied to the high-order system of Volterra integro-differential equation of the form

$$\sum_{i=1}^{n} \sum_{j=0}^{m} a_{ijs}(x) \, y_i^{(j)}(x) = f_s(x) + \sum_{i=1}^{n} \int_a^x k_{is}(x,t) y_i(t) dt, \qquad s = 1, 2, \cdots, n, \tag{4}$$

where $a_{ijs}(x)$ , $f_s(x) \, (s = 1, 2, \cdots, n)$ and $k_{is}(x,t)$ are known functions which are $l$th derivatable on interval $a \leq x, t \leq b$.

We assume that (4) has a unique solution. Suppose the solution of (4), can be expressed in the form:

$$y_i(x) = \sum_{r=0}^{N} \frac{1}{r!} y_i^{(r)}(\xi) \, (x - \xi)^r, \; a \leq x, \xi \leq b, \tag{5}$$

which is a Taylor polynomial of degree $N$, where $N \geq \{n_{ijs}, n_s\}$, and $y^{(s)}(\xi) \, (s = 0, 1, \cdots, N)$ are the coefficients to be determined.

## 2 Analysis of Method

First, we rewrite (4) in the following form

$$D(x) = I(x), \tag{6}$$

where $D(x) = [D_1(x), D_2(x), ..., D_n(x)]^T, \quad I(x) = [I_1(x), I_2(x), ..., I_n(x)]^T$,

$$D_s(x) = \sum_{i=1}^{n} \sum_{j=0}^{m} a_{ijs}(x) y_i^{(j)}(x), \qquad I_s(x) = f_s(x) + \sum_{i=1}^{n} V_{is}(x), \qquad s = 1, 2, \cdots, n, \tag{7}$$

with

$$V_{is}(x) = \int_a^x k_{is}(x,t) y_i(t) dt. \tag{8}$$

Then $D(x)$ is called the differential part and $I(x)$ the integral part of (4). Differentiating Eq. (6) $N$ times with respect to $x$, we get

$$D_s^l(x) = I_s^l(x), \quad l = 0, 1, \cdots, N, \; s = 1, 2, \cdots, n. \tag{9}$$

In the following part, we will analyse the expressions $D_s^l(x)$ and $I_s^l(x)$. It is easy to see that

$$\begin{aligned} D_s^{(l)}(x) &= \left[\sum_{i=1}^{n}\sum_{j=0}^{m} a_{ijs}(x)\, y_i^{(j)}(x)\right]^{(l)} \\ &= \left[\sum_{j=0}^{m} a_{1js}(x)\, y_1^{(j)}(x)\right]^{(l)} + \cdots + \left[\sum_{j=0}^{m} a_{njs}(x)\, y_n^{(j)}(x)\right]^{(l)}, \\ & \qquad l = 0, 1, \cdots, N,\ s = 1, 2, \cdots, n \end{aligned} \tag{10}$$

Using Leibnitz's rule (dealing with differentiation of products of functions), simplifying and then substituting $x = \xi$ into the resulting relation, we can get

$$D_s^{(l)}(x) = \sum_{i=1}^{n}\sum_{j=0}^{m}\sum_{p=0}^{l} \binom{l}{p} a_{ijs}^{(l-p)}(x)\, y_i^{(p+j)}(x), \quad l = 1, 2, \cdots, N,\ s = 0, 1, \cdots, n. \tag{11}$$

The system (11) can be written in the matrix form as:

$$\mathbf{D} = \mathbf{W}\mathbf{Y}, \tag{12}$$

where $\mathbf{Y} = \left[y_1^{(0)}, y_1^{(1)}, \cdots, y_1^{(N)}, y_2^{(0)}, \cdots, y_2^{(N)}, \cdots, y_n^{(0)}, \cdots, y_n^{(N)}\right]^T$. Note that

$$\mathbf{W} = [W_{is}] \qquad i, s = 1, 2, \cdots, n, \tag{13}$$

is a matrix, where each $W_{is}$ is again a matrix:

$$w_{is}^{lp} = \sum_{q=0}^{m} \binom{l}{p-m+q} a_{im-qs}^{(l-p+m-q)}(\xi), \quad l, p = 0, 1, \cdots, N. \tag{14}$$

**Note:** For $r < 0$, $a_{ijs}^{(r)} = 0$ and for $j < 0$ and $j > i$, $\binom{i}{j} = 0$, where $i, j$ and $r$ are integers. On the other hand, for the integral part $I_s^l(x)$, it is easy to know that

$$I_s^{(l)}(x) = f_s^{(l)}(x) + \sum_{i=1}^{n} V_{is}^{(l)}(x), \quad l = 0, 1, \cdots, N, \tag{15}$$

where

$$\begin{aligned} V_{is}^{(l)}(x) &= \frac{\partial^l}{\partial x^l}\int_a^x k_{is}(x,t) y_i(t)\,dt \\ &= \sum_{j=0}^{l-1}\left[h_{is}^j(x) y_i(x)\right]^{l-j-1} + \int_a^x \frac{\partial^l k_{is}(x,t)}{\partial x^l} y_i(t)\,dt \\ &= \sum_{r=0}^{l-1}\sum_{j=0}^{l-r-1}\binom{l-j-1}{r}\left(h_{is}^j(x)\right)^{(l-r-j-1)} y_i^{(r)}(x) + \int_a^x \frac{\partial^l k_{is}(x,t)}{\partial x^l} y_i(t)\,dt, \end{aligned} \tag{16}$$

with

$$h_{is}^{j}(x)=\frac{\partial^{j}k_{is}(x,t)}{\partial x^{j}}|_{t=x}.$$

By Using Leibnitz's rule and substituting (5) in (16), we can get

$$\begin{aligned} I_s^{(l)}(\xi) &= f_s^{(l)}(\xi)+\sum_{r=0}^{l-1}\sum_{j=0}^{l-r-1}\binom{l-j-1}{r}\left(h_{is}^{j}(\xi)\right)^{(l-r-j-1)}y_i^{(r)}(\xi) \\ &\quad+\int_a^{\xi}\frac{\partial^{l}k_{is}(x,t)}{\partial x^{l}}|_{x=\xi}\left[\sum_{r=0}^{\infty}\frac{1}{r!}y_i^{(r)}(\xi)\,(t-\xi)^{r}\right]dt \qquad (17)\\ &= f_s^{(l)}(x)+\sum_{r=0}^{l-1}(H_{is}^{lr}+T_{is}^{lr})y_i^{(r)}(\xi)+\sum_{r=l}^{\infty}T_{is}^{lr}y_i^{(r)}(\xi). \end{aligned}$$

For the case of computing in practice, the approximate form of system (17) can be put in as follows:

$$I_s^{(l)}(\xi)=f_s^{(l)}(\xi)+\sum_{r=0}^{l-1}(H_{is}^{lr}+T_{is}^{lr})y_i^{(r)}(\xi)+\sum_{r=l}^{N}T_{is}^{lr}y_i^{(r)}(\xi), \qquad (18)$$

where for $l=1,2,\cdots,N;\ \ r=0,1,\cdots,l-1\ \ (l>r)$

$$H_{is}^{lr}=\sum_{j=0}^{l-r-1}\binom{l-j-1}{r}\left(h_{is}^{j}(\xi)\right)^{(l-r-j-1)} \qquad (19)$$

and for $l\le r$, $H_{is}^{lr}=0$. and

$$T_{is}^{lr}=\frac{1}{r!}\int_a^{\xi}\frac{\partial^{l}k_{is}(x,t)}{\partial x^{l}}|_{x=\xi}\,(t-\xi)^{r}dt, \quad l,r=0,1,\cdots,N. \qquad (20)$$

This system can be put in the matrix form as

$$\mathbf{I}=\mathbf{F}+\mathbf{TY}. \qquad (21)$$

(21) combined with (13)

$$\mathbf{WY}=\mathbf{F}+\mathbf{TY}\quad\textbf{or}\quad(\mathbf{W}-\mathbf{T})\mathbf{Y}=\mathbf{F}, \qquad (22)$$

where

$$\mathbf{W}=[w_{is}^{lr}]=\begin{bmatrix} w_{11}^{00} & w_{11}^{01} & \cdots & w_{11}^{0N} & \cdots & w_{1n}^{00} & w_{1n}^{01} & \cdots & w_{1n}^{0N}\\ w_{11}^{10} & w_{11}^{11} & \cdots & w_{11}^{1N} & \cdots & w_{1n}^{00} & w_{1n}^{01} & \cdots & w_{1n}^{0N}\\ \cdots & \cdots & \cdots & \cdots & \cdots & \cdots & \cdots & \cdots & \cdots\\ w_{11}^{N0} & w_{11}^{N1} & \cdots & w_{11}^{NN} & \cdots & w_{1n}^{N0} & w_{1n}^{N1} & \cdots & w_{1n}^{NN}\\ \cdots & \cdots & \cdots & \cdots & \cdots & \cdots & \cdots & \cdots & \cdots\\ w_{n1}^{00} & w_{n1}^{01} & \cdots & w_{n1}^{0N} & \cdots & w_{nn}^{00} & w_{nn}^{01} & \cdots & w_{nn}^{0N}\\ w_{n1}^{10} & w_{n1}^{11} & \cdots & w_{n1}^{1N} & \cdots & w_{nn}^{00} & w_{nn}^{01} & \cdots & w_{nn}^{0N}\\ \cdots & \cdots & \cdots & \cdots & \cdots & \cdots & \cdots & \cdots & \cdots\\ w_{n1}^{N0} & w_{n1}^{N1} & \cdots & w_{n1}^{NN} & \cdots & w_{nn}^{N0} & w_{nn}^{N1} & \cdots & w_{nn}^{NN} \end{bmatrix},$$

$$\mathbf{F} = \left[f_1^{(0)},\, f_1^{(1)}, \cdots, f_1^{(N)}, f_2^{(0)}, \cdots, f_2^{(N)}, \cdots, f_n^{(0)}, \cdots, f_n^{(N)}\right]^T, \tag{23}$$

$$\mathbf{T} \quad = [H_{is}^{lr} + T_{is}^{lr}] = \begin{bmatrix} \mathbf{A_{11}} & \mathbf{A_{12}} & \cdots & \mathbf{A_{1n}} \\ \mathbf{A_{21}} & \mathbf{A_{22}} & \cdots & \mathbf{A_{2n}} \\ \cdots & \cdots & \cdots & \cdots \\ \mathbf{A_{n1}} & \mathbf{A_{n2}} & \cdots & \mathbf{A_{nn}} \end{bmatrix},$$

$$\mathbf{A_{is}} = \begin{bmatrix} T_{is}^{00} & T_{is}^{01} & T_{is}^{02} & \cdots & T_{is}^{0N} \\ H_{is}^{10} + T_{is}^{10} & T_{is}^{11} & T_{is}^{12} & \cdots & T_{is}^{1N} \\ H_{is}^{20} + T_{is}^{20} & H_{is}^{21} + T_{is}^{21} & T_{is}^{22} & \cdots & T_{is}^{2N} \\ \cdots & \cdots & \cdots & \cdots & \cdots \\ H_{is}^{N0} + T_{is}^{N0} & H_{is}^{N1} + T_{is}^{N1} & H_{is}^{N2} + T_{is}^{N2} & \cdots & T_{is}^{NN} \end{bmatrix},$$

$$\begin{aligned} \mathbf{Y} &= \left[y_1^{(0)}(\xi),\, y_1^{(1)}(\xi), \cdots, y_1^{(N)}(\xi), y_2^{(0)}(\xi), \cdots, y_2^{(N)}(\xi), \cdots, y_n^{(0)}(\xi), \cdots, y_n^{(N)}(\xi)\right]^T \\ &\equiv [y_{10},\, y_{11}, \cdots, y_{1N}, y_{20}, \cdots, y_{2N}, \cdots, y_{n0}, \cdots, y_{nN}]^T, \end{aligned} \tag{24}$$

which is to be solved.

Substituting (23) in (22), we can convert (22) into an algebraic equations with variables $y_{10},\, y_{11}, \cdots, y_{1N}, y_{20}, \cdots, y_{2N}, \cdots, y_{n0}, \cdots, y_{nN}$, we can determine the variables $y_{ir}$ (i=1,2,...,n; r=0,1,...,N), i.e., the unknown Taylor coefficients $y_i^{(r)}(\xi)$ (i=1,2,...,n; r = 0,1,...,N), thus we can get the Taylor polynomial solution of the system (4) as follows:

$$y_i(x) = \sum_{r=0}^{N} \frac{1}{r!} y_i^{(r)}(\xi)\,(x-\xi)^r. \tag{25}$$

**Example 2.1** Consider the following Volterra system of integro-differential equations:

$$\begin{cases} y_1 - y_1^{'} + 2y_1^{''} - 4y_2 - \frac{3}{2}y_2^{'} + \frac{5}{4}y_2^{''} - 2y_3^{'} - \frac{1}{3}y_3^{''} = f_1(x) + \int_0^x (t-x)\, y_1(t)dt \\ \qquad + \int_0^x 5\, y_2(t)dt + \int_0^x (5x + \frac{1}{2})\, y_3(t)dt, \\ -\frac{1}{4}y_1^{''} + y_2 + y_2^{'} - 2y_2^{''} + \frac{1}{6}y_3^{''} = f_2(x) + \int_0^x (x+1)\, y_1(t)dt + \int_0^x t^2\, y_2(t)dt \\ \qquad + \int_0^x y_3(t)dt, \\ \frac{2}{3}y_1^{'} + \frac{1}{6}y_1^{''} - \frac{1}{2}y_2 + y_2^{''} + \frac{3}{4}y_3 = f_3(x) + \int_0^x (3x-t)\, y_2(t)dt + \int_0^x x\, y_3(t)dt, \end{cases} \tag{26}$$

where $f_1(x) = -x^6 - \frac{5}{4}x^5 - \frac{1}{8}x^4 - 3x^3 + \frac{1}{2}x^2$, $f_2(x) = -\frac{9}{10}x^5 - x^4$ , $f_3(x) = -\frac{1}{5}x^6 - \frac{1}{4}x^5 + \frac{7}{12}x^3 - \frac{23}{6}$ and the matrix form of the above system for $N = 4$ and $\xi = 0$ is as follows:

$$WY - KY = F,$$

where

$$W=\begin{bmatrix}
1 & -1 & 2 & 0 & 0 & -4 & -\frac{3}{2} & \frac{5}{4} & 0 & 0 & 0 & -2 & \frac{-1}{3} & 0 & 0\\
0 & 1 & -1 & 2 & 0 & 0 & -4 & -\frac{3}{2} & \frac{5}{4} & 0 & 0 & 0 & -2 & \frac{-1}{3} & 0\\
0 & 0 & 1 & -1 & 2 & 0 & 0 & -4 & -\frac{3}{2} & \frac{5}{4} & 0 & 0 & 0 & -2 & \frac{-1}{3}\\
0 & 0 & 0 & 1 & -1 & 0 & 0 & 0 & -4 & -\frac{3}{2} & 0 & 0 & 0 & 0 & -2\\
0 & 0 & 0 & 0 & 1 & 0 & 0 & 0 & 0 & -4 & 0 & 0 & 0 & 0 & 0\\
0 & 0 & -\frac{1}{4} & 0 & 0 & 1 & 1 & -2 & 0 & 0 & 0 & 0 & \frac{1}{6} & 0 & 0\\
0 & 0 & 0 & -\frac{1}{4} & 0 & 0 & 1 & 1 & -2 & 0 & 0 & 0 & 0 & \frac{1}{6} & 0\\
0 & 0 & 0 & 0 & -\frac{1}{4} & 0 & 0 & 1 & 1 & -2 & 0 & 0 & 0 & 0 & \frac{1}{6}\\
0 & 0 & 0 & 0 & 0 & 0 & 0 & 0 & 1 & 1 & 0 & 0 & 0 & 0 & 0\\
0 & 0 & 0 & 0 & 0 & 0 & 0 & 0 & 0 & 1 & 0 & 0 & 0 & 0 & 0\\
0 & \frac{2}{3} & \frac{1}{6} & 0 & 0 & -\frac{1}{2} & 0 & 1 & 0 & 0 & \frac{3}{4} & 0 & 0 & 0 & 0\\
0 & 0 & \frac{2}{3} & \frac{1}{6} & 0 & 0 & -\frac{1}{2} & 0 & 1 & 0 & 0 & \frac{3}{4} & 0 & 0 & 0\\
0 & 0 & 0 & \frac{2}{3} & \frac{1}{6} & 0 & 0 & -\frac{1}{2} & 0 & 1 & 0 & 0 & \frac{3}{4} & 0 & 0\\
0 & 0 & 0 & 0 & \frac{2}{3} & 0 & 0 & 0 & -\frac{1}{2} & 0 & 0 & 0 & 0 & \frac{3}{4} & 0\\
0 & 0 & 0 & 0 & 0 & 0 & 0 & 0 & 0 & -\frac{1}{2} & 0 & 0 & 0 & 0 & \frac{3}{4}
\end{bmatrix},$$

$$F=\begin{bmatrix} 0\\ 0\\ 1\\ -18\\ -3\\ 0\\ 0\\ 0\\ 0\\ -24\\ -\frac{23}{6}\\ 0\\ 0\\ \frac{7}{2}\\ 0 \end{bmatrix},\ K=\begin{bmatrix}
0 & 0 & 0 & 0 & 0 & 0 & 0 & 0 & 0 & 0 & 0 & 0 & 0 & 0 & 0\\
0 & 0 & 0 & 0 & 0 & 5 & 0 & 0 & 0 & 0 & \frac{1}{2} & 0 & 0 & 0 & 0\\
-1 & 0 & 0 & 0 & 0 & 0 & 5 & 0 & 0 & 0 & 10 & \frac{1}{2} & 0 & 0 & 0\\
0 & -1 & 0 & 0 & 0 & 0 & 0 & 5 & 0 & 0 & 0 & 15 & \frac{1}{2} & 0 & 0\\
0 & 0 & -1 & 0 & 0 & 0 & 0 & 0 & 5 & 0 & 0 & 0 & 20 & \frac{1}{2} & 0\\
0 & 0 & 0 & 0 & 0 & 0 & 0 & 0 & 0 & 0 & 0 & 0 & 0 & 0 & 0\\
1 & 0 & 0 & 0 & 0 & 0 & 0 & 0 & 0 & 0 & 1 & 0 & 0 & 0 & 0\\
2 & 1 & 0 & 0 & 0 & 0 & 0 & 0 & 0 & 0 & 0 & 1 & 0 & 0 & 0\\
0 & 3 & 1 & 0 & 0 & 2 & 0 & 0 & 0 & 0 & 0 & 0 & 1 & 0 & 0\\
0 & 0 & 4 & 1 & 0 & 0 & 6 & 0 & 0 & 0 & 0 & 0 & 0 & 1 & 0\\
0 & 0 & 0 & 0 & 0 & 0 & 0 & 0 & 0 & 0 & 0 & 0 & 0 & 0 & 0\\
0 & 0 & 0 & 0 & 0 & 0 & 0 & 0 & 0 & 0 & 0 & 0 & 0 & 0 & 0\\
0 & 0 & 0 & 0 & 0 & 5 & 0 & 0 & 0 & 0 & 2 & 0 & 0 & 0 & 0\\
0 & 0 & 0 & 0 & 0 & 0 & 7 & 0 & 0 & 0 & 0 & 3 & 0 & 0 & 0\\
0 & 0 & 0 & 0 & 0 & 0 & 0 & 9 & 0 & 0 & 0 & 0 & 4 & 0 & 0
\end{bmatrix}.$$

Then we can get the following algebraic equations:

$$\begin{cases}
-\frac{1}{4}y_{12}+y_{20}+y_{21}-2y_{22}+\frac{1}{6}y_{32}=0,\\
-\frac{1}{4}y_{14}+y_{22}+y_{23}-2y_{24}+\frac{1}{6}y_{34}-2y_{10}-y_{11}-y_{31}=0,\\
\frac{2}{3}y_{12}+\frac{1}{6}y_{13}-\frac{1}{2}y_{21}+y_{23}+\frac{3}{4}y_{31}=0,\\
-\frac{1}{4}y_{13}+y_{21}+y_{22}-2y_{23}+\frac{1}{6}y_{33}-y_{10}-y_{30}=0,\\
-\frac{1}{2}y_{24}+\frac{3}{4}y_{34}-9y_{22}-4y_{32}=0,\\
y_{23}+y_{24}-3y_{11}-y_{12}-2y_{20}-y_{32}=0,\\
y_{13}-y_{14}-4y_{23}-\frac{3}{2}y_{24}-2y_{34}+y_{11}-5y_{22}-15y_{31}-\frac{1}{2}y_{32}=-18,\\
\frac{2}{3}y_{13}+\frac{1}{6}y_{14}-\frac{1}{2}y_{22}+y_{24}+\frac{3}{4}y_{32}-5y_{20}-2y_{30}=0,\\
y_{24}-4y_{12}-y_{13}-6y_{21}-y_{33}=-24,\\
y_{10}-y_{11}+2y_{12}-4y_{20}-\frac{3}{2}y_{21}+\frac{5}{4}y_{22}-2y_{31}-\frac{1}{3}y_{32}=0,\\
\frac{2}{3}y_{11}+\frac{1}{6}y_{12}-\frac{1}{2}y_{20}+y_{22}+\frac{3}{4}y_{30}=-\frac{23}{6},\\
\frac{2}{3}y_{14}-\frac{1}{2}y_{23}+\frac{3}{4}y_{33}-7y_{21}-3y_{31}=\frac{7}{2},\\
y_{14}-4y_{24}+y_{12}-5y_{23}-20y_{32}-\frac{1}{2}y_{33}=-3,\\
y_{11}-y_{12}+2y_{13}-4y_{21}-\frac{3}{2}y_{22}+\frac{5}{4}y_{23}-2y_{32}-\frac{1}{3}y_{33}-5y_{20}-\frac{1}{2}y_{30}=0,\\
y_{12}-y_{13}+2y_{14}-4y_{22}-\frac{3}{2}y_{23}+\frac{5}{4}y_{24}-2y_{33}-\frac{1}{3}y_{34}+y_{10}-5y_{21}-10y_{30}-\frac{1}{2}y_{31}=1.
\end{cases}$$

The solution of this system of algebraic equations is as follows:

$$\begin{aligned} Y \;=\; & \{y_{12}=0, y_{23}=0, y_{30}=-4, y_{22}=2, y_{11}=-2, y_{20}=3, y_{31}=-2, y_{10}=5, \\ & y_{34}=24, y_{14}=0, y_{33}=6, y_{21}=1, y_{32}=0, y_{13}=12, y_{24}=0\}. \end{aligned}$$

Then in view of (25) we can obtain the solution of (26) as

$$\begin{aligned} y_1(x) &= 2x^3-2x+5, \\ y_2(x) &= x^2+x+3, \\ y_3(x) &= x^4+x^3-2x-4. \end{aligned}$$

which is exact solution.

**Example 2.2** Consider the following Volterra system of integro-differential equations:

$$\begin{cases} y_1+y_1^{'}=f_1(x)+\int_0^x(sin(x-t)-1)\,y_1(t)dt+\int_0^x(1-tcos(x))\,y_2(t)dt, \\ -y_1+y_2=f_2(x)+\int_0^x\,y_1(t)dt+\int_0^x(x-t)\,y_2(t)dt, \end{cases}$$

where $f_1(x)$ and $f_2(x)$ are chosen such that the exact solution is $f_1(x)=cos(x)$ and $f_2(x)=sin(x)$. Numerical results for N=12 and $\xi=0$ are given in Table 1.

| $x$ | $y_1(x)$ | | $y_2(x)$ | |
|---|---|---|---|---|
| | Exact | Approximate | Exact | Approximate |
| 0.0 | 1.0 | 1.002264127 | 0.0 | -0.002264127328 |
| 0.1 | 0.9950041653 | 0.9970320650 | 0.09983341665 | 0.09759183946 |
| 0.2 | 0.9800665778 | 0.9818454811 | 0.1986693308 | 0.1965212957 |
| 0.3 | 0.9553364891 | 0.9568714640 | 0.2955202067 | 0.2936886078 |
| 0.4 | 0.9210609940 | 0.9224004551 | 0.3894183423 | 0.3885026325 |
| 0.5 | 0.8775825619 | 0.8788683493 | 0.4794255386 | 0.4806769283 |
| 0.6 | 0.8253356149 | 0.8268785893 | 0.5646424734 | 0.5702225351 |
| 0.7 | 0.7648421873 | 0.7672136234 | 0.6442176872 | 0.6572875444 |
| 0.8 | 0.6967067093 | 0.7008073298 | 0.7173560909 | 0.7415468153 |
| 0.9 | 0.6216099683 | 0.6285990889 | 0.7833269096 | 0.8203856200 |
| 1.0 | 0.5403023059 | 0.5510745228 | 0.8414709848 | 0.8842821006 |

**Table 1**: Numerical results for N=12 and $\xi=0$.

## 3 Conclusion

In this paper, we use modified Taylor-series expansion method for solving a system of Volterra integro-differential equations. By using the theories and methods of mathematical analysis and computer algebra, we convert the system of integro-differential equations into a system of linear algebraic equations and then we obtain the solution of the system of integro-differential equations. The Taylor polynomial method proposed in this investigation is simple and effective for solving various system of integro-differential equations and can provide an accuracy approximate solution or exact solution.
Maple has been used for computations in this paper.

## References


[1] Kanwal, R.P. and Liu, K.C. A Taylor expansion approach for solving integral equations. *Int. J. Math. Educ. Sci. Technol.* **20** (3) (1989) 411–414.

[2] Ren, Y. Zhang and Bo. Qiao, Hong. A simple Taylor-series expansion method for a class of second kind integral equations. *J. Comput. Appl. Math* **110** (1999) 15–24.

[3] Dabas, J. Existence and Uniqueness of Solutions to Quasilinear Integro-differential Equations by the Method of Lines. *Nonlinear Dynamics and Systems Theory* **11** (4) (2011) 397–410.

[4] Daftardar-Gejji, V. Dehghan and M. Jafari, H. An algorithm for solving a System of linear ordinary differential Equations. *Far East Journal of Applied Mathematics* **29** (3) (2007) 445–453.

[5] Maleknejad and K. Aghazadeh, N. Numerical solution of Volterra integral equations of the second kind with convolution kernel by using Taylor-series expansion method. *Appl. Math. Comput.* **161** (2005) 915–922.

[6] Jafari, H. Hoseinzadeh, H. and Azad, A. A computational method for solving a System of Fredholm integro-differential Equations. *Icfai Journal of Computational Mathematics (IJCM)* **2** (2009) 35–44.

[7] Rabbani, M. Maleknejad and K. Aghazadeh, N. Numerical computational solution of the Volterra integral equations system of the second kind by using an expantion method. *Appl. Math. Comput.* **187** (2007) 1143–1146.

[8] Yalcinbas, S. and Sezer, M. The approximate solution of high-order linear Volterra–Fredholm integro-differential equations in terms of Taylor polynomials. *Appl. Math. Comput.* **112** (2000) 291–308.

[9] Wang, W. An algorithm for solving the high-order nonlinear Volterra–Fredholm integro-differential equation with mechanization. *Appl. Math. Comput.* **172** (1) (2006) 1–23.

[10] Yalcinbas, S. Taylor polynomial solutions of nonlinear Volterra–Fredholm integral equations. *Appl. Math. Comput.* **127** (2002) 195–206.

Nonlinear Dynamics and Systems Theory, **12** (2) (2012) 397–434

# Universal Spectrum for Atmospheric Aerosol Size Distribution: Comparison with PCASP-B Observations of VOCALS 2008

A.M. Selvam *

*(Retired) Indian Institute of Tropical Meteorology, Pune 411008, India*

Received: August 31, 2011; Revised: October 8, 2012

**Abstract:** Atmospheric flows exhibit scale-free fractal fluctuations. A general systems theory based on classical statistical physical concepts visualizes the fractal fluctuations to result from the coexistence of eddy fluctuations in an eddy continuum, the larger scale eddies being the integrated mean of enclosed smaller scale eddies. The model predicts (i) the eddy energy (variance) spectrum and corresponding eddy amplitude probability distribution are quantified by the same universal inverse power law distribution incorporating the golden mean. (ii) The steady state ordered hierarchical growth of atmospheric eddy continuum is associated with maximum entropy production. (iii) Atmospheric particulate size spectrum is derived in terms of the predicted universal inverse power law for atmospheric eddy energy spectrum. Model predictions are in agreement with observations. Universal inverse power law for power spectra of fractal fluctuations rules out linear secular trends in meteorological parameters. Global warming related climate change, if any, will be seen as intensification of fluctuations of all scales manifested immediately in high frequency fluctuations. The universal aerosol size spectrum may be computed for any location with two measured parameters, namely, the mean volume radius and the total number concentration and may be incorporated in climate models for computation of radiation budget of earth-atmosphere system.

**Keywords:** *complex systems and statistical physics; general systems theory; maximum entropy principle; universal inverse power law spectrum; universal spectrum for atmospheric suspended particulates; fractal fluctuations; chaos and nonlinear dynamics.*

**Mathematics Subject Classification (2010):** 60G18, 76F20, 76F55, 28A80.

* Corresponding author: mailto:amselvam@gmail.com

 

## 1 Introduction

Atmospheric flows exhibit self-similar fractal space-time fluctuations on all space-time scales associated with inverse power law distribution or $1/\nu$ noise, where $\nu$ is the frequency, for power spectra of meteorological parameters such as wind, temperature, etc [60]. Such $1/\nu$ noise imply long-range correlations, identified as self-organized criticality generic to dynamical systems in nature and are independent of the exact physical, chemical, physiological and other properties of the dynamical system.

Mathematical modelling of Nonlinear dynamics is a multidisciplinary area of intensive study in recent years. Real world and mathematical models of dynamical systems are characterized by unpredictable or chaotic fractal fluctuations. Simple mathematical models of dynamical systems exhibit very complicated or chaotic dynamics [3]. A review of the several real world models was presented by Martunyuk [62] to illustrate the importance of the theory and applications of the general methods of stability analysis [5, 22, 23]. Slane and Tragesser [89] analysed a class of near-periodic systems in which the dynamics can be described by a set of nonlinear differential equations with no known equilibrium solution. Special solutions to rotating stratified Boussinesq equations were discussed by Desale and Sharma [24]. A fuzzy approach for the optimal design of robust control for uncertain systems was proposed by Chen [19]. Fuzzy theory was originally introduced to describe information (for example, the linguistic information) that is in lack of a sharp boundary with its environment [103].

The signature of fractals, namely, inverse power law form for power spectra of fluctuations was identified for isotropic homogeneous turbulence by Kolmogorov in the 1940s. The concept of fractals and its quantitative measure for space-time fluctuations of all scales was introduced by Mandelbrot in the late 1960s. The robust pattern of selfsimilar space-time fluctuations was identified by Bak, Tang and Wiesenfeld in the late 1980s as self-organised criticality (SOC) whereby the cooperative existence of fluctuations of all space-time scales maintains the dynamical equilibrium in dynamical systems. In this paper the author presents a general systems theory model applicable to all dynamical systems. The quantitative characteristics of the observed fractal space-time fluctuations and SOC are derived directly as a natural consequence of model concepts based on collective statistical probabilities of fluctuations such as in kinetic theory of gases as explained in the following. Visconti [97] states that according to Edward Lorenz the atmosphere may be intrinsically unpredictable. Today there is no theory that could predict the evolution of a cloud in the presence of updraft, wind, humidity advection, etc. In a completely different context, the kinetic theory of gases solves another impossible problem and avoids the question of how to describe the exact position of each molecule in a gas. Instead it gives their collective properties, describing their statistical behavior [97]. The most important problem of statistical mechanics is the Kinetic Theory of Gases. Notions like pressure, temperature and entropy were based on the statistical properties of a large number of molecules [20]. Recent work in dynamical systems theory has shown that many properties that are associated with irreversible processes in fluids can be understood in terms of the dynamical properties of reversible, Hamiltonian systems. That is, stochastic-like behavior is possible for these systems [27]. Maxwell's (1860s) and Boltzmann's (1870s) work on the kinetic theory of gases, and the creation of the more general theory of statistical mechanics persuaded many thinkers that certain very important large scale regularities – the various gas laws, and eventually the second law of thermodynamics were indeed to be explained as the combined effect of the probability distributions governing those systems parts [90].

A general systems theory developed by the author visualizes the fractal fluctuations to result from the coexistence of eddy fluctuations in an eddy continuum, the larger scale eddies being the integrated mean of enclosed smaller scale eddies. The model predicts that the probability distributions of component eddy amplitudes and the corresponding variances (power spectra) are quantified by the same universal inverse power law distribution which is a function of the golden mean. Atmospheric particulates are held in suspension by the vertical velocity distribution (spectrum). The atmospheric particulate size spectrum is derived in terms of the model predicted universal inverse power law characterizing atmospheric eddy energy spectrum.

Information on the size distribution of atmospheric suspended particulates (aerosols, cloud drops, raindrops) is important for the understanding of the physical processes relating to the studies in weather, climate, atmospheric electricity, air pollution and aerosol physics. Atmospheric suspended particulates affect the radiative balance of the Earth/atmosphere system via the direct effect whereby they scatter and absorb solar and terrestrial radiation, and via the indirect effect whereby they modify the microphysical properties of clouds thereby affecting the radiative properties and lifetime of clouds [36]. At present empirical models for the size distribution of atmospheric suspended particulates is used for quantitative estimation of earth-atmosphere radiation budget related to climate warming/cooling trends. The empirical models for different locations at different atmospheric conditions, however, exhibit similarity in shape implying a common universal physical mechanism governing the organization of the shape of the size spectrum. The pioneering studies during the last three decades by Lovejoy and his group [59, 60] show that the particulates are held in suspension in turbulent atmospheric flows which exhibit selfsimilar fractal fluctuations on all scales ranging from turbulence (mm-sec) to climate (kms-years). Lovejoy and Schertzer [59] have shown that the rain drop size distribution should show a universal scale invariant shape. The non-linear coupling between statistical mechanics, particle microphysics and atmospheric dynamics must be studied from scaling point of view [51].

In the present study a general systems theory for fractal space-time fluctuations developed by the author [78, 84-86] is applied to derive universal (scale independent) inverse power law distribution incorporating the golden mean for atmospheric eddy energy distribution. Atmospheric particulates are held in suspension by the spectrum of atmospheric eddy fluctuations (vertical). The suspended atmospheric particulate size distribution is expressed in terms of the atmospheric eddy energy spectrum and is expressed as a function of the golden mean $\tau$ ($\approx 1.618$), the total number concentration and the mean volume radius (or diameter) of the particulate size spectrum. A knowledge of the mean volume radius and total number concentration is sufficient to compute the total particulate size spectrum at any location. Model predicted atmospheric eddy energy spectrum is in agreement with earlier observational results [79, 81-83, 87]. Model predicted suspended particulate (aerosol) size spectrum is in agreement with observations using VOCALS 2008 PCASP-B data (Sections 8 and 9).

The paper is organized as follows. Section 2 contains the current state of knowledge of the size distribution of atmospheric suspended particulates. Section 3 contains a brief summary of the observed characteristics of selfsimilar fractal fluctuations in atmospheric flows. Section 4 summarizes the general systems theory for fractal space-time fluctuations in atmospheric flows. The normalized (scale independent) atmospheric eddy energy spectrum and the associated aerosol size spectrum are derived in Section 5. In

Section 6 it is shown that the General Systems Theory presented in this paper satisfies the Maximum Entropy Principle of classical Statistical Physics. Section 7 contains details of observational data sets used for validating the model predictions. Sections.8 and 9 contain results of analyses of the data sets and conclusions of the study respectively.

## 2 Atmospheric Suspended Particulates: Current State of Knowledge

### 2.1 Aerosol size distribution

As aerosol size is one of the most important parameters in describing aerosol properties and their interaction with the atmosphere, its determination and use is of fundamental importance. Aerosol size covers several decades in diameter and hence a variety of instruments are required for its determination. This necessitates several definitions of the diameter, the most common being the geometric diameter d. The size fraction with d > 1-2 $\mu$m is usually referred to as the coarse mode, and the fraction d < 1-2 $\mu$m is the fine mode. The latter mode can be further divided into the accumulation d$\backsim$ 0.1-1 $\mu$m, Aitken d $\backsim$ 0.01-0.1 $\mu$m, and nucleation d < 0.01m modes. Due to the $d^3$ dependence of aerosol volume (and mass), the coarse mode is typified by a maximum volume concentration and, similarly, the accumulation mode by the surface area concentration and the Aitken and nucleation modes by the number concentration. As the sources and sinks of the coarse and fine modes are different, there is only a weak association of particles in both modes [37]. The aerosol chemistry data organized first by Peter Mueller and subsequently analyzed by Friedlander and co-workers showed that the fine and coarse mass modes were chemically distinctly different [38]. Based on tedious and careful size distribution measurements performed over many different parts of the world, Junge and co-workers[43-46] have observed that there is a remarkable similarity in the gathered size distributions (number concentration $N$ versus radius $r_a$): they follow a power law function over a wide range from 0.1 to over 20$\mu$ m in particle radius [38]

$$\frac{\mathrm{d}N}{\mathrm{dlog}r_a} = \mathrm{c}r_a^{-\alpha}.$$

The inverse power law exponent $\alpha$ of the number distribution function ranged between 3 and 5 with a typical value of 4. This power-law form of the size distribution became known as the *Junge distribution* of atmospheric aerosols. In the 1960s the physical mechanisms that were responsible for maintaining the observed *quasi-stationary* size distribution of the size spectra were not known.

Whitby [99] introduced the concept of the multimodal nature of atmospheric aerosol and Jaenicke and Davies [41] added the mathematical formalism used today. Semi-quantitative explanation of the observed fine particle dynamics provided the scientific support for the bimodal concept and became the basis of regional dynamically coupled gas-aerosol models. Typically, the planetary boundary layer (PBL) aerosol is combination of three modes corresponding to Aitken nuclei, accumulation mode aerosols, and coarse aerosols, the shape of which is often modeled as the sum of lognormal modes [100, 18]. In a nutshell, the bimodal distribution concept states that the atmospheric aerosol mass is distributed in two distinct size ranges, fine and coarse and that each aerosol mode has a characteristic size distribution, chemical composition and optical properties [38].

## 3 Selfsimilar Fractal Fluctuations from Turbulence to Climate Scales in Atmospheric Flows

The Atmospheric particulates are suspended in the selfsimilar wind fluctuation pattern ranging from turbulence to climate scales manifested as inverse power law form for power spectra of temporal fluctuations of wind speed. A brief summary of observed long-range correlations on all space-time scales in atmospheric flows and implications for modeling atmospheric dynamical transport processes is given in the following.

Atmospheric flows exhibit self-similar fractal fluctuations generic to dynamical systems in nature. Self-similarity implies long-range space-time correlations identified as self-organized criticality [4]. The physics of self-organized criticality ubiquitous to dynamical systems in nature and in finite precision computer realizations of non-linear numerical models of dynamical systems is not yet identified. During the past three decades, Lovejoy and his group [60] have done extensive observational and theoretical studies of fractal nature of atmospheric flows and emphasized the urgent need to formulate and incorporate quantitative theoretical concepts of fractals in mainstream classical theory relating to Atmospheric Physics.

The empirical analyses summarized by Lovejoy and Schertzer [60], Bunde et al.[15], Bunde and Havlin [13, 14], Eichner et al. [28], Rybski et al. [73, 74], directly demonstrate the strong scale dependencies of many atmospheric fields, showing that they depend in a power law manner on the spacetime scales over which they are measured. In spite of intense efforts over more than 50 years, analytic approaches have been surprisingly ineffective at deducing the statistical properties of turbulence. Atmospheric Science labors under the misapprehension that its basic science issues have long been settled and that its task is limited to the application of known laws albeit helped by ever larger quantities of data themselves processed in evermore powerful computers and exploiting ever more sophisticated algorithms. Conclusions about anthropogenic influences on the atmosphere can only be drawn with respect to the null hypothesis, i.e. one requires a theory of the natural variability, including knowledge of the probabilities of the extremes at various resolutions. At present, the null hypotheses are classical so that they assume there are no long-range statistical dependencies and that the probabilities are thin-tailed (i.e. exponential). However observations show that cascades involve long-range dependencies and (typically) have fat tailed (algebraic) distributions in which extreme events occur much more frequently and can persist for much longer than classical theory would allow [60, 10, 11, 29, 12, 9].

A general systems theory for the observed fractal space-time fluctuations of dynamical systems developed by the author [78, 85] helps formulate a simple model to explain the observed vertical distribution of number concentration and size spectra of atmospheric aerosols. The atmospheric aerosol size spectrum is derived in terms of the universal inverse power law characterizing atmospheric eddy energy spectrum. The physical basis and the theory relating to the model are discussed in Section 4. The model predictions are (i) The fractal fluctuations can be resolved into an overall logarithmic spiral trajectory with the quasiperiodic Penrose tiling pattern for the internal structure. (ii) The probability distribution of fractal space-time fluctuations (amplitude) also represents the power (variance or square of amplitude) spectrum for fractal fluctuations and is quantified as universal inverse power law incorporating the golden mean. Such a result that the additive amplitudes of eddies when squared represent probability distribution is observed in the subatomic dynamics of quantum systems such as the electron or photon. Therefore the irregular or unpredictable fractal fluctuations exhibit quantum-like chaos. (iii) Atmospheric aerosols are held in suspension by the vertical velocity fluctuation distribution (spectrum). The normalized (scale independent) atmospheric aerosol size spectrum is derived in terms of the universal inverse power law characterizing atmospheric eddy energy spectrum. Model predicted spectrum is in agreement (within two standard deviations on either side of the mean) with experimentally determined data sets for homogeneous aerosol size intervals (Sections 7 and 8).

## 4 General Systems Theory for Fractal Space-Time Fluctuations in Atmospheric Flows

The study of the spontaneous, i.e., self-organized formation of structures in systems far from thermal equilibrium in open systems belongs to the multidisciplinary field of synergetics [35]. Formation of structure begins by aggregation of molecules in a turbulent fluid (gas or liquid) medium. Turbulent fluctuations are therefore not dissipative, but serve to assemble and form coherent structures [63, 69, 70, 39], for example, the formation of clouds in turbulent atmospheric flows. Traditionally, turbulence is considered dissipative and disorganized. Yet, coherent (organized) vortex roll circulations (vortices) are ubiquitous to turbulent fluid flows [93, 50, 32]. The exact physical mechanism for the formation and maintenance of coherent structures, namely vortices or large eddy circulations in turbulent fluid flows is not yet identified.

Turbulence, namely, seemingly random fluctuations of all scales, therefore, plays a key role in the formation of selfsimilar coherent structures in the atmosphere. Such a concept is contrary to the traditional view that turbulence is dissipative, i.e., ordered growth of coherent form is not possible in turbulent flows. The author [78, 85] has shown that turbulent fluctuations self-organize to form selfsimilar structures in fluid flows.

In summary, spatial integration of enclosed turbulent fluctuations give rise to large eddy circulations in fluid flows. Therefore, starting with turbulence scale fluctuations, progressively larger scale eddy fluctuations can be generated by integrating circulation structures at different scale ranges. Such a concept envisages only the magnitude (intensity) of the fluctuations and is independent of the properties of the medium in which the fluctuations are generated. Also, self-similar space-time growth structure is implicit to hierarchical growth process, i.e., the large scale structure is the envelope of enclosed smaller scale structures. Successively larger scale structures form a hierarchical network and function as a unified whole. Large eddy is the integrated mean of enclosed turbulent eddies and functions as a fuzzy logic network with two-way energy (information) flow between the scales. Fuzzy descriptions of system performance adds more insight to view the system performance [19].

The role of surface frictional turbulence in weather systems is discussed in Section 4.1. The common place occurrence of long-lived organized cloud patterns and their important contribution to the radiation budget of the earths atmosphere is briefly discussed in Section 4.1.1.

### 4.1 Frictional convergence induced weather

Roeloffzen et al. [72] discussed the importance of frictional convergence induced weather as follows. The coastline generally represents a marked discontinuity in surface roughness. The resulting mechanical forcing leads to a secondary circulation in the boundary layer, and consequently to a vertical motion field that may have a strong influence on the weather in the coastal zone. In potentially unstable air masses, frictional convergence may cause a more-or-less stationary zone of heavy shower activity, for example. Of all meteorological phenomena typical for coastal regions, the fair weather sea-breeze circulation has probably been studied most extensively, e.g., Estoque [30], Walsh [98], Pielke [68], Pearson et al. [67]. In contrast to this thermally-driven circulation, the mechanical forcing due to the discontinuity in surface roughness may create circulation patterns of similar amplitude and scale. Frictional convergence is mentioned in some studies as the cause of increased precipitation in coastal zones under specific conditions, e.g., Bergeron [7], Timmerman [94], Oerlemans [64]; but its effect is generally underestimated [72].

Frictional convergence is analogous to Ekman pumping, namely, the process of inducing vertical motions by boundary layer friction [91].

Cotton and Anthes [21] emphasized the importance of the role of Ekman pumping on large scale weather systems. The strong control of cumulus convection by the larger scales of motion in tropical cyclones has been recognized for a long time. Syono et al. [92] showed that the rate of precipitation in typhoons was related to the updrafts produced by frictional convergence in the PBL (so-called Ekman pumping). Later observational and modeling studies have confirmed the cooperative interaction between cumulus convection and the tropical cyclones through frictionally induced moisture convergence and enhanced evaporation in the PBL (see review in Anthes [2]). Local winds such as Sea breezes actually are very important because they are determined mainly by the interaction of large scale motions with local topography [97].

New research suggests that rough areas of land, including city buildings and naturally jagged land cover like trees and forests can actually attract passing hurricanes. It was observed that storms traveling over river deltas hold together longer than those over dry ground. As a result, the city of New Orleans might feel a greater impact of hurricanes coming off the Gulf of Mexico than existing computer models predict [61].

#### 4.1.1 Mesoscale cellular convection and radiation budget of the earth

Feingold et al. [31] discussed the importance of the observed large scale organized pattern of clouds in the radiation budget of the earths atmosphere. Cloud fields adopt many different patterns that can have a profound effect on the amount of sunlight reflected back to space, with important implications for the Earths climate. These cloud patterns can be observed in satellite images of the Earth and often exhibit distinct cell-like structures associated with organized convection at scales of tens of kilometers [49, 1, 33], i.e. mesoscale cellular convection. These clouds are important because they increase the reflectance of shortwave radiation and therefore exert a cooling effect on the climate system that is not compensated by appreciable changes in outgoing longwave radiation [96].

### 4.2 Growth of macro-scale coherent structures from microscopic domain fluctuations in atmospheric flows

The non-deterministic model [78, 85, 86] incorporates the physics of the growth of macro-scale coherent structures from microscopic domain fluctuations in atmospheric flows. In summary, the mean flow at the planetary ABL possesses an inherent upward momentum flux of *frictional origin* at the planetary surface. This turbulence-scale upward momentum flux is progressively amplified by the exponential decrease of the atmospheric density with height coupled with the buoyant energy supply by micro-scale fractional condensation on hygroscopic nuclei, even in an unsaturated environment [71]. The mean large-scale upward momentum flux generates helical vortex-roll (or large eddy) circulations in the planetary atmospheric boundary layer and under favourable conditions of moisture supply, is manifested as cloud rows and (or) streets, and mesoscale cloud clusters MCC in the global cloud cover pattern. A conceptual model of large and turbulent eddies in the planetary ABL is shown in Figures 1 and 2. The mean airflow at the planetary surface carries the signature of the fine scale features of the planetary surface topography as turbulent fluctuations with a net upward momentum flux. This persistent upward momentum flux of *surface frictional origin* generates large-eddy (or vortex-roll) circulations, which carry upward the turbulent eddies as internal circulations. Progressive upward growth of a large eddy occurs because of buoyant energy generation in turbulent fluctuations as a result of the latent heat of condensation of atmospheric water vapour on suspended hygroscopic nuclei such as common salt particles. The latent heat of condensation generated by the turbulent eddies forms a distinct warm envelope or a micro-scale capping inversion layer at the crest of the large-eddy circulations as shown in Figure 1.

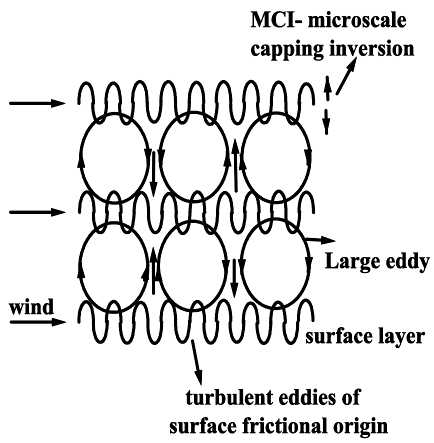


**Figure 1**: Micro-scale capping inversion (MCI) layer at the crest of the large-eddy circulations.

Progressive upward growth of the large eddy occurs from the turbulence scale at the planetary surface to a height $R$ and is seen as the rising inversion of the daytime atmospheric boundary layer (Figure 2).

The turbulent fluctuations at the crest of the growing large-eddy mix overlying environmental air into the large-eddy volume, i.e. there is a two-stream flow of warm air upward and cold air downward analogous to superfluid turbulence in liquid helium [25, 26]. The convective growth of a large eddy in the atmospheric boundary layer therefore occurs by vigorous counter flow of air in turbulent fluctuations, which releases stored buoyant energy in the medium of propagation, e.g. latent heat of condensation of atmospheric water vapour. Such a picture of atmospheric convection is different from the traditional concept of atmospheric eddy growth by diffusion, i.e. analogous to the molecular level momentum transfer by collision. Molecules and turbulence eddies must

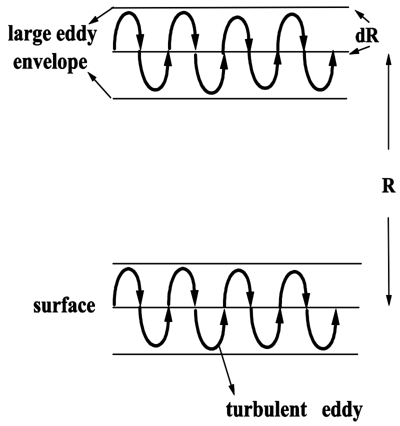


**Figure 2**: Progressive upward growth of the large eddy from the turbulence scale at the planetary surface.

have influence on atmospheric particles. However most theories on particle diffusional growth emphasize molecular effects, e.g., based on classical transport laws (Fick's first law for mass diffusion, Fourier law for heat diffusion) whereas the effects of turbulence are underestimated [51].

The generation of turbulent buoyant energy by the micro-scale fractional condensation is maximum at the crest of the large eddies and results in the warming of the large-eddy volume. The turbulent eddies at the crest of the large eddies are identifiable by a micro-scale capping inversion that rises upward with the convective growth of the large eddy during the course of the day. This is seen as the rising inversion of the daytime planetary boundary layer in echosonde and radiosonde records and has been identified as the entrainment zone [8, 34] where mixing with the environment occurs.

The general systems theory for eddy growth discussed so far for planetary atmospheric boundary layer (ABL) can be extended up to the upper atmospheric levels. In summary, a gravity wave feedback mechanism for the vertical mass exchange between the troposphere and the stratosphere is proposed. The vertical mass exchange takes place through a chain of eddy systems. The atmospheric boundary layer (ABL) contains large eddies (vortex rolls) which carry on their envelopes turbulent eddies of *surface frictional origin* [76, 78, 85]. The buoyant energy production by *microscale-fractional-condensation* (MFC) in turbulent eddies is responsible for the sustenance and growth of large eddies [77, 78, 85]. The buoyant energy production of turbulent eddies by the *microscale-fractional-condensation* (MFC) process is maximum at the crest of the large eddies and results in the warming of the large eddy volume. The turbulent eddies at the crest of the large eddies are identifiable by a *microscale-capping-inversion* (MCI) layer which rises upwards with the convective growth of the large eddy in the course of the day. The MCI layer is a region of enhanced aerosol concentrations. As the *microscale-fractional-condensation* (MFC) generated warm parcel of air corresponding to the large eddy rises in the stable environment of the *microscale-capping-inversion* (MCI), Brunt Vaisala oscillations are generated [77, 78, 85]. The growth of the large eddy is associated with generation of a continuous spectrum of gravity (buoyancy) waves in the atmosphere. The atmosphere contains a stack of large eddies. Vertical mixing of overlying environmental air into the large eddy volume occurs by turbulent eddy fluctuations [76, 78, 85]. The circulation speed of the large eddy is related to that of the turbulent eddy according to the following expression [95, 78]

$$W^2 = \frac{2r}{\pi R} w^2. \tag{1}$$

In the above equation (1), $W$ and $w$ are respectively the r.m.s (root mean square) circulation speeds of the large and turbulent eddies and $R$ and $r$ are their respective radii.

The relationship between the time scales $T$ and $t$ respectively of the large and turbulent eddies can be derived in terms of the circulation speeds $W$ and $w$ and their respective length scales $R$ and $r$ from equation (1) [78] as follows

$$T = \frac{2\pi R}{W} \text{ and } t = \frac{2\pi r}{w},$$
$$\frac{T}{t} = \frac{Rw}{rW} = \frac{R}{r}\sqrt{\frac{\pi R}{2r}} = \left[\frac{R}{r}\right]^{\frac{3}{2}} \sqrt{\frac{\pi}{2}}.$$

As seen from Figures 1 and 2 and from the concept of eddy growth, vigorous counter flow (mixing) characterizes the large-eddy volume. The total fractional volume dilution rate of the large eddy by vertical mixing across unit cross-section is derived from equation (1) [76, 78, 85] and is given as follows

$$k = \frac{wr}{\mathrm{d}WR}. \tag{2}$$

In equation (2), $w$ is the increase in vertical velocity per second of the turbulent eddy due to microscale fractional condensation (MFC) process and d$W$ is the corresponding increase in vertical velocity of large eddy.

The fractional volume dilution rate $k$ is equal to 0.4 for the scale ratio $z$, i.e. $R/r$ =10. Identifiable large eddies can exist in the atmosphere for scale ratios more than 10 only since, for smaller scale ratios the fractional volume dilution rate $k$ becomes more than half. Thus atmospheric eddies of various scales, i.e., convective, meso-, synoptic and planetary scale eddies are generated by successive decadic scale range eddy mixing process starting from the basic turbulence scale [77, 78, 85]. From equation (2) the following logarithmic wind profile relationship for the ABL is obtained [76, 78, 85].

$$W = \frac{w}{k} \ln z. \tag{3}$$

The steady state fractional upward mass flux $f$ of surface air at any height $z$ can be derived using equation (3) and is given by the following expression [76, 78, 85].

$$f = \sqrt{\frac{2}{\pi z}}. \tag{4}$$

In equation (4) $f$ represents the steady state fractional volume of surface air at any level $z$. Since atmospheric aerosols originate from surface, the vertical profile of mass and number concentration of aerosols follow the $f$ distribution.

The magnitude of the steady state vertical aerosol mass flux is dependent on $m_*$, the aerosol mass concentration at the initial level (earth surface) and is equal to $m_* f$ from (4), the non-zero values of $f$ being given in terms of the non-dimensional length scale ratio $z$. Similarly the aerosol number concentration $N$ at normalized height $z$ is equal to $N_* f$, where $N_*$ is the number concentration at the surface.

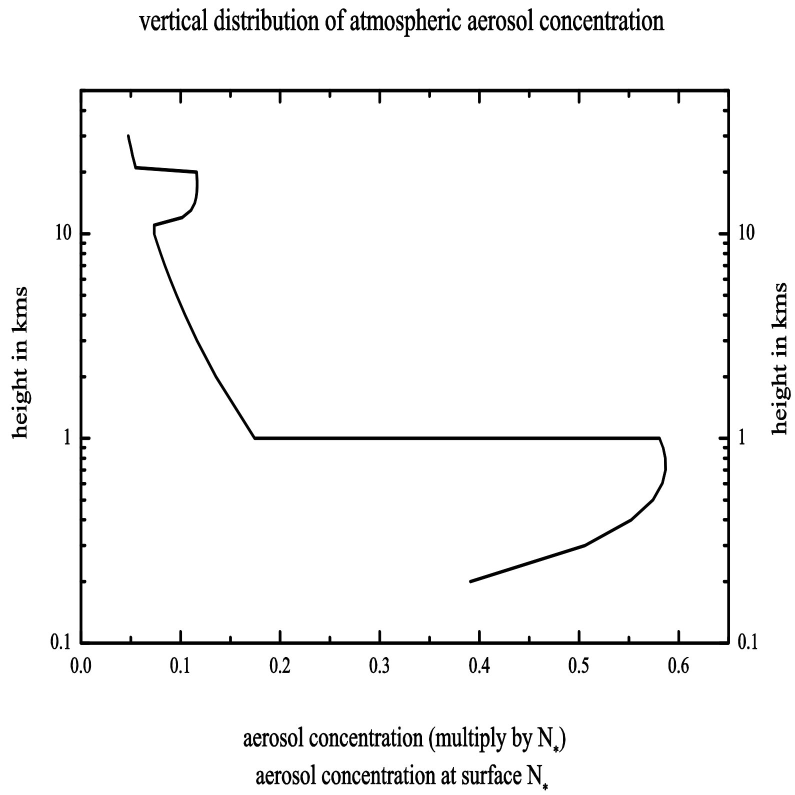


**Figure 3**: Model predicted aerosol vertical distribution.

The aerosol concentration vertical profile in Figure 3 is computed using equation (4) with appropriate length scale ratio $z$ values corresponding to the associated steady state fractional volume dilution $k$ values (2). The fractional volume dilution rate $k$ is equal to 0.4 for the scale ratio $z$, i.e., $R/r$ =10. Identifiable large eddies can exist in the atmosphere only for scale ratios more than 10 since, for smaller scale ratios the fractional volume dilution rate $k$ becomes more than half. Thus atmospheric eddies of various scales, i.e., convective, meso-, synoptic and planetary scale eddies are generated by successive decadic scale range eddy mixing process starting from the basic turbulence scale [42, 76-87].

The peaks in the aerosol concentration at 1 km (lifting condensation level) and at about 10-15 km (stratosphere) identify the microscale capping inversion (MCI, Figure 1) at the crests of the convective and meso-scale eddies respectively, the appropriate scale ratios for the convective and meso-scale eddies being 10 and 100 with respect to the turbulence scale. Thus for the turbulent eddy of radius 100m, the MCI's for the convective and meso-scale eddies occur at 1 km and 10 km respectively.

The model predicted profiles closely resemble the observed profiles associated with major quasi-permanent tropospheric inversion (temperature) layers reported by other investigators [46].

The vertical mass exchange mechanism predicts the $f$ distribution for the steady state vertical transport of aerosols at higher levels. Thus aerosol injection into the stratosphere by volcanic eruptions gives rise to the enhanced peaks in the regions of microscale capping inversion (MCI) in the stratosphere and other higher levels determined by the radius of the dominant turbulent eddy at that level.

The time $T$ taken for the steady state aerosol concentration $f$ to be established at the normalised height $z$ is equal to the time taken for the large eddy to grow to the height $z$ and is computed using the following relation (see Section 4.3.2 below)

$$T = \frac{r}{w}\sqrt{\frac{\pi}{2}}\mathrm{li}\sqrt{z}. \tag{5}$$

In equation (5), li is the logarithm integral.

The vertical dispersion rate of aerosols/pollutants from known sources (e.g., volcanic eruptions, industrial emissions) can be computed using the relation for $f$ and $T$ (equations 4 and 5).

### 4.3 Computations of model predictions and comparison with observations

#### 4.3.1 Vertical velocity profile

The microscale fractional condensation (MFC) generated values of vertical velocity have been calculated for different heights above the surface for clear-air conditions and above the cloud-base for in-cloud conditions for a representative tropical environment with favourable moisture supply. A representative cloud-base height is considered to be 1000m above sea level (a.s.l) and the corresponding meteorological parameters are, surface pressure 1000 mb, surface temperature 30 $^o$C, relative humidity at the surface 80%, turbulent length scale 1 cm. The values of the latent heat of vapourisation $\mathrm{L_V}$ and the specific heat of air at constant pressure $\mathrm{C_p}$ are 600 cal gm$^{-1}$ and 0.24 cal gm$^{-1}$ respectively. The density of air at surface is 1.1495 Kg m$^{-3}$. The ratio values of $m_\mathrm{w}/m_0$, where $m_0$ is the mass of the hygroscopic nuclei per unit volume of air and $m_\mathrm{w}$ is the mass of water condensed on $m_0$, at various relative humidities as given by Winkler and Junge [101, 102] have been adopted and the value of $m_\mathrm{w}/m_0$ is equal to about 3 for relative humidity 80%. For a representative value of $m_0$ equal to 100g m$^{-3}$ the temperature perturbation $\theta$' is equal to 0.00065$^0$C and the corresponding vertical velocity perturbation (turbulent) $w_*$ is computed and is equal to 21.1x10$^{-4}$ cm sec$^{-1}$ from the following relationship between the corresponding virtual potential temperature $\theta_v$, and the acceleration due to gravity g equal to 980.6 cm sec$^{-2}$

$$w_* = \frac{\mathrm{g}}{\theta_v}\theta'.$$

Heat generated by condensation of water equal to 300 $\mu$g on 100 $\mu$g of hygroscopic nuclei per metre$^3$ generates vertical velocity perturbation $w_*$ (cm sec$^{-2}$) equal to 21.1x10$^{-4}$ cm sec$^{-2}$ at surface levels. In the following it is shown that a value of $w_*$ equal to 30x10$^{-7}$

cm sec$^{-2}$, i.e. about three orders of magnitude less than that shown in the above example is sufficient to generate clouds as observed in practice.

From the logarithmic wind profile relationship (3) and the steady state fractional upward mass flux $f$ of surface air at any height $z$ (4) the corresponding vertical velocity perturbation $W$ can be expressed in terms of the primary vertical velocity perturbation $w_*$ as

$$W = w_* f z. \tag{6}$$

$W$ may be expressed in terms of the scale ratio $z$ as given below.

From equation (4)

$$f = \sqrt{\frac{2}{\pi z}} \ln z.$$

Therefore,

$$W = w_* z \sqrt{\frac{2}{\pi z}} \ln z = w_* \sqrt{\frac{2z}{\pi z}} \ln z.$$

The steady state values of large eddy vertical velocity perturbation $W$ equal to $w_* f z$ at normalized heights $z$ produced by the constant value of primary perturbation $w_*$ generated by microscale fractional condensation at surface levels are computed from (6) and given in the Table 1.

| Height z above surface i.e., large eddy radius | Vertical velocity perturbation $W = w_* f z$ cm sec$^{-1}$ |
|---|---|
| 1 cm | 30x10$^{-7}$ |
| 100 cm | 1.10x10$^{-4}$ |
| 100 m | 2.20x10$^{-3}$ |
| 1000 m | 8.71x10$^{-3}$ $\approx$ 0.01 |

**Table 1**: The steady state values of large eddy vertical velocity perturbation $W$.

Microscale fractional condensation generated turbulent eddy perturbation speed increases progressively with height $z$ from surface, the turbulent eddies being carried on the envelope of large eddy circulation of radius $z$ and may be visualized as follows:
The 1 cm eddy at the surface generates perturbation speed $w_*$ by microscale fractional condensation. At height $z$ cm corresponding to the envelope of large eddy of $z$ cm radius, the 1 cm eddy carried on the envelope of the large eddy has a perturbation speed of $w_* f z$. Thus at 1000m corresponding to large eddy radius 1000m, the 1cm eddy on the envelope has a perturbation speed of 0.01 cm sec$^{-1}$. The large eddy circulation time period at height $z$ can be expressed in terms of the primary 1 cm radius eddy perturbation speed on its envelope as given in (5) (see Section 4.3.2 for the detailed derivation).

The above values of microscale fractional condensation related vertical velocities, although small in magnitude, are present for long enough periods in the lower levels and contribute for the formation and development of clouds as explained below.

### 4.3.2 Large eddy growth time

The time required for the large eddy of radius $R$ to grow from the primary turbulence scale radius $r_*$ is computed as follows

$$\text{The scale ratio } z = \frac{R}{r_*}.$$

Therefore for constant turbulence radius $r_*$

$$\mathrm{d}z = \frac{\mathrm{d}R}{r_*}.$$

The incremental growth d$R$ of large eddy radius is equal to

$$\mathrm{d}R = r_* \mathrm{d}z.$$

The time d$t$ for the incremental cloud growth is expressed as follows

$$\mathrm{d}t = \frac{\mathrm{d}R}{W} = \frac{r_* \mathrm{d}z}{W}.$$

$W$ is the increase in large eddy circulation speed resulting from enclosed turbulent eddy circulations of speed $w_*$ and is given as $W = w_* f z$ from (6). Therefore

$$\mathrm{d}t = \frac{r_* \mathrm{d}z}{w_* f z} = \frac{r_* \mathrm{d}z}{w_* z \sqrt{\frac{2}{\pi z}} \ln z},$$

$$t = \frac{r_*}{w_*} \sqrt{\frac{\pi}{2}} \int_2^z \frac{\mathrm{d}z}{\sqrt{z} \ln z}.$$

The above equation can be written in terms of $\sqrt{z}$ as follows

$$\sqrt{\mathrm{z}} = \frac{\mathrm{d}z}{2\sqrt{z}},$$

$$\mathrm{d}z = 2\sqrt{z}\mathrm{d}(\sqrt{z}).$$

Therefore,

$$t = \frac{r_*}{w_*} \sqrt{\frac{\pi}{2}} \int_{x_1}^{x_2} \frac{\mathrm{d}\sqrt{z}}{\ln\sqrt{z}} = \frac{r_*}{w_*} \sqrt{\frac{\pi}{2}} \int_{x_1}^{x_2} \mathrm{li}(\sqrt{z}),$$

$$x_1 = \sqrt{z}_1, \quad x_2 = \sqrt{z}_2.$$

In the above equation $z_1$ and $z_2$ refer respectively to lower and upper limits of integration and li is the Soldner′s integral or the logarithm integral. The large eddy growth time $t$ (equation 5 in Section 4.2) can be computed from the above equation in terms of the internal primary small eddy radius $r_*$ (equal to 1 cm) and the corresponding eddy acceleration $w_* f z$.

Starting from surface, the time $t$ seconds taken for the evolution of the 1000m ($10^5$ cm) eddy from the 1 cm radius ($r_*$) eddy energized by the microscale fractional condendensation (MFC) induced primary perturbation $w_* f z$ equal to 0.01cm sec$^{-2}$ can be computed from the above equation by substituting for $z_1 = 1$cm and $z_2 = 10^5$ cm such that $x_1 = \sqrt{1}$=1 and $x_2$=$\sqrt{10^5} \approx 317$ ,

$$t = \frac{1}{.001}\sqrt{\frac{\pi}{2}}\int_1^{317} \mathrm{li}\sqrt{z}.$$

The value of $\int_1^{317} \mathrm{li}\sqrt{z}$ is equal to 71.3. Hence $t \approx 8938$ sec $\approx$ 2 hrs 30 mins.

Thus starting from the surface level cloud growth begins after a time period of 2 hrs 30 mins. This is consistent with the observations that convective cloud growth is visible in the afternoon hours.

## 5 Atmospheric Aerosol Size Spectrum

### 5.1 Vertical variation of aerosol number concentration

The atmospheric eddies hold in suspension the aerosols and thus the mass size spectrum of the atmospheric aerosols is dependent on the vertical velocity fluctuation spectrum of the atmospheric eddies as explained in the following. The distribution of atmospheric aerosols is not only determined by turbulence, but also by dry and wet chemistry, sedimentation, gas to particle conversion, coagulation, (fractal) variability at the surface, amongst others. However, at any instant, the mass (and therefore the radius for homogeneous aerosols) size distribution of atmospheric suspensions (aerosols) is directly related to the wind vertical velocity (eddy energy) spectrum which is shown to be universal (scale independent). The source for aerosols in the fine mode (diameter less than 1 $\mu$m) and coarse mode (diameter greater than 1$\mu$m) are different [38] and may account for the differences in the departures of the observed from model predicted radius size spectrum for the fine and coarse aerosol modes (Section 6).

From the logarithmic wind profile relationship (3) and the steady state fractional upward mass flux $f$ of surface air at any height $z$ (4) the vertical velocity perturbation $W$ is expressed in (6) as

$$W = w_* f z.$$

The corresponding moisture content $q$ at height z is related to the moisture content $q_*$ at the surface (or reference level) and is given as (6)

$$q = q_* f z. \tag{7}$$

The aerosols are held in suspension by the eddy vertical velocity perturbations. Thus the suspended aerosol mass concentration $m$ at any level $z$ will be directly related to the vertical velocity perturbation $W$ at $z$, i.e., $W \approx m$g where g is the acceleration due to gravity. Therefore

$$m = m_* f z. \tag{8}$$

In (8), $m_*$ is the suspended aerosol (homogeneous) mass concentration in the surface layer. Let $r_a$ and $N$ represent the mean volume radius and number concentration of aerosols at level $z$. The variables $r_{as}$ and $N_*$ relate to corresponding parameters at the surface levels. Substituting for the average mass concentration in terms of mean radius $r_a$ and number concentration $N$ at normalized height $z$ above surface

$$\frac{4}{3}\pi {r_a}^3 N = \frac{4}{3}\pi {r_{as}}^3 N_* f z. \tag{9}$$

The number concentration $N$ of aerosol decreases with normalised height $z$ according to the $f$ distribution as shown earlier in Section 4.2 and is expressed as follows:

$$N = N_* f. \tag{10}$$

### 5.2 Vertical variation of aerosol mean volume radius

The mean volume radius of aerosol increases with height (eddy radius) $z$ as shown in the following. At any height $z$, the fractal fluctuations (of wind, temperature, etc.) carry the signatures of eddy fluctuations of all size scales since the eddy of length scale $z$ encloses smaller scale eddies and at the same time forms part of internal circulations of eddies larger than length scale $z$.

The wind velocity perturbation $W$ is represented by an eddy continuum of corresponding size (length) scales $z$. The aerosol mass flux across unit cross-section per unit time is obtained by normalizing the velocity perturbation $W$ with respect to the corresponding length scale $z$ to give the volume flux of air equal to $Wz$ and can be expressed as follows from (6):

$$Wz = (w_* f z) z. \tag{11}$$

The corresponding normalized moisture flux perturbation is equal to $qz$ where $q$ is the moisture content per unit volume at level $z$. Substituting for $q$ from (7)

$$\text{normalised moisture flux at level } z = q_* f z^2. \tag{12}$$

The moisture flux increases with height resulting in increase of mean volume radius of CCN (cloud condensation nuclei) because of condensation of water vapour. The corresponding CCN (aerosol) mean volume radius $r_a$ at height $z$ is given in terms of the aerosol number concentration $N$ at level $z$ and mean volume radius $r_{as}$ at the surface (or reference level) as follows from (12)

$$\frac{4}{3}\pi {r_a}^3 = \frac{4}{3}\pi {r_{as}}^3 N_* f z^2. \tag{13}$$

Substituting for $N$ from (10) in terms of $N_*$ and $f$

$$\begin{aligned} {r_a}^3 &= {r_{as}}^3 z^2, \\ r_a &= r_{as} z^{\frac{2}{3}}. \end{aligned} \tag{14}$$

The mean aerosol size increases with height according to the cube root of $z^2$ (14). As the large eddy grows in the vertical, the aerosol size spectrum extends towards larger sizes while the total number concentration decreases with height according to the $f$ distribution. The atmospheric aerosol size spectrum is dependent on the eddy energy spectrum and may be expressed in terms of the recently identified universal characteristics of fractal fluctuations generic to atmospheric flows [86, 87] as shown in Section 5.3 below.

### 5.3 Probability distribution of fractal fluctuations in atmospheric flows

The atmospheric eddies hold in suspension the aerosols and thus the size spectrum of the atmospheric aerosols is dependent on the vertical velocity spectrum of the atmospheric eddies. Atmospheric air flow is turbulent, i.e., consists of irregular fluctuations of all space-time scales characterized by a broadband spectrum of eddies. The suspended aerosols will also exhibit a broadband size spectrum closely related to the atmospheric eddy energy spectrum.

Atmospheric flows exhibit self-similar fractal fluctuations generic to dynamical systems in nature such as fluid flows, heart beat patterns, population dynamics, spread of forest fires, etc. Power spectra of fractal fluctuations exhibit inverse power law of form $\nu^{-\alpha}$ where $\alpha$ is a constant indicating long-range space-time correlations or persistence. Inverse power law for power spectrum indicates scale invariance, i.e., the eddy energies at two different scales (space-time) are related to each other by a scale factor ($\alpha$ in this case) alone independent of the intrinsic properties such as physical, chemical, electrical etc of the dynamical system.

A general systems theory for turbulent fluid flows predicts that the eddy energy spectrum, i.e., the variance (square of eddy amplitude) spectrum is the same as the probability distribution $P$ of the eddy amplitudes, i.e. the vertical velocity $W$ values. Such a result that the additive amplitudes of eddies, when squared, represent the probabilities is exhibited by the subatomic dynamics of quantum systems such as the electron or photon. Therefore, the unpredictable or irregular fractal space-time fluctuations generic to dynamical systems in nature, such as atmospheric flows is a signature of quantum-like chaos. The general systems theory for turbulent fluid flows predicts [78, 84-87] that the atmospheric eddy energy spectrum follows inverse power law form incorporating the golden mean $\tau$ [ 86, 87] and the normalized deviation for values of $\sigma \geq 1$ and $\sigma \leq$ -1 as given below

$$P = \tau^{-4\sigma}. \tag{15}$$

The vertical velocity $W$ spectrum will therefore be represented by the probability distribution $P$ for values of $\sigma \geq 1$ and $\sigma \leq$ -1 given in (15) since fractal fluctuations exhibit quantum-like chaos as explained above:

$$W = P = \tau^{-4\sigma}. \tag{16}$$

Values of the normalized deviation $\sigma$ in the range -1 $< \sigma <$ 1 refer to regions of primary eddy growth where the fractional volume dilution $k$ (2) by eddy mixing process has to be taken into account for determining the probability distribution $P$ of fractal fluctuations (see Section 5.4 below).

### 5.4 Primary eddy growth region fractal space-time fluctuation probability distribution

Normalized deviation $\sigma$ ranging from -1 to +1 corresponds to the primary eddy growth region. In this region the probability $P$ is shown to be equal to $P = \tau^{-4k}$ (see below), where $k$ is the fractional volume dilution by eddy mixing (2).

For the primary eddy growth region, the normalized deviation $\sigma$ represents the length step growth number for growth stages more than one. The first stage of eddy growth is the primary eddy growth starting from unit length scale perturbation, the complete eddy forming at the tenth length scale growth, i.e., $R = 10r$ and scale ratio $z$ equals to 10 [78, 85]. The steady state fractional volume dilution k of the growing primary eddy by internal smaller scale eddy mixing is given by (2) as

$$k = \frac{wr}{WR}. \tag{17}$$

The expression for $k$ in terms of the length scale ratio$z$ equal to $\frac{R}{r}$ is obtained from (1) as

$$k = \sqrt{\frac{\pi}{2z}}. \tag{18}$$

A fully formed large eddy length $R = 10r$ ($z$=10) represents the average or mean level zero and corresponds to a maximum of 50% probability of occurrence of either positive or negative fluctuation peak at normalized deviation $\sigma$ value equal to zero by convention. For intermediate eddy growth stages, i.e., $z$ less than 10, the probability of occurrence of the primary eddy fluctuation does not follow conventional statistics, but is computed as follows taking into consideration the fractional volume dilution of the primary eddy by internal turbulent eddy fluctuations. Starting from unit length scale fluctuation, the large eddy formation is completed after 10 unit length step growths, i.e., a total of 11 length steps including the initial unit perturbation. At the second step ($z = 2$) of eddy growth the value of normalized deviation $\sigma$ is equal to 1.1 - 0.2 (= 0.9) since the complete primary eddy length plus the first length step is equal to 1.1. The probability of occurrence of the primary eddy perturbation at this $\sigma$ value however, is determined by the fractional volume dilution $k$ which quantifies the departure of the primary eddy from its undiluted average condition and therefore represents the normalized deviation $\sigma$. Therefore, the probability density $P$ of fractal fluctuations of the primary eddy is given using the computed value of $k$ as shown in the following equation

$$P = \tau^{-4k}. \tag{19}$$

The vertical velocity $W$ spectrum will therefore be represented by the probability density distribution $P$ for values of -1 $\leq \sigma \leq$ 1 given in (19) since fractal fluctuations exhibit quantum-like chaos as explained above (16):

$$W = P = \tau^{-4k}. \tag{20}$$

The probabilities of occurrence ($P$) of the primary eddy for a complete eddy cycle either in the positive or negative direction starting from the peak value ($\sigma = 0$) are given for progressive growth stages ($\sigma$ values) in the following Table 2. The statistical normal probability density distribution corresponding to the normalized deviation $\sigma$ values are also given in the Table 2.

The model predicted probability density distribution $P$ along with the corresponding statistical normal distribution with probability values plotted on linear and logarithmic scales respectively on the left and right hand sides are shown in Fig.4. The model predicted probability distribution $P$ for fractal space-time fluctuations is very close to the statistical normal distribution for normalized deviation $\sigma$ values less than 2 as seen on the left hand side of Figure 4. The model predicts progressively higher values of probability $P$ for values of $\sigma$ greater than 2 as seen on a logarithmic plot on the right hand side of Figure 4.

### 5.5 Atmospheric wind spectrum and aerosol size spectrum

The steady state flux d$N$ of cloud condensation nuclei (CCN) at level $z$ in the normalized vertical velocity perturbation (d$W$)$z$ is given as

$$\mathrm{d}N = N(\mathrm{d}W)z. \tag{21}$$

| Growth step no | $\pm\sigma$ | $k$ | Probability(%) model predicted | Probability (%) Statistical normal |
|---|---|---|---|---|
| 2 | .9000 | .8864 | 18.1555 | 18.4060 |
| 3 | .8000 | .7237 | 24.8304 | 21.1855 |
| 4 | .7000 | .6268 | 29.9254 | 24.1964 |
| 5 | .6000 | .5606 | 33.9904 | 27.4253 |
| 6 | .5000 | .5118 | 37.3412 | 30.8538 |
| 7 | .4000 | .4738 | 40.1720 | 34.4578 |
| 8 | .3000 | .4432 | 42.6093 | 38.2089 |
| 9 | .2000 | .4179 | 44.7397 | 42.0740 |
| 10 | .1000 | .3964 | 46.6250 | 46.0172 |
| 11 | 0 | .3780 | 48.3104 | 50.0000 |

**Table 2**: Primary eddy growth.

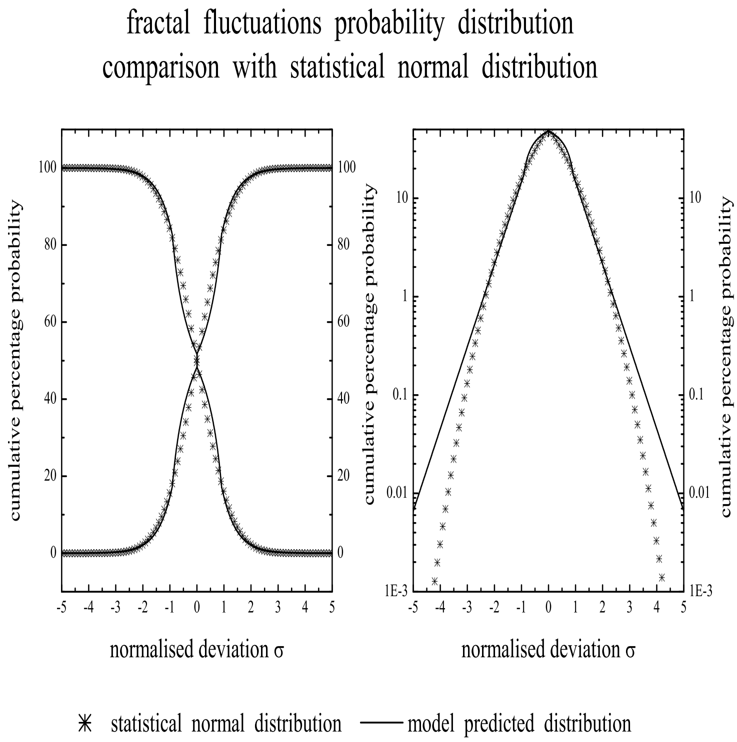


**Figure 4**: Model predicted probability distribution $P$ along with the corresponding statistical normal distribution with probability values plotted on linear and logarithmic scales respectively on the left and right hand sides.

The logarithmic wind profile relationship for $W$ at (3) gives

$$\mathrm{d}N = Nz\frac{w_*}{k}(\mathrm{d}\ln z). \tag{22}$$

The general systems theory predicts universal logarithmic wind profile [78, 83] as manifested in the spiralling vortex air flows of tornadoes and the hurricane spiral cloud circulations.

Substituting for $k$ from (2)

$$\mathrm{d}N = Nz\frac{w_*}{w_*}Wz(\mathrm{d}\ln z) = NWz^2(\mathrm{d}\ln z). \tag{23}$$

The length scale $z$ is related to the aerosol radius $r_a$ (14). Therefore

$$\ln z = \frac{3}{2}\ln\left(\frac{r_a}{r_{as}}\right). \tag{24}$$

Defining a normalized radius $r_{an}$ equal to $r_a/r_{as}$ , i.e., $r_{an}$ represents the CCN mean volume radius $r_a$ in terms of the CCN mean volume radius $r_{as}$ at the surface (or reference level). Therefore,

$$\ln z = \frac{3}{2}\ln r_{an}, \tag{25}$$

$$\mathrm{d}\ln z = \frac{3}{2}\mathrm{d}\ln r_{an}. \tag{26}$$

Substituting for $\mathrm{d}\ln z$ in (23)

$$\mathrm{d}N = NWz^2\frac{3}{2}(\mathrm{d}\ln r_{an}), \tag{27}$$

$$\frac{\mathrm{d}N}{(\mathrm{d}\ln r_{an})} = \frac{3}{2}NWz^2. \tag{28}$$

Substituting for $W$ from equations (16) and (20) in terms of the universal probability density $P$ for fractal fluctuations

$$\frac{\mathrm{d}N}{(\mathrm{d}\ln r_{an})} = \frac{3}{2}NPz^2. \tag{29}$$

The general systems theory predicts that fractal fluctuations may be resolved into an overall logarithmic spiral trajectory with the quasiperiodic Penrose tiling pattern for the internal structure such that the successive eddy lengths follow the Fibonacci mathematical series [78, 85]. The eddy length scale ratio $z$ for length step $\sigma$ is therefore a function of the golden mean $\tau$ given as

$$z = \tau^{\sigma}. \tag{30}$$

Expressing the scale length $z$ in terms of the golden mean $\tau$ in (29)

$$\frac{\mathrm{d}N}{\mathrm{d}(\ln r_{an})} = \frac{3}{2}NP\tau^{2\sigma}. \tag{31}$$

In (31) $N$ is the steady state aerosol concentration at level $z$. The normalized aerosol concentration at any level $z$ is given as

$$\frac{1}{N}\frac{\mathrm{d}N}{\mathrm{d}(\ln r_{an})} = \frac{3}{2}P\tau^{2\sigma}. \tag{32}$$

The fractal fluctuations probability density is $P = \tau^{-4\sigma}$ (16) for values of the normalized deviation $\sigma \geq 1$ and $\sigma \leq$ -1 on either side of $\sigma = 0$ as explained earlier (Sections 5.3 and 5.4). Values of the normalized deviation -1 $\leq \sigma \leq$ 1 refer to regions of primary eddy growth where the fractional volume dilution $k$ (2) by eddy mixing process has to be taken into account for determining the probability density $P$ of fractal fluctuations. Therefore the probability density $P$ in the primary eddy growth region ($\sigma \geq 1$ and $\sigma \leq$ -1) is given using the computed value of $k$ as $P = \tau^{-4k}$ (20).

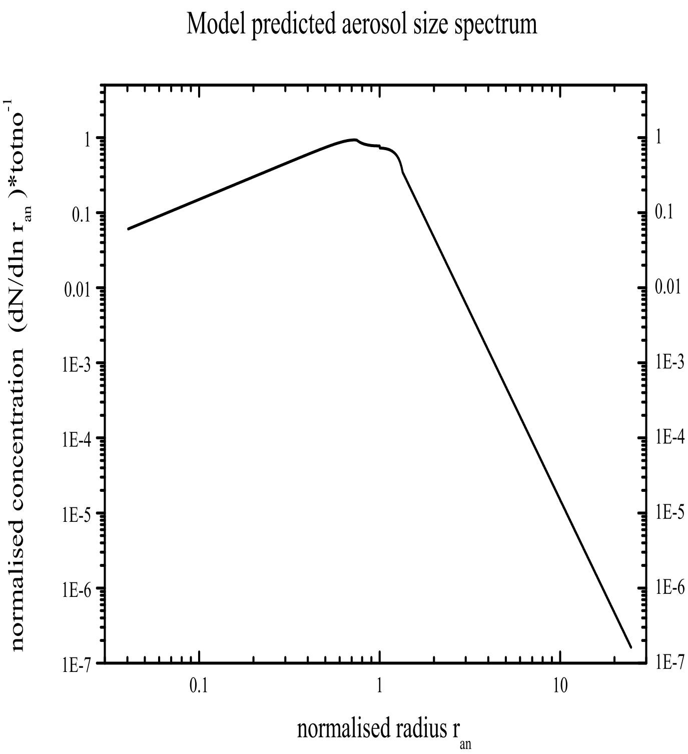


**Figure 5**: Model predicted universal (scale independent) aerosol size spectrum.

The normalized radius $r_{an}$ is given in terms of $\sigma$ and the golden mean $\tau$ from equations (25) and (30) as follows

$$\ln z = \frac{3}{2}\ln r_{an}, \tag{33}$$
$$r_{an} = z^{\frac{2}{3}} = \tau^{\frac{2\sigma}{3}}.$$

The normalized aerosol size spectrum is obtained by plotting a graph of normalized aerosol concentration $\frac{1}{N}\frac{\mathrm{d}N}{\mathrm{d}(\ln r_{an})} = \frac{3}{2}P\tau^{2\sigma}$ (32) versus the normalized aerosol radius $r_{an} = \tau^{\frac{2\sigma}{3}}$ (33). The normalized aerosol size spectrum is derived directly from the universal probability density $P$ distribution characteristics of fractal fluctuations (equations 16 and 20) and is independent of the height $z$ of measurement and is universal for aerosols in turbulent atmospheric flows. The aerosol size spectrum is computed starting from the minimum size, the corresponding probability density $P$ (32) refers to the cumulative probability density starting from 1 and is computed as equal to $P = 1 - \tau^{-4\sigma}$ . The universal normalized aerosol size spectrum represented by $\frac{1}{N}\frac{\mathrm{d}N}{\mathrm{d}(\ln r_{an})}$ versus the normalized aerosol radius $r_{an}$ is shown in Figure 5.

## 6 General Systems Theory and Maximum Entropy Principle of Classical Statistical Physics

Kaniadakis [47] states that the correctness of an analytic expression for a given power-law tailed distribution, used to describe a statistical system, is strongly related to the validity of the generating mechanism. In this sense the maximum entropy principle, the cornerstone of statistical physics, is a valid and powerful tool to explore new roots in searching for generalized statistical theories [47]. The concept of entropy is fundamental in the foundation of statistical physics. It first appeared in thermodynamics through the second law of thermodynamics. In statistical mechanics, we are interested in the disorder in the distribution of the system over the permissible microstates. The measure of disorder first provided by Boltzmann principle (known as Boltzmann entropy) is given by $S = K_B \ln M$, where $K_B$ is the thermodynamic unit of measurement of entropy and is known as Boltzmann constant equal to $1.38\times10^{-16}$ erg/$^o$C. The variable $M$, called thermodynamic probability or statistical weight, is the total number of microscopic complexions compatible with the macroscopic state of the system and corresponds to the degree of disorder or missing information [16].

The maximum entropy principle concept of classical statistical physics is applied to determine the fidelity of the inverse power law probability distribution $P$ (15) for exact quantification of the observed space-time fractal fluctuations of dynamical systems ranging from the microscopic dynamics of quantum systems to macro-scale real world systems. The eddy energy probability distribution ($P$) of fractal space-time fluctuations for each stage of hierarchical eddy growth is given by (15) derived earlier, namely

$$P = \tau^{-4t}.$$

The r.m.s circulation speed $W$ of the large eddy follows a logarithmic relationship with respect to the length scale ratio $z$ equal to $R/r$ (3) as given below

$$W = \frac{w_*}{k}\log z.$$

In the above equation the variable $k$ represents for each step of eddy growth, the fractional volume dilution of large eddy by turbulent eddy fluctuations carried on the large eddy envelope [78] and is given as (2)

$$k = \frac{w_* r}{WR}.$$

Substituting for $k$ in (3), we have

$$W = w_* \frac{WR}{w_* r} \log z = \frac{WR}{r} \log z, \tag{34}$$
$$\text{and } \frac{r}{R} = \log z.$$

The ratio $r/R$ represents the fractional probability $P$ of occurrence of small-scale fluctuations ($r$) in the large eddy ($R$) environment. Since the scale ratio $z$ is equal to $r/R$, (34) may be written in terms of the probability $P$ as follows

$$\frac{r}{R} = \log z = \log\left(\frac{R}{r}\right) = \log\left(\frac{1}{(r/R)}\right), \tag{35}$$
$$P = \log\left(\frac{1}{P}\right) = -\log P.$$

For a probability distribution among a discrete set of states the generalized entropy for a system out of equilibrium is given as [75, 16, 6, 88]

$$S = -\sum_{j=1}^{n} P_j \ln P_j. \tag{36}$$

In (36) $P_j$ is the probability for the $j^{th}$ stage of eddy growth in the present study and the entropy $S$ represents the missing information regarding the probabilities. Maximum entropy $S$ signifies minimum preferred states associated with scale-free probabilities.

The validity of the probability distribution $P$ (15) is now checked by applying the concept of maximum entropy principle [47]. Substituting for $\log P_j$ (36) and for the probability$P_j$ in terms of the golden mean $\tau$ derived earlier (15) the entropy $S$ is expressed as

$$S = -\sum_{j=1}^{n} P_j \ln P_j = \sum_{j=1}^{n} P_j^2 = \sum_{j=1}^{n} \left(\tau^{-4n}\right)^2, \tag{37}$$
$$S = \sum_{j=1}^{n} \tau^{-8n} \approx 1 \text{ for large } n.$$

In (37) $S$ is equal to the square of the cumulative probability density distribution and it increases with increase in $n$, i.e., the progressive growth of the eddy continuum and approaches 1 for large $n$. According to the second law of thermodynamics, increase in entropy signifies approach of dynamic equilibrium conditions with scale-free characteristic of fractal fluctuations and hence the probability distribution $P$ (15) is the correct analytic expression quantifying the eddy growth processes visualized in the general systems theory. The ordered growth of the atmospheric eddy continuum is associated with maximum entropy production.

Paltridge [65] states that the principle of maximum entropy production (MEP) is the subject of considerable academic study, but is yet to become remarkable for its practical applications. The ability of a system to dissipate energy and to produce entropy "ought to be" some increasing function of the systems structural complexity. It would be nice if there were some general rule to the effect that, in any given complex system, the steady state which produces entropy at the maximum rate would at the same time be the steady state of maximum order and minimum entropy [65].

Selvam [87] has shown that the eddy continuum energy distribution $P$ (15) is the same as the *Boltzmann distribution* for molecular energies. The derivation of *Boltzmann's equation* from general systems theory concepts visualises the eddy energy distribution as follows: (i) The primary small-scale eddy represents the molecules whose eddy kinetic energy is equal to $K_B T$ where $K_B$ is the *Boltzmann's constant* and $T$ is the temperature as in classical physics. (ii) The energy pumping from the primary small-scale eddy generates growth of progressive larger eddies [78]. The r.m.s circulation speeds $W$ of larger eddies are smaller than that of the primary small-scale eddy (1). (iii) The space-time *fractal* fluctuations of molecules (atoms) in an ideal gas may be visualized to result from an eddy continuum with the eddy energy $E$ per unit volume relative to primary molecular kinetic energy $K_B T$ decreasing progressively with increase in eddy size.

The eddy energy probability distribution ($P$) of fractal space-time fluctuations also represents the *Boltzmann distribution* for each stage of hierarchical eddy growth and is given by (15) derived earlier, namely

$$P = \tau^{-4t}.$$

The general systems theory concepts are applicable to all space-time scales ranging from microscopic scale quantum systems to macroscale real world systems such as atmospheric flows.

A systems theory approach based on maximum entropy principle has been applied earlier in cloud physics to obtain useful information on droplet size distributions without regard to the details of individual droplets [51-57]. Liu, Daum et al. [57] conclude that a combination of the systems idea with multiscale approaches seems to be a promising avenue. Checa and Tapiador [17] have presented a maximum entropy approach to Rain Drop Size Distribution (RDSD) modelling. Liu, Liu and Wang [58] have given a review of the concept of entropy and its relevant principles, on the organization of atmospheric systems and the principle of the Second Law of thermodynamics, as well as their applications to atmospheric sciences. The Maximum Entropy Production Principle (MEPP), at least as used in climate science, was first hypothesised by Paltridge [66].

## 7 Data

VOCALS PCASP-B data sets were used for comparison of observed with model predicted suspended particle size spectrum in turbulent atmospheric flows.

During October and November, 2008, Brookhaven National Laboratory (BNL) participated in VOCALS (VAMOS Ocean-Cloud-Atmosphere Land Study), a multi agency, multi-national atmospheric sampling field campaign conducted over the Pacific Ocean off the coast of Arica, Chile. Support for BNL came from DOE's Atmospheric Science Program (ASP) which is now part of the Atmospheric System Research (ASR) program following a merger with DOE's Atmospheric Radiation (ARM) program. A description of the VOCALS field campaign can be found at http://www.eol.ucar.edu/projects/vocals/

Measurements made from the DOE G-1 aircraft are being used to assess the effects of anthropogenic and biogenic aerosol on the microphysics of marine stratus. Aerosols affect the size and lifetime of cloud droplets thereby influencing the earth climate by making clouds more or less reflective and more or less long-lived. Climatic impacts resulting from interactions between aerosols and clouds have been identified by the IPCC (2007) as being highly uncertain and it is toward the improved representation of these processes in climate models that BNL's efforts are directed.

The parent data set from which the Excel spreadsheet has been derived is archived at the BNL anonymous ftp site:
ftp://ftp.asd.bnl.gov/pub/ASP%20Field%20Programs/2008VOCALS/Processed_Data/PCASP_BPart/.

Data are archived as ASCII files.

### 7.1 VOCALS 2008 PCASP-B aerosol size spectrum

Data from the DOE G-1 Research Aircraft Facility operating during the 2008 VAMOS Ocean Cloud Atmosphere Land Study (VOCALS) 2008 based in part at Chacalluta Airport (ARI) north of Arica, CHILE.

PCASP_BPart - Contains detailed size-binned (30 bins, 0.1 - 3 $\mu$m diameter) data obtained from the PCASP (Passive Cavity Aerosol Spectrometer Probe, Unit B). This probe was on the isokinetic inlet in the cabin before 10/29/08. On flight 081029a it was moved to the nose pylon of the plane.

The following 17 data sets were used for the study, the file names giving Flight Designation (yymmddflight of day letter), 081014a_10.txt, 081017a_10.txt, 081018a_10.txt, 081022a_10.txt, 081023a_10.txt, 081025a_10.txt, 081026a_10.txt, 081028a_10.txt, 081029a_10.txt, 081101a_10.txt, 081103a_10.txt, 081104a_10.txt, 081106a_10.txt, 081108a_10.txt, 081110a_10.txt, 081112a_10.txt, 081113a_10.txt. The letter is a for first flight. Max.Data Frequency is 10s-1 indicated as _10 in the file name.

## 8 Analysis and Discussion of Results

The atmospheric suspended particulate size spectrum is closely related to the vertical velocity spectrum (Section 5). The mean volume radius of suspended aerosol particulates increases with height (or reference level $z$) in association with decrease in number concentration. At any height (or reference level) $z$, the fractal fluctuations (of wind, temperature, etc.) carry the signatures of eddy fluctuations of all size scales since the eddy of length scale $z$ encloses smaller scale eddies and at the same time forms part of internal circulations of eddies larger than length scale $z$ (Section 5.2). The observed atmospheric suspended particulate size spectrum also exhibits a decrease in number concentration with increase in particulate radius. At any reference level $z$ of measurement the mean volume radius $r_{as}$ will serve to calculate the normalized radius $r_{an}$ for the different radius class intervals as explained below.

The general systems theory for fractal space-time fluctuations in dynamical systems predicts universal mass size spectrum for atmospheric suspended particulates (Section 5). For homogeneous atmospheric suspended particulates, i.e. with the same particulate substance density, the atmospheric suspended particulate mass and radius size spectrum is the same and is given as (Section 5.5) the normalized aerosol number concentration equal to $\frac{1}{N}\frac{\mathrm{d}N}{\mathrm{d}(\ln r_{an})}$ versus the normalized aerosol radius $r_{an}$, where (i) $r_{an}$ is equal to $\frac{r_a}{r_{as}}$, $r_a$ being the mean class interval radius and $r_{as}$ being the mean volume radius for the total aerosol size spectrum (ii) $N$ is the total aerosol number concentration and $\mathrm{d}N$ is the aerosol number concentration in the aerosol radius class interval $\mathrm{d}r_a$ (iii) $\mathrm{d}(\ln r_{an})$ is equal to $\frac{\mathrm{d}r_a}{r_a}$ for the aerosol radius class interval $r_a$ to $r_a+\mathrm{d}r_a$.

### 8.1 Analysis results, VOCALS PCASP-B aerosol size spectrum

A total of 17 data sets between 14 October and 13 November 2008 are available for the study. The data used in this study for each of the 17 flights are (i) average and standard deviation for particle number concentration per cc in 29 class intervals ranging from .1 to 3 $\mu$m for the particle diameter (ii) average and standard deviation for total particle number concentration per cc (bins 2 to 30) (iii) average and standard deviation for total volume (cc).

Details of data sets used for the study are shown in Figure 6(a - d) as follows. (i) Figure 6a: lower and upper radius size limits for bin numbers 2 to 30 (ii) Figure 6b: average and standard deviation for total particle number concentration per cc for the 17 flights (iii) Figure 6c: average and standard deviation for total volume (cc) for the 17 flights (bins 2 to 30) (iv) Figure 6d: average and standard deviation for mean volume radius ($\mu$m) for the 17 flights. The dispersion (equal to standard deviation/mean) expressed as percentage gives a statistical measure of variability of measured particle number concentration. Computed dispersion (%) values are plotted for the two size ranges (i) less than 1 $\mu$m diameter (bins 2 to 20) and (ii) 1 to 3 $\mu$m diameter (bins 21 to 30) in Figure 7a and Figure 7b respectively.

The average total number concentration exhibits a variability of about $\pm 100$ cc$^{-1}$ around a mean value of about 200 cc$^{-1}$ except for the first three flights which show larger variability (Figure 6b). The total volume is one order of magnitude larger for flight numbers 10 onwards compared to earlier flights (Figure 6c) consistent with larger median volume radii for flight numbers 10 onwards (Figure 6d) and exhibit large variability, particularly for size ranges more than 1 $\mu$m (Figure 6d).

For particle diameter range less than 1 $\mu$m (bins 2 to 20) the computed dispersion (%) for particle number concentration is within 100% for bins 2 to 14 size range and thereafter increases rapidly to a maximum of 500%. The computed dispersion (%) for particle number concentration for bins 21 to 30 (1 to 3 $\mu$m diameter) increases steeply from 500% to nearly 5000% with increase in particle size.

The mid-point diameter of the class interval was used to compute the corresponding value of d(ln$r_{an}$). The average aerosol size spectra for each of the 17 data sets are plotted on the left hand side and the total average spectrum for the 17 data sets is plotted on the right and side in Figure 8 along with the model predicted scale independent aerosol size spectrum. The corresponding standard deviations for the average spectra are shown as error bars in Figure 8.

The total average aerosol size spectrum (right hand side of Figure 8a) for size (radius) range less than about 0.5$\mu$m (accumulation mode) is closer to the model predicted spectrum while for particle size range greater than 0.5$\mu$m (coarse) the spectrum shows appreciable departure from model predicted size spectrum possibly attributed to different aerosol substance densities in the accumulation and coarse modes. The aerosol size spectra for the two different homogeneous aerosol substance densities corresponding to the two size (radius) ranges, namely (i) 0.1 to about 0.5 $\mu$m (accumulation mode) and (ii) 0.5 to 1.5$\mu$m (coarse mode) were computed separately and shown in Figures 9 and 10 respectively. The observed aerosol size distribution for the two size categories now follow closely the model predicted universal size spectrum for homogeneous atmospheric suspended particulates. Earlier studies [38] have shown that the source for submicron (diameter) size accumulation mode aerosols is different from the larger (greater than 1 $\mu$m diameter) coarse mode particles in the atmosphere and therefore may form two different homogeneous aerosol size groups.

The amount and longitudinal gradient of aerosol sulfate, and a consideration of the locations of Cu smelters and power plants in Chile, strongly suggest that the sub micron aerosol is dominated by anthropogenic emissions [48].

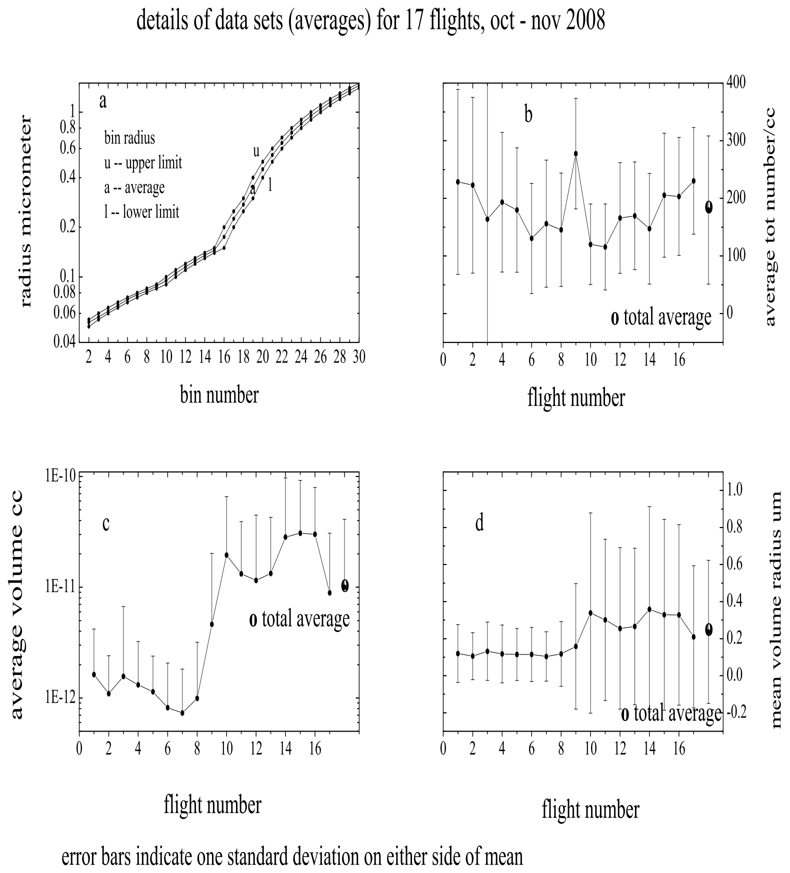


**Figure 6**: (a): lower and upper radius size limits for bin numbers 2 to 30 (b) average and standard deviation for total particle number concentration per cc for the 17 flights (c) average and standard deviation for total volume (cc) for the 17 flights (bins 2 to 30) (d) average and standard deviation for mean volume radius ($\mu$m) for the 17 flights.

## 9 Conclusions

The apparently irregular (turbulent) atmospheric flows exhibit selfsimilar fractal fluctuations associated with inverse power law distribution for power spectra of meteorological parameters on all time scales signifying an eddy continuum underlying the fluctuations. A general systems theory [78] visualizes each large eddy as the envelope (average) of enclosed smaller-scale eddies, thereby generating the eddy continuum, a concept analogous to Kinetic Theory of Gases in Classical Statistical Physics. It is shown that the ordered growth of atmospheric eddy continuum in dynamical equilibrium is associated with Maximum Entropy Production.

Two important model predictions of the general systems theory for turbulent atmospheric flows and their applications are given in the following:

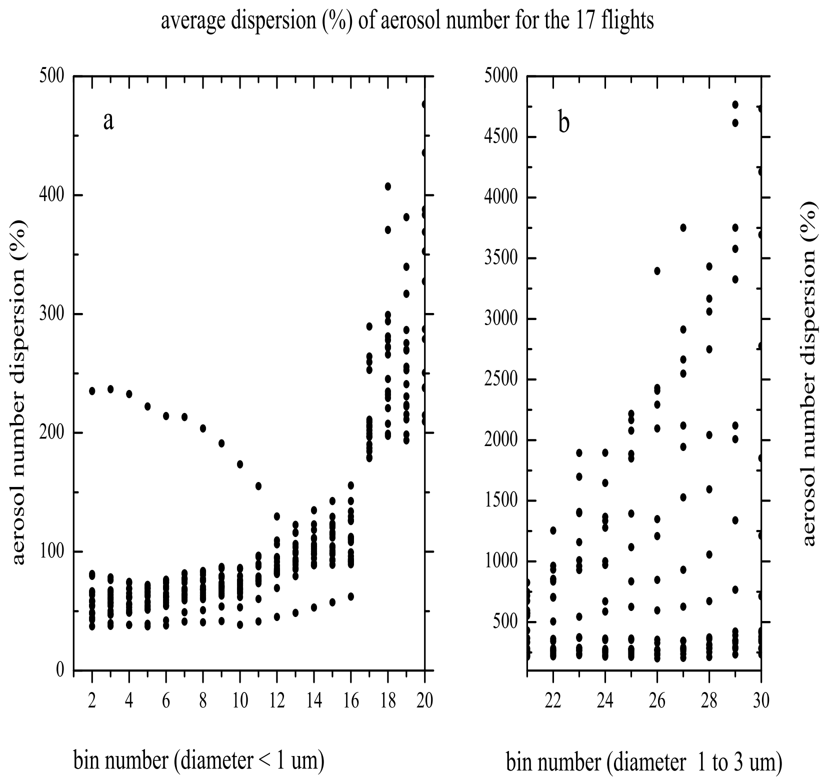


**Figure 7**: Computed dispersion (%) values for size range (a) less than 1 $\mu$m diameter (bins 2 to 20) (b) 1 to 3 $\mu$m diameter (bins 21 to 30).

- The probability distributions of amplitude and variance (square of amplitude) of fractal fluctuations are quantified by the same universal inverse power law incorporating the golden mean. Universal inverse power law for power spectra of fractal fluctuations rules out linear secular trends in meteorological parameters. Global warming related climate change, if any, will be seen as intensification of fluctuations of all scales manifested immediately in high frequency fluctuations [79, 87].

- The mass or radius (size) distribution for homogeneous suspended atmospheric particulates is expressed as a universal scale-independent function of the golden mean $\tau$, the total number concentration and the mean volume radius. Model predicted aerosol size spectrum is in agreement (within two standard deviations on either side of the mean) with total averaged radius size spectra for the VOCALS

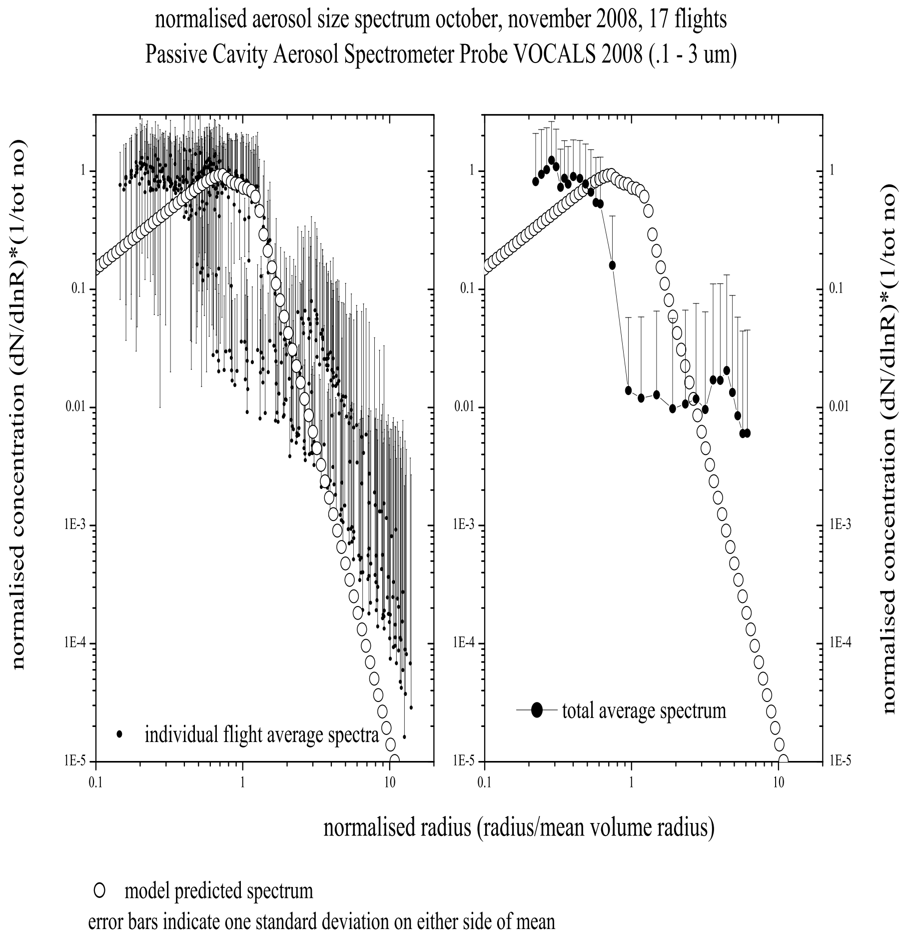


**Figure 8**: The average aerosol size spectra (bins 2 to 30) for each of the 17 data sets are plotted on the left hand side and the total average spectrum for the 17 data sets is plotted on the right along with the model predicted scale independent aerosol size spectrum.

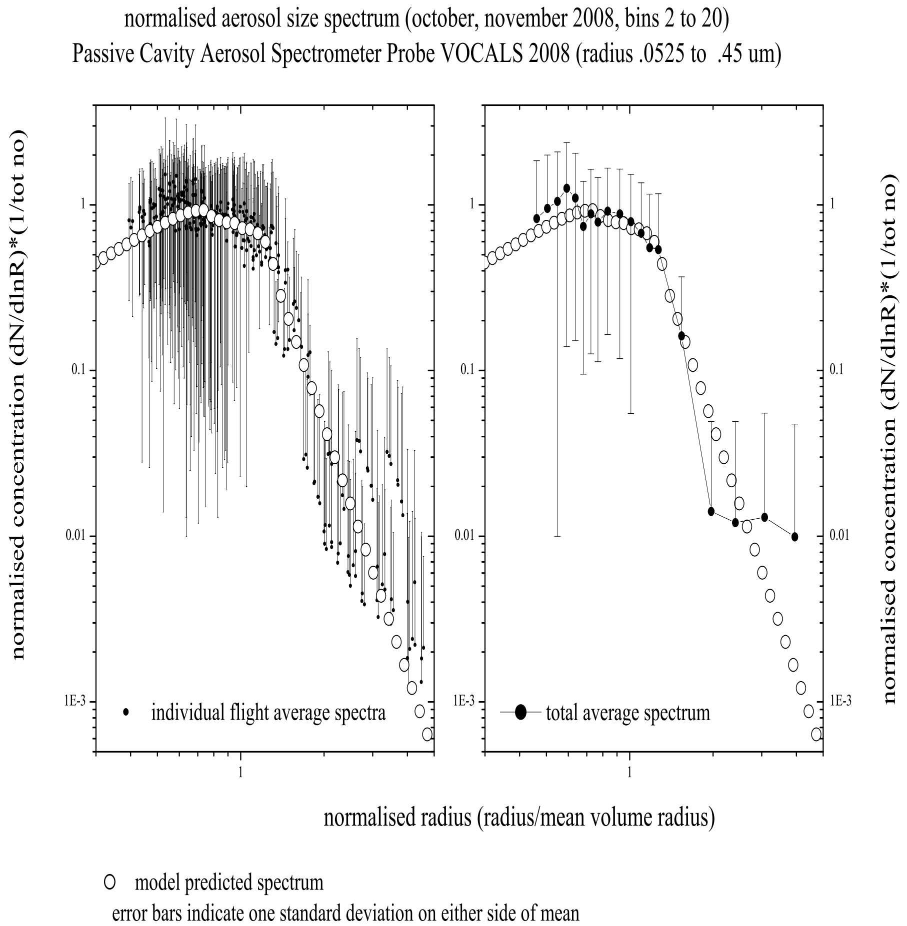


**Figure 9**: The aerosol size spectra for homogeneous aerosol substance density in the accumulation mode corresponding to the size (radius) range 0.1 to about 0.5 $\mu$m (bins 2 to 20). The average aerosol size spectra for each of the 17 data sets are plotted on the left hand side and the total average spectrum for the 17 data sets is plotted on the right along with the model predicted scale independent aerosol size spectrum

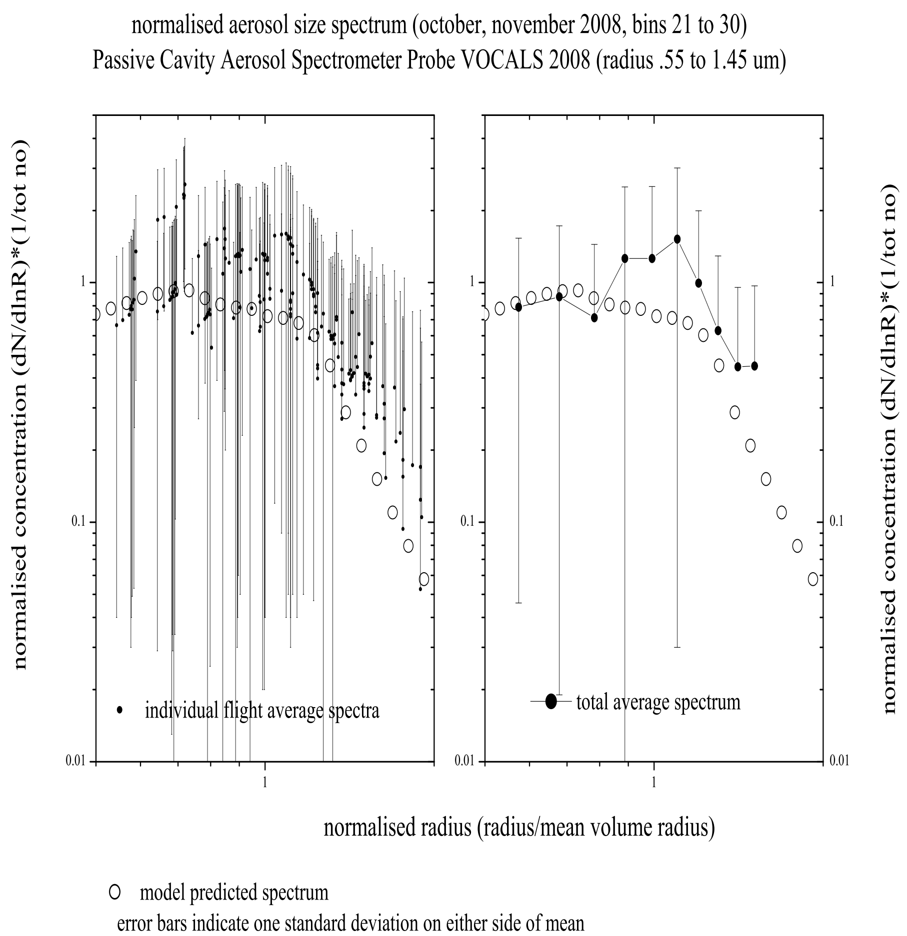


**Figure 10**: The aerosol size spectra for homogeneous aerosol substance density in the coarse mode corresponding to the size (radius) range 0.5 to 1.5 $\mu$m (bins 21 to 30). The average aerosol size spectra for each of the 17 data sets are plotted on the left hand side and the total average spectrum for the 17 data sets is plotted on the right along with the model predicted scale independent aerosol size spectrum

2008 PCASP-B data sets. SAFARI 2000 aerosol size distributions reported by Haywood et al. [36] also show similar shape for the distributions. Specification of cloud droplet size distributions is essential for the calculation of radiation transfer in clouds and cloud-climate interactions, and for remote sensing of cloud properties. The general systems theory model for aerosol size distribution is scale free and is derived directly from atmospheric eddy dynamical concepts. At present empirical models such as the log normal distribution with arbitrary constants for the size distribution of atmospheric suspended particulates is used for quantitative estimation of earth-atmosphere radiation budget related to climate warming/cooling trends (Section 2.1). The universal aerosol size spectrum presented in this paper may be computed for any location with two measured parameters, namely, the mean volume radius and the total number concentration and may be incorporated in climate models for computation of radiation budget of earth-atmosphere system.

**Acknowledgment**

The author is grateful to Dr. A. S. R. Murty for encouragement during the course of the study.

**Appendix I: List of frequently used Symbols:**

$\nu$: frequency,

$d$: aerosol diameter,

$N$: aerosol number concentration,

$N_*$: surface (or initial level) aerosol number concentration,

$r_a$: aerosol radius,

$\alpha$: exponent of inverse power law,

$W$: circulation speed (root mean square) of large eddy,

$w$: circulation speed (root mean square) of turbulent eddy,

$R$: radius of the large eddy,

$r$: radius of the turbulent eddy,

$w_*$: primary (initial stage) turbulent eddy circulation speed,

$r_*$: primary (initial stage) turbulent eddy radius,

$T$: time period of large eddy circulation,

$t$: time period of turbulent eddy circulation,

$k$: fractional volume dilution rate of large eddy by turbulent eddy fluctuations,

$z$: eddy length scale ratio equal to it R/ $r$,

$f$: steady state fractional upward mass flux of surface (or initial level) air,

$q$: moisture content at height $z$,

$q_*$: moisture content at primary (initial stage) level,

$m$: suspended aerosol mass concentration at any level $z$,

$m_*$: suspended aerosol mass concentration at primary (initial stage) level,

$r_a$: mean volume radius of aerosols at level $z$,

$r_{as}$: mean volume radius of aerosols at primary (initial stage) level,

$r_{an}$: normalized mean volume radius equal to $r_a/r_{as}$,

$P$: probability density distribution of fractal fluctuations,

$\sigma$: normalized deviation.

## References


[1] Agee, E.M. Observations from space and thermal convection: a historical perspective. *Bull. Am. Meteorol. Soc.* **65** (1984) 938–949.

[2] Anthes, R.A. *Tropical Cyclones-Their Evolution Structure and Effects.* Meteorol. Monogr. **41**, 1982.

[3] Aulbach, B. and Kieninger, B. On three definitions of chaos. *Nonlinear Dynamics and Systems Theory* **1** (1) (2001) 23–37.

[4] Bak, P.C., Tang, C. and Wiesenfeld, K. Self-organized criticality. *Phys. Rev. A.* **38** (1988) 364–374.

[5] Barbashin, E. A. *Introduction to the Theory of Stability.* Moscow: Nauka, 1967.

[6] Beck, C. Generalized information and entropy measures in physics. *Contemp. Phys.* **50** (2009) 495–510. arXiv:0902.1235v2 [cond-mat.stat-mech]

[7] Bergeron, T. The problem of artificial control of rainfall on the globe: II. The coastal orographic maxima of precipitation in autumn and winter. *TeIIus* **1** (1949) I5–32.

[8] Boers, R. A parameterization of the depth of the entrainment zone. *J. Atmos. Sci.* **28** (1989) 107–111.

[9] Bogachev, M.I., Eichner, J.F. and Bunde, A. Effect of nonlinear correlations on the statistics of return intervals in multifractal data sets. *Physical Review Letters* **99** (2007) 240601 (1–4).

[10] Bogachev, M.I., Eichner, J.F. and Bunde, A. On the occurrence of extreme events in long-term correlated and multifractal data sets. *Pure Appl. Geophys.* **165** (2008) 1195–1207.

[11] Bogachev, M.I., Eichner, J.F. and Bunde, A. The effects of multifractality on the statistics of return intervals. *Eur. Phys. J. Special Topics* **161** (2008) 181–193.

[12] Bunde, A., Eichner, J.F., Kantelhardt, J.W. and Havlin, S. Long-term memory: a natural mechanism for the clustering of extreme events and anomalous residual times in climate records. *Physical Review Letters* **94** (2005) 048701 (1–4).

[13] Bunde, A. and Havlin, S. Power-law persistence in the atmosphere and in the oceans. *Physica A* **314** (2002) 15–24.

[14] Bunde, A. and Havlin, S. Scaling in the atmosphere: on global laws of persistence and tests of climate models. *Fractals* **11** Supplementary Issue (2003) 205-216.

[15] Bunde, A., Eichner, J., Govindan, R., Havlin, S., Koscielny-Bunde, E., Rybskia, D. and Vjushin, D. Power-law persistence in the atmosphere: analysis and applications. In: *Nonextensive Entropy - Interdisciplinary Applications* (Eds.: M. Gell-Mann, C. Tsallis) Oxford University Press, New York. 2003. arXiv:physics/0208019 v2 27 May 2003

[16] Chakrabarti, C.G. and De, K. Boltzmann-Gibbs entropy: axiomatic characterization and application. *Intern. J. Math. and Math. Sci.* **23** (4) (2000) 243–251.

[17] Checa, R. and Tapiador, F.J. A maximum entropy modelling of the rain drop size distribution. *Entropy* **13** (2011) 293–315.

[18] Chen, W.N., Chang, S.Y., Chou, C.C.K. and Fang, G.C. Total scatter-to-backscatter ratio of aerosol derived from aerosol size distribution measurement. *International Journal of Environment and Pollution* **37** (1) (2009) 45–54.

[19] Chen, Ye-Hwa. Optimal design of robust control for uncertain systems: a fuzzy approach. *Nonlinear Dynamics and Systems Theory* **1** (2) (2001) 133–143.

[20] Contopoulos, G. *Order and Chaos in Dynamical Astronomy.* Springer, USA, 2010.

[21] Cotton, W.R. and Anthes, R.A. *Storm and Cloud Dynamics.* Vol. 44, International Geophysics Series, Academic Press, 1989.

[22] De Luca, F. and Manes, C. Hybrid force/position control for robots on contact with dynamic environments. *Proc. Robot Control, SYROCO'91*, 1988, 377–382.

[23] Denysenko, V.S., Martynyuk, A.A. and Slyn'ko, V.I. Stability analysis of impulsive Takagi-Sugeno systems. *International Journal of Innovative Computing, Information and Control* **5** (10A) (2009) 3141–3155.

[24] Desale, B.S. and Sharma, V. Special solutions to rotating stratified Boussinesq equations. *Nonlinear Dynamics and Systems Theory* **10** (1) (2010) 29–38.

[25] Donnelly, R. J. Superfluid turbulence. *Sci. Am.* **259** (5) (1988) 100–109.

[26] Donnelly, R.J. *Quantized Vortices in Helium II.* Cambridge University Press, USA, 1990.

[27] Dorfman, J.R. Deterministic chaos and the foundations of the kinetic theory of gases. arXiv:chao-dyn/9712005v1 4 Dec 1997, 1–61, 1997.

[28] Eichner, J.F., Koscielny-Bunde, E., Bunde, A., Havlin, S. and Schellnhuber, H-J. Power-law persistence and trends in the atmosphere: a detailed study of long temperature records. *Physical Review E* **68** (2003) 046133(4).

[29] Eichner, J.F., Kantelhardt, J.W., Bunde, A. and Havlin, S. Extreme value statistics in records with long-term persistence. *Physical Review E* **73** (2006) 016130 (1–10).

[30] Estoque, M.A. The sea breeze as a function of the prevailing synoptic situation. *Atmos. Sci.* **19** (1962) 244–250.

[31] Feingold, G., Koren, I., Wang, H., Xue, H. and Brewer, W.A. Precipitation-generated oscillations in open cellular cloud fields. *Nature* **466** (2010) 849–852.

[32] Frisch, U. and Orszag, S.A. Turbulence: Challenges for theory and experiment. *Physics Today* **Jan.** (1990) 24–32.

[33] Garay, M.J., Davies, R., Averill, C. and Westphal, J.A. Actinoform clouds: overlooked examples of cloud self-organization at the mesoscale. *Bull. Am. Meteorol. Soc.* **85** (2004) 1585–1594.

[34] Gryning, S-E. and Batchvarova, E. Parametrization of the depth of the entrainment zone above the daytime mixed layer. *Quart. J. Roy. Meteorol. Soc.* **120(515)** (2006) 47-58.

[35] Haken, H. Synergetics: An overview. *Reports on Progress in Physics* **52** (7) (1989) 517–552.

[36] Haywood, J., Francis, P., Dubovik, O., Glew, M. and Holben, B. Comparison of aerosol size distributions, radiative properties, and optical depths determined by aircraft observations. *Journal of Geophysical Research* **108**(D13) 8471 (2003) SAF 7-1 to 12 doi:10.1029/2002JD002250.

[37] Hewitt, C.N. and Jackson, A.V. *Handbook of Atmospheric Science: Principles and Applications.* Wiley-Blackwell, USA, 2003.

[38] Husar, R.B. The emergence of the bimodal distribution concept. In: *History and Reviews of Aerosol Science* (Eds.: G. J. Sem, D. Boulaud, P. Brimblecombe, E. S. Ensor, J. W. Gentry, J. C. M. Marijnissen, O. Preining) American Association for Aerosol Research, 2005.

[39] Insinnia, E.M. Synchronicity and coherent excitations in microtubules. *Nanobiology* **1** (2) (1992) 191–208.

[40] IPCC *Climate Change 2007: The Physical Science Basis, Contribution of Working Group I to the Fourth Assessment Report of the Intergovernmental Panel on Climate Change* (Eds.: S. Solomon, D. Qin, M. Manning, Z. Chen, M. Marquis, K. B. Averyt, M. Tignor, H. L. Miller, Cambridge University Press, Cambridge, UK and New York, NY, USA, 2007.

[41] Jaenicke, R. and Davies, C.N. The mathematical expression of the size distribution of atmospheric aerosols. *J. Aerosol Sci.* **7** (1976) 255–259.

[42] Joshi, R.R. and Selvam, A.M. Identification of self-organized criticality in atmospheric low frequency variability. *Fractals* **7** (4) (1999) 421–425.

[43] Junge, C. Gesetzmigkeiten in der Grenverteilung atmosphrischer Aerosoleber dem Kontinent. *Ber. Deut. Wetterdienst US-Zone* **35** (1952) 261–277.

[44] Junge, C.E. Die Rolle der Aerosols und der gasformigen Beimengungen der Luft im Spurenstoffhaushalt der Troposhere. *Tellus* **5** (1953) 1–26.

[45] Junge, C.E. The size distribution and aging of natural aerosols as determined from electrical and optical data on the atmosphere. *Journal of Meteorology* **12** (1955) 13–25.

[46] Junge, C.E. *Air chemistry and Radioactivity.* Academic Press, London, 1963, pp.382.

[47] Kaniadakis, G. Maximum entropy principle and power-law tailed distributions. *Eur. Phys. J. B* **70** (2009) 3–13.

[48] Kleinman, L.I., Springston, S.R., Daum, P.H., Lee, Y-N., Sedlacek, A.J., Senum, G. and Wang, J. *Pre-Cloud Aerosol, Cloud Droplet Concentration, and Cloud Condensation Nuclei from the VAMOS Ocean-Cloud-Atmosphere Land Study (VOCALS) Field Campaign, First Quarter 2010, ASR Program Metric Report.* (2009) pp. 1–11, December 2009, Research sponsored by the U.S. Department of Energy Office of Science, Office of Biological and Environmental Research.

[49] Krueger, A.F. and Fritz, S. Cellular cloud patterns revealed by TIROS I. *Tellus* **13** (1961) 1–7.

[50] Levich, E. Certain problems in the theory of developed hydrodynamic turbulence. *Physics Reports* **151** (3,4) (1987) 129–238.

[51] Liu, Y. On the generalized theory of atmospheric particle systems. *Adv. Atmos. Sci.* **12** (1995) 419–438.

[52] Liu, Y., Laiguang, Y., Weinong, Y. and Feng, L. On the size distribution of cloud droplets. *Atmos. Res.* **35** (1995) 201-216.

[53] Liu, Y. and Hallett, J. The 1/3 power-law between effective radius and liquid water content. *Quart. J. Roy. Meteor. Soc.* **123** (1997) 1789–1795.

[54] Liu, Y. and Hallett, J. On size distributions of droplets growing by condensation: A new conceptual model. *J. Atmos. Sci.* **55** (1998) 527–536.

[55] Liu, Y. and Daum, P.H. *Statistical Physics, Information Theory and Cloud Droplet Size Distributions, Eleventh ARM Science Team Meeting Proceedings.* (2001) Atlanta, Georgia, March 19–23, 2001.

[56] Liu, Y., Daum, P.H. and Hallett, J. A generalized systems theory for the effect of varying fluctuations on cloud droplet size distributions. *Journal of the Atmospheric Sciences* **59** (2002) 2279–2290.

[57] Liu, Y., Daum, P.H., Chai, S.K. and Liu, F. Cloud parameterizations, cloud physics, and their connections: An overview. *Recent Res. Devel. Geophysics* **4** (2002) 119-142.

[58] Liu, Y., Liu, C. and Wang, D. Understanding atmospheric behaviour in terms of entropy: a review of applications of the second law of thermodynamics to meteorology. *Entropy* **13** (2011) 211–240.

[59] Lovejoy, S. and Schertzer, D. Turbulence, raindrops and the $l^{1/2}$ number density law. *New Journal of Physics* **10** (2008) 075017(1-32), doi:10.1088/1367-2630/10/7/075017.

[60] Lovejoy, S. and Schertzer, D. Towards a new synthesis for atmospheric dynamics: space-time cascades. *Atmos. Res.* **96** (2010) 1–52. http://www.physics.mcgill.ca/~gang/eprints/eprintLovejoy/neweprint/ Atmos.Res.8.3.10.finalsdarticle.pdf

[61] Lucibella, M., *Cities attract hurricanes.* (2010) http://www.physorg.com/ news201800721.html

[62] Martunyuk, A.A. Stability in the models of real world phenomena.*Nonlinear Dynamics and Systems Theory* **11** (1) (2011) 7–52.

[63] Nicolis, G. and Prigogine, I. *Self-Organization in Non-Equilibrium Systems.* Wiley, New York, 1977.

[64] Oerlemans, J. A case study of a subsynoptic disturbance in a polar outbreak. *Q.J.R. Meteorol. Soc.* **106** (1980) 313–325.

[65] Paltridge, G.W. A story and a recommendation about the principle of maximum entropy production. *Entropy* **11** (2009) 945–948.

[66] Paltridge, G.W. Climate and thermodynamic systems of mximum dissipation. *Nature* **279** (1978) 630–631.

[67] Pearson, R.A., Carboni, C. and Brusasca, G. The sea breeze with mean flow. *Q.J.R. Meteorol. Soc.* **109** (1983) 809–830.

[68] Pielke, R.A. A three dimensional numerical model of the sea breeze over South Florida. *Mon. Wea. Rev.* **102** (1974) 115–139.

[69] Prigogine, I. *From Being to Becoming.* Freeman San Francisco, CA, USA, 1980.

[70] Prigogine, I. and Stengers, I. *Order Out of Chaos.* 3rd edn. Fontana Paperbacks, London, 1988.

[71] Pruppacher, H.R. and Klett, J.D. *Microphysics of Clouds and Precipitation.* Kluwer Academic Publishers, The Netherlands, 1997.

[72] Roeloffzen, J.C., Van den Berg, W.D. and Oerlemans, J. Frictional convergence at coastlines. *Tellus* **38A** (1986) 397–411.

[73] Rybski, D., Bunde, A., Havlin, S. and von Storch, H. Long-term persistence in climate and the detection problem. *Geophysical Research Letters* **33** (2006) L06718(1–4) doi:10.1029/2005GL025591.

[74] Rybski, D., Bunde, A. and von Storch, H. Long-term memory in 1000-year simulated temperature records. *Journal of Geophysical Research* **113** (2008) D02106(1–9). doi:10.1029/2007JD008568.

[75] Salingaros, N.A. and West, B.J. A universal rule for the distribution of sizes. *Environment and Planning B: Planning and Design* **26** (1999) 909–923, Pion Publications.

[76] Selvam, A.M., Murty, A.S.R. and Ramana Murty, Bh.V. A new hypothesis for vertical mixing in clouds. *Preprint volume, 9th International Cloud Physics Conference, Tallinn, USSR.* 1984.

[77] Selvam, A.M., Murty, A.S.R. and Ramana Murty, Bh.V. Role of frictional turbulence in the evolution of cloud systems. *Preprint volume, 9th International Cloud Physics Conference, Tallinn, USSR.* 1984.

[78] Selvam, A.M. Deterministic chaos, fractals and quantumlike mechanics in atmospheric flows. *Can. J. Phys.* **68** (1990) 831–841. http://xxx.lanl.gov/html/physics/0010046

[79] Selvam, A.M., Pethkar, J.S. and Kulkarni, M.K. Signatures of a universal spectrum for atmospheric interannual variability in rainfall time series over the Indian Region. *Int'l J. Climatol.* **12** (1992) 137-152.

[80] Selvam, A.M. Universal quantification for deterministic chaos in dynamical systems. *Applied Math. Modelling* **17** (1993) 642–649. http://xxx.lanl.gov/html/physics/0008010.

[81] Selvam, A.M., Joshi, R.R. Universal spectrum for interannual variability in COADS global air and sea surface temperatures. *Int'l. J. Climatol.* **15** (1995) 613-623.

[82] Selvam, A.M., Pethkar, J.S., Kulkarni, M.K. and Vijayakumar, R. Signatures of a universal spectrum for atmospheric interannual variability in COADS surface pressure time series. *Int. J. Climatol.* **16** (1996) 393–404.

[83] Selvam, A.M. and Fadnavis, S. Signatures of a universal spectrum for atmospheric interannual variability in some disparate climatic regimes. *Meteorology and Atmospheric Physics* **66** (1998) 87–112. http://xxx.lanl.gov/abs/chao-dyn/9805028.

[84] Selvam, A.M. A general systems theory for chaos, quantum mechanics and gravity for dynamical systems of all space-time scales. *ELECTROMAGNETIC PHENOMENA* **5** (2(15)) (2005) 160–176. http://arxiv.org/pdf/physics/0503028; http://www.emph.com.ua/15/selvam.htm.

[85] Selvam, A.M. *Chaotic Climate Dynamics.* Luniver Press, U. K., 2007.

[86] Selvam, A.M. Fractal fluctuations and statistical normal distribution. *Fractals* **17** (3) (2009) 333–349. http://arxiv.org/pdf/0805.3426

[87] Selvam, A.M. Signatures of universal characteristics of fractal fluctuations in global mean monthly temperature anomalies. *Journal of Systems Science and Complexity* **24** (1) (2011) 14–38. http://arxiv.org/abs/0808.2388.

[88] Sethna, J.P. *Statistical Mechanics: Entropy, Order Parameters, and Complexity.* Clarendon Press, Oxford, 2009. http://www.freebookcentre.net/physics-books-download/Statistical-Mechanics-Entropy,-Order-Parameters,-and-Complexity-[PDF-371].html.

[89] Slane, J. and and Tragesser, S. Analysis of periodic nonautonomous inhomogeneous systems.*Nonlinear Dynamics and Systems Theory* **11** (2) (2011) 183–198.

[90] Strevens, M. *Bigger than Chaos: Understanding Complexity through Probability.* Harvard University Press, USA, 2006.

[91] Stull, R.B. *An Introduction to Boundary Layer Meteorology.* Atmospheric and Oceanographic Sciences Library, Vol. 13, Springer, 1988.

[92] Syono, Y., Ogura, Y., Gambo, K. and Kasahara, A. On the negative vorticity in a typhoon. *J. Meteorol. Soc. Jpn.* **29** (1951) 397–415.

[93] Tennekes, H. and Lumley, J. L. *A First Course in Turbulence.* The MIT Press, USA, 1972.

[94] Timmerman, H. The influence of topography and orography on the precipitation patterns in the Netherlands. *KNMl Mededelingen en Verhandelingen nr* **80** (1963) 49 pp.

[95] Townsend, A.A. *The Structure of Turbulent Shear Flow.* 2nd ed. Cambridge University Press, London, U. K., 1956, 115–130.

[96] Twomey, S. The influence of pollution on the shortwave albedo of clouds. *J. Atmos. Sci.* **34** (1977) 1149–1152.

[97] Visconti, G. *Fundamentals of Physics and Chemistry of the Atmosphere.* Springer, USA, 2001.

[98] Walsh, J.E. Sea breeze theory and applications. *J. Atmos. Sci.* **31** (1974) 2012–2019.

[99] Whitby, K.T. On the multimodal nature of atmospheric aerosol size distribution. *Paper presented at the VIII International Conference on Nucleation, Leningrad*, 1973.

[100] Whitey, K.T. The physical characteristics of sulfur aerosols. *Atmos. Environ.* **41** Supplement 1 (2007) 25–49.

[101] Winkler, P. and Junge, C.E. Comments on Anomalous deliquescence of sea spray aerosols. *J. Appl. Meteorol.* **10** (1971) 159–163.

[102] Winkler, P. and Junge, C. The growth of atmospheric aerosol particles as a function of the relative humidity. *J. de Recherches Atmospheriques* **6** (1972) 617–637.

[103] Zadeh, L.A. Fuzzy sets. *Information and Control* **8** (1965) 338–353.

Nonlinear Dynamics and Systems Theory, **12** (4) (2012) 435–436

# Contents of Volume 12, 2012

## Volume 12 Number 1 March 2012



## Volume 12 Number 2 June 2012

## Volume 12 Number 3 September 2012



## Volume 12 Number 4 December 2012